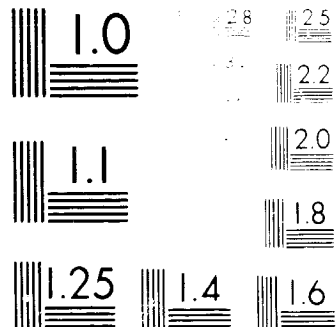


| OF |

N 78 32049

UNCLAS



# NASA Technical Memorandum 74033

(NASA-TM-74033) AERODYNAMIC CHARACTERISTICS  
OF A 1/4 SCALE POWERED HELICOPTER MODEL WITH  
A V-TYPE EMPENNAGE (NASA) 65 p HC A04/MF  
AD1

N78-32049

CSCL 01A

Unclass

G3/02 31572

## AERODYNAMIC CHARACTERISTICS OF A 1/4-SCALE POWERED HELICOPTER MODEL WITH A V-TYPE EMPENNAGE

Carl E. Freeman, Arthur E. Phelps III,  
and Raymond E. Mineck

August 1978



National Aeronautics and  
Space Administration

Langley Research Center  
Hampton Virginia 23665

## SUMMARY

An investigation was made in the Langley V/STOL tunnel to determine rotor induced effects on a 1/4-scale helicopter model with a conventional empennage and also a V-type empennage with dihedral angles of 45°, 50°, 55°, and 60°. Static longitudinal and lateral-directional stability data are presented for rotor advance ratios of 0.057, 0.102, and 0.192 in level flight and climb attitudes. The data are presented without analysis or discussion.

## INTRODUCTION

Conventionally powered, single main rotor helicopters have experienced directional control problems while operating in low velocity, left rear quartering winds in ground effect, and during low-speed sideward flight in ground effect (refs. 1 and 2). Investigations have been conducted to determine the source of these directional control problems and possible means of alleviating them (refs. 3 to 5). Reference 4 showed that a V-type empennage presents significant advantages over conventional horizontal-vertical control surfaces with respect to helicopter directional control at low speeds. The principal advantages are: (1) smaller adverse fin forces and (2) increased tail rotor efficiency.

A subsequent unpowered investigation was conducted (ref. 6) to parametrically determine a V-type empennage configuration that approximated the directional and longitudinal characteristics of the conventional helicopter empennage. On the basis of that test, V-type empennages with 45°, 50°, 55°, and 60° dihedral have been tested in the Langley V/STOL tunnel to determine the rotor wake effect on the characteristics of the V-type empennage in forward flight.

## SYMBOLS

Units used for the physical quantities defined in this paper are given in the International System of Units (SI) and parenthetically in U.S. Customary Units. All measurements and calculations were made in U.S. Customary Units. Conversion factors are presented in reference 7.

Positive senses of forces, moments, and angles are presented in figure 1. Relative strain-gage balance positions and location of the model moment reference centers are shown in figure 2. Fuselage and tail longitudinal data are given in the stability axis system and lateral-directional data are presented in the body axis system. Rotor forces and moments are given in the control axis system.

$a_0$       rotor precone angle, deg

$a_{1s}$       first-harmonic rotor longitudinal flapping angle, deg

$A_1$       lateral cyclic control, deg

A	rotor disk area, $\pi R^2$
b	number of rotor blades
$b_{1s}$	first-harmonic rotor lateral flapping angle, deg
$B_1$	longitudinal cyclic control, deg
c	rotor blade chord, m (ft)
$C_D$	drag coefficient, $F_D/q_\infty A$
$C_I$	rolling-moment coefficient, $M_x/q_\infty \pi R^3$
$C_L$	lift coefficient, $F_L/q_\infty A$
$C_{L\alpha}$	lift-curve slope, deg <sup>-1</sup>
$C_m$	pitching-moment coefficient, $M_y/q_\infty \pi R^3$
$C_n$	yawing-moment coefficient, $M_z/q_\infty \pi R^3$
$C_H/\sigma$	rotor horizontal force coefficient, $H_R/\rho_\infty A V_T^2 \sigma$
$C_Q/\sigma$	rotor torque coefficient, $Q_R/\rho_\infty A V_T^2 \sigma R$
$C_T/\sigma$	rotor thrust coefficient, $T_R/\rho_\infty A V_T^2 \sigma$
$C_y$	side-force coefficient, $F_y/\rho_\infty A$
$C_{y\beta}$	directional stability parameter, deg <sup>-1</sup>
D	rotor diameter, m (ft)
$F_D$	drag force, N (lbf)
$F_L$	lift force, N (lbf)
h/d	ratio of rotor height above test section floor to rotor diameter
$h_h$	distance of center of hub above shaft inclination point, cm (in.)
$H_R$	rotor horizontal force, N (lbf)
$i_H$	horizontal-tail incidence, deg
$i_V$	V-tail incidence, deg
$M_x$	rolling moment, N-m (lbf-ft)
$M_y$	pitching moment, N-m (lbf-ft)

$M_z$	yawing moment, N-m (lbf-ft)
$q_\infty$	free-stream dynamic pressure, Pa (lbf/ft <sup>2</sup> )
$Q_R$	rotor torque, N-m (lbf-ft)
R	rotor radius, m (ft)
S	V-tail planform area, m <sup>2</sup> (ft <sup>2</sup> )
$T_R$	rotor thrust, N (lbf)
$V_T$	rotor tip speed, $\Omega R$ , m/sec (ft/sec)
$V_\infty$	free-stream velocity, m/sec (ft/sec)
X,Y,Z	model axis system
$x_s, z_s$	distance from model reference system to rotor shaft inclination point, cm (in.)
$\alpha$	angle of attack, deg
$\beta$	angle of sideslip, deg
$\gamma$	rotor shaft tilt angle, deg
$\Gamma$	dihedral angle, deg
$\theta_c$	collective pitch angle measured at 0.75R, deg
$\mu$	rotor advance ratio, $V_\infty/V_T$
$\rho_\infty$	free-stream density, kg/m <sup>3</sup> (slugs/ft <sup>3</sup> )
$\sigma$	rotor solidity, $b c R/A$
$\phi$	roll ang'e, deg
$\psi$	blade azimuth position, deg
$\Omega$	rotor rotational speed, rad/sec

Model component designations:

F	fuselage
R	rotor
S	conventional empennage

**W wing**

**Vabc** V-tail empennage where a, b, and c are as indicated in the following table:

a	$\Gamma$	b	s		c	$i_v$
			$m^2$	$ft^2$		
1	45	1	0.186	(2.000)	1	5
2	50	2	.244	(2.625)	2	8
3	55	3	.302	(3.250)	3	10
4	60					

**Notation:**

**B.L.** butt line

**F.S.** fuselage station

**HP** hub plane (shaft axis)

**NFP** no feathering plane (control axis)

**TPP** tip path plane

**W.L.** water line

**MODEL AND APPARATUS**

The model used in this investigation was the same model as described in reference 6 with the addition of a two-bladed rotor system. A photograph of the model in the Langley V/STOL tunnel is given in figure 3 and geometric characteristics are given in table I. The model consisted of the general rotor model system (GRMS) configured to approximate the attack helicopter of reference 1. Detailed descriptions of the model and drive system are given in references 6 and 8, respectively.

Schematics of the basic configuration and the empennages tested are given in figures 2 and 4. As shown in figure 2, the fuselage was wider than the exact 1/4 scale to accommodate the GRMS. The V-tail (fig. 4) had variable dihedral, incidence, and planform area features in order to investigate a variety of tail configurations.

The main rotor was a two-bladed teetering type with blades formed from fiberglass laid over nylon honeycomb cores. The geometric characteristics of the blades are given in table II and figure 5. One blade was instrumented with strain gages to measure blade loads during testing. Rotor collective and cyclics were remotely controlled. The model was mounted on the V/STOL tunnel high alpha-beta sting assembly. This model support system allows high angles

of attack and sideslip be obtained and keeps the model near the center of the test section for pitch and yaw excursions.

#### TESTS AND CORRECTIONS

The tests were conducted in the Langley V/STOL tunnel, which is an atmospheric, closed-circuit wind tunnel. The test section, which measures 4.42 m by 6.63 m, can be configured three ways: (1) closed; (2) open (no walls or ceiling); and (3) slotted. The bulk of the tests were made at rotor advance ratios of 0.057 (open test section), 0.102 (closed), and 0.192 (closed). The normal rotor operating sweep was 1200 r.p.m. Angle-of-attack, angle-of-side-slip, rotor-collective, and longitudinal cyclic sweeps were made about measured trim conditions for the conventional horizontal tail set at 10° incidence.

Angle of attack and test section dynamic pressure were corrected for wall effects as suggested in reference 9. Drag data for the empennage were not corrected for tail cone chamber pressure.

The data were recorded on a digital data acquisition system. A data point consisted of an average of 50 samples of data acquired over a 5 second interval. All data presented in this paper were filtered above 2 Hz.

#### PRESENTATION OF DATA

Data obtained during this investigation are presented in a plotted form in figures 6 to 23. The rotor data are in the model control axis system with the hub being the moment reference center. Fuselage data are the forces on the total configuration with rotor and tail loads subtracted out. The tail data are the forces and moments on the tail surfaces and the tail cone from fuselage station 271.7 aft. Longitudinal data for the fuselage and tail are in the stability axis system. Lateral data are in the body axis system. The data are presented without analysis or discussion in the following order:

#### Figure

##### Longitudinal characteristics

##### Comparison of conventional tail and baseline

V-tail in 1-g flight . . . . .	6
V-tail in climb . . . . .	7

Effect of V-tail dihedral on the aerodynamic characteristics of the model . . . . .	8
--	---

Effect of V-tail planform area on the aerodynamic characteristics of the model . . . . .	9
---	---

Effect of V-tail incidence on the aerodynamic characteristics of the model . . . . .	10
---	----

Figure

Comparison of the baseline V-tail with right or left surfaces removed. . . . .	11
Comparison of the baseline V-tail with two nonsymmetrical dihedral configurations. . . . .	12
Effect of horizontal tail (conventional) incidence on the aerodynamic characteristics of the model . . . . .	13
Lateral-directional characteristics	
Comparison of conventional tail and baseline V-tail	
1-g flight . . . . .	14
Climb. . . . .	15
Effect of V-tail dihedral on the aerodynamic characteristics of the model . . . . .	16
Effect of V-tail planform on the aerodynamic characteristics of the model . . . . .	17
Effect of V-tail incidence on the aerodynamic characteristics of the model . . . . .	18
Comparison of the baseline V-tail with right or left surfaces removed. . . . .	19
Comparison of the baseline V-tail with two nonsymmetrical dihedral configurations. . . . .	20

Miscellaneous

Comparison of rotor collective effects on the conventional tail and baseline V-tail . . . . .	21
Comparison of rotor longitudinal cyclic effects on the conventional tail and baseline V-tail . . . . .	22

Although it is not the intention of this paper to present an analysis of the data, an explanation of some of the data is necessary; in particular the fuselage and tail drag data. Due to a high ratio of downwash to free-stream velocities at low advance ratios, a large effective angle of attack is induced on the fuselage and tail. This induced angle of attack creates lift forces not necessarily perpendicular with the free stream, thereby creating negative drag (thrust) as can be seen in the data. Also, due to physical characteristics of the tail balance installation, the tail loads include the aft section of the tail cone. Since the data are presented as comparisons of one tail configuration with other tail configurations, all having the same tail cone, no corrections were made for the effect of chamber pressure on drag of the tail.

## REFERENCES

1. Connor, William J.: The Huey Cobra in Vietnam. 1968 Report to the Aerospace Profession, Tech. Rev., vol. 9, no. 2, Soc. Exp. Test Pilots, 1968, pp. 25-32
2. Lynn, R. R.; Robinson, F. D.; Batra, N. N.; and Duhon, J. M.: Tail Rotor Design. Pt. I: Aerodynamics. J. Am. Helicopter Soc., vol. 15, no. 4, Oct. 1970, pp. 2-15
3. Huston, Robert J.; and Morris, Charles E. K., Jr.: A Wind-Tunnel Investigation of Helicopter Directional control in Rearward Flight in Ground Effect. NASA TN D-6118, 1971
4. Yeager, William T., Jr.; Young, Warren H., Jr.; and Mantay, Wayne R.: A Wind-Tunnel Investigation of Parameters Affecting Helicopter Directional Control at Low Speeds in Ground Effect. NASA TN D-7694, 1974
5. Wiesner, Wayne; and Kohley, Gary: Tail Rotor Design Guide. USAAMRDL Tech. Rep. 73-99, U.S. Army, Jan. 1974. (Available from DDC as AD-775391.)
6. Freeman, Carl E.; and Yeager, William T., Jr.: A Wind-Tunnel Investigation of an Unpowered Helicopter Fuselage Model with a V-Type Empennage. NASA TN D-3476, 1977
7. Mechtly, E. A.: The International System of Units - Physical Constants and Conversion Factors (Second Revision). NASA SP-7012, 1973
8. Mineck, Raymond E.; and Freeman, Carl E.: Aerodynamic Characteristics of a 1/6-Scale Powered Model of the Rotor Systems Research Aircraft. NASA TM X-3489, 1977
9. Heyson, Harry H.: Use of Superposition in Digital Computers to Obtain Wind-Tunnel Interference Factors for Arbitrary Configurations, With Particular References to V/STOL Models. NASA TR R-302, 1969

TABLE I.- MODEL GEOMETRY

**Wing:****Airfoil:**

Root . . . . .	NACA 0030
Tip . . . . .	NACA 0024
Span, m (ft) . . . . .	0.786 (2.58)
Area, m <sup>2</sup> (ft <sup>2</sup> ) . . . . .	0.159 (1.71)

**Chord:**

Root, m (ft) . . . . .	0.213 (0.700)
Tip, m (ft) . . . . .	0.158 (0.520)
Incidence angle (chord line), deg. . . . .	14
Leading-edge sweep, deg. . . . .	14
Dihedral angle, deg. . . . .	0

**Horizontal tail:**

Airfoil. . . . .	Inverted Clark Y
Span, m (ft) . . . . .	0.573 (1.88)
Area, m <sup>2</sup> (ft <sup>2</sup> ) . . . . .	0.0975 (1.05)
Chord:	
Root, m (ft) . . . . .	0.183 (0.60)
Tip, m (ft). . . . .	0.137 (0.45)
Incidence angle (chord line), deg. . . . .	0, 6, 10
Leading-edge sweep, deg . . . . .	20

**Vertical tail:**

Span, m (ft) . . . . .	0.378 (1.24)
Area, m <sup>2</sup> (ft <sup>2</sup> ) . . . . .	0.0966 (1.04)
Chord:	
Root, m (ft) . . . . .	0.341 (1.12)
Tip, m (ft). . . . .	0.171 (0.56)
Incidence angle (chord line), deg. . . . .	0
Leading-edge sweep, deg. . . . .	50

**V-tails:<sup>a</sup>**

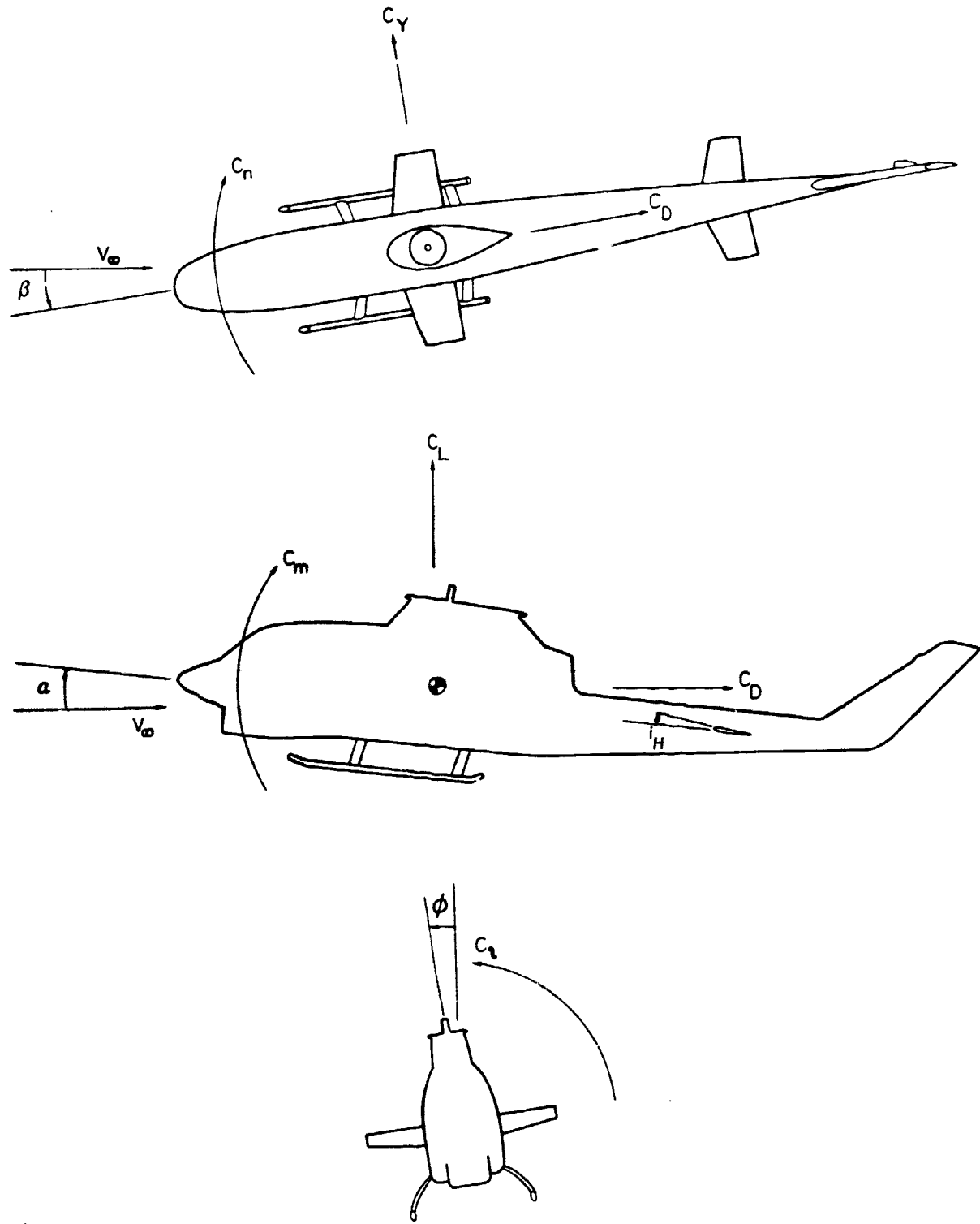
Airfoil. . . . .	NACA 4415
------------------	-----------

<sup>a</sup>See figure 4 and Symbols for details.

TABLE II.- ROTOR GEOMETRY

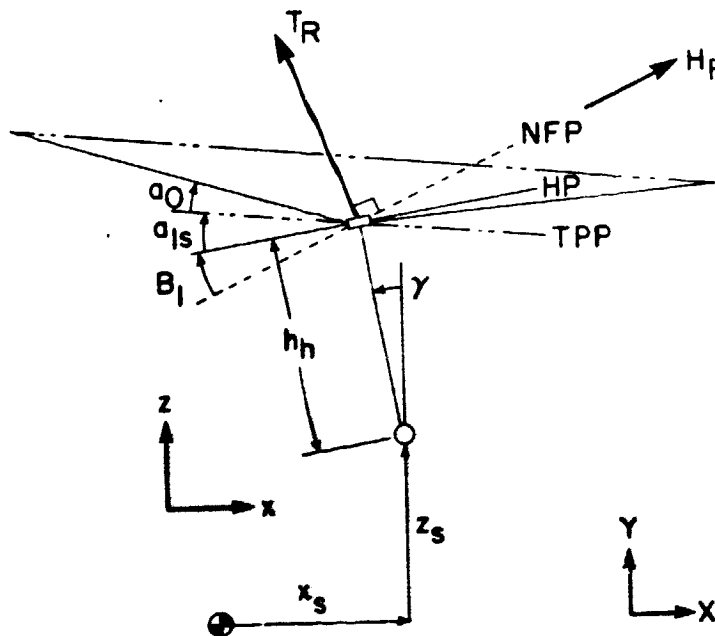
Radius, m (ft) . . . . .	1.68 (5.50)
Disk area, $m^2$ ( $ft^2$ ) . . . . .	8.83 (95.0)
Chord, cm (in.) . . . . .	17.14 (6.75)
Twist, deg. . . . .	$10^\circ$
Precone, deg. . . . .	$2.5^\circ$
Solidity. . . . .	0.065
Airfoil section . . . . .	(a)
Cutout, percent R . . . . .	16.7%
$b_h$ , cm (in.) . . . . .	0.00 (0.00)
$x_s$ , cm (in.) . . . . .	0.00 (0.00)
$z_s$ , cm (in.) . . . . .	51.80 (20.39)
$\gamma$ , deg. . . . .	0
$a_0$ , deg . . . . .	2.5

(a) Coordinates are given in reference 3.

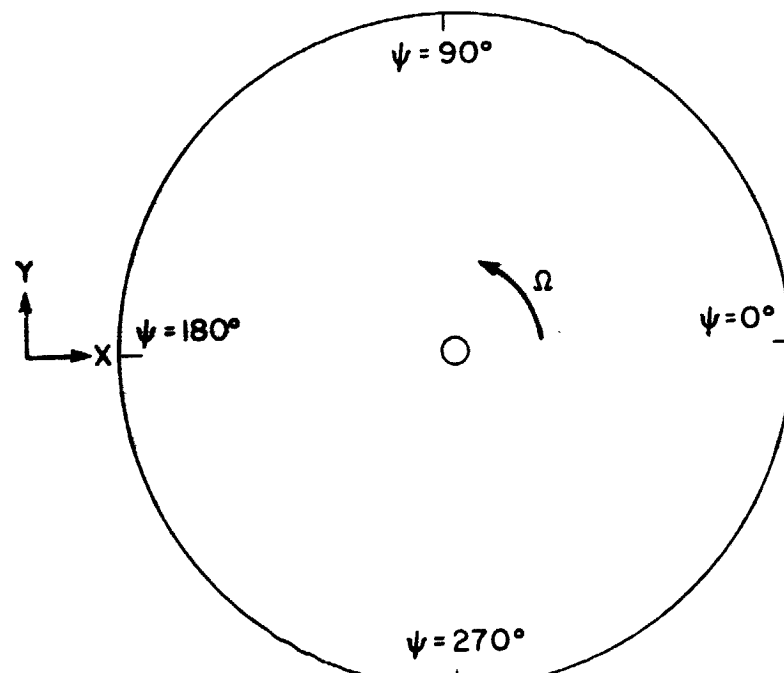


(a) Fuselage

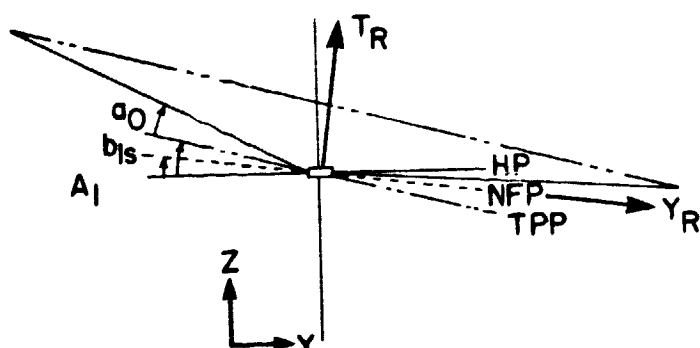
Figure 1. - Axes and sign conventions. Positive directions are indicated by arrows.



View from left



View from top



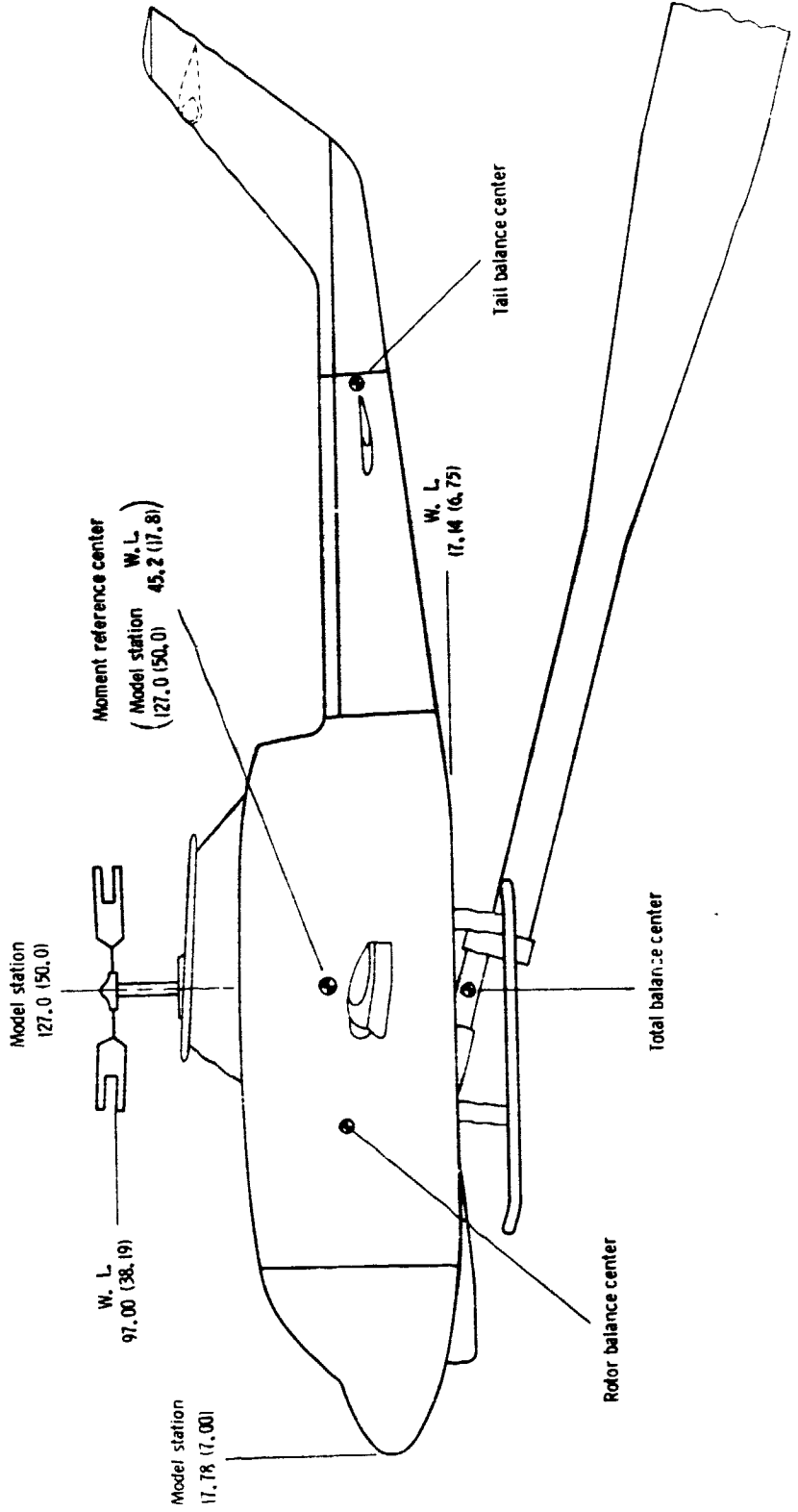
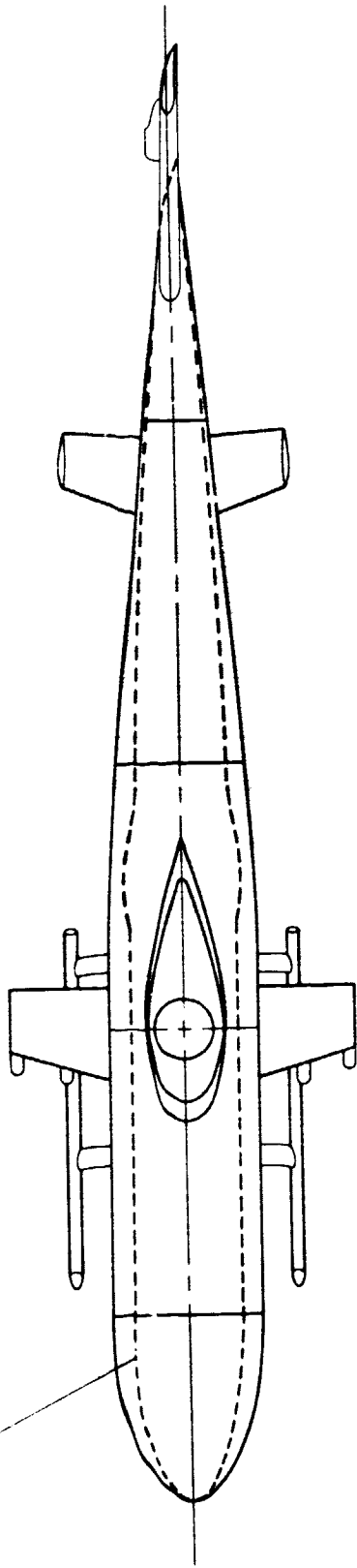
View from rear

(b) Rotor system

Figure 1.- Concluded.

OPTIONAL IMAGE IS  
OF POOR QUALITY

1/4 scale attack helicopter (ref. 1)



ORIGINAL IMAGE IS  
OF POOR QUALITY

Figure 2 - Rockwell R-44 Helicopter dimensions (in.)



Figure 3.- Model in test section.

ORIGINAL PAGE IS  
OF POOR QUALITY

ORIGINAL PAGE IS  
OF POOR QUALITY

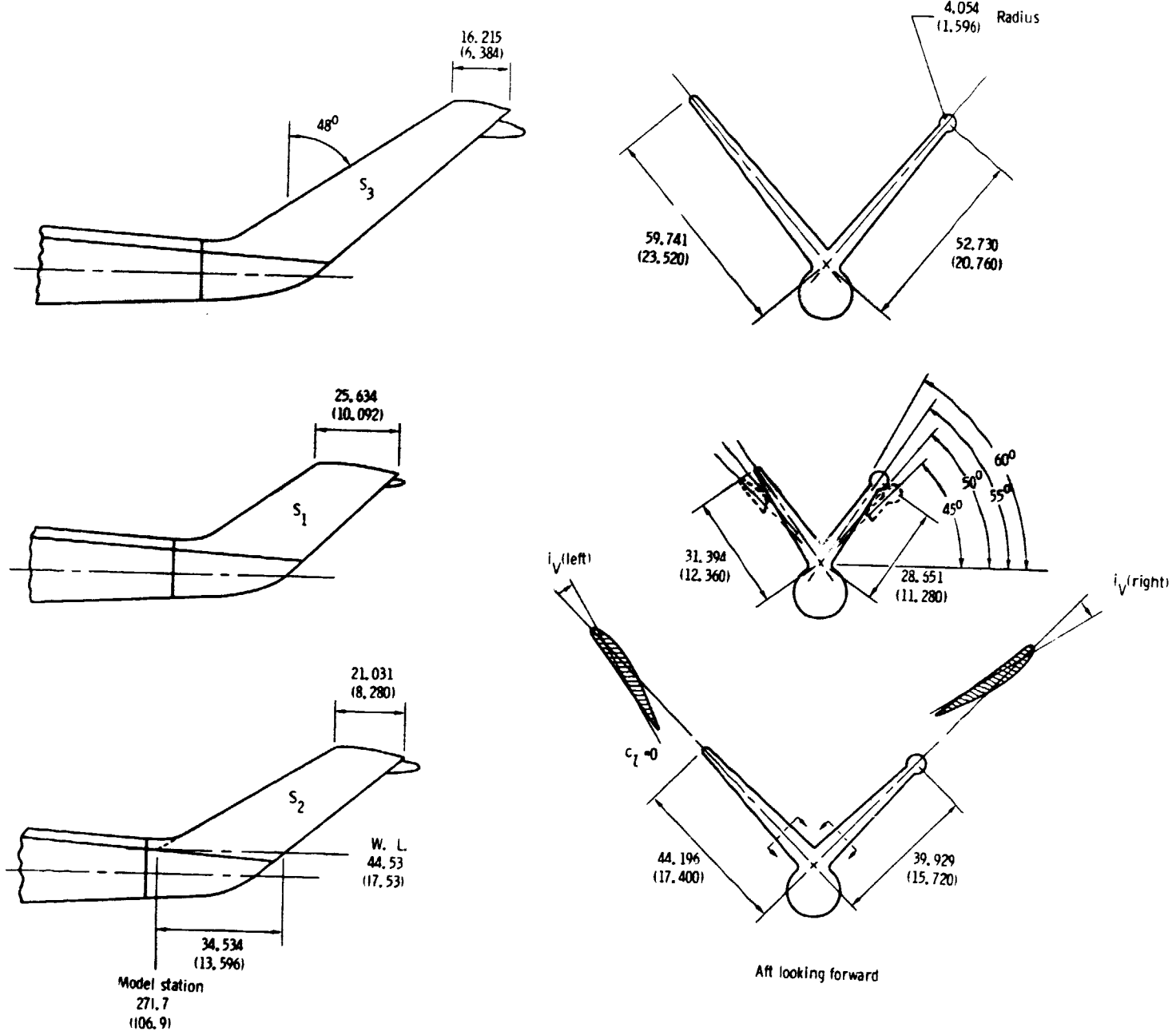


Figure 4. - V-tail geometry.

Dimensions: cm(in.)

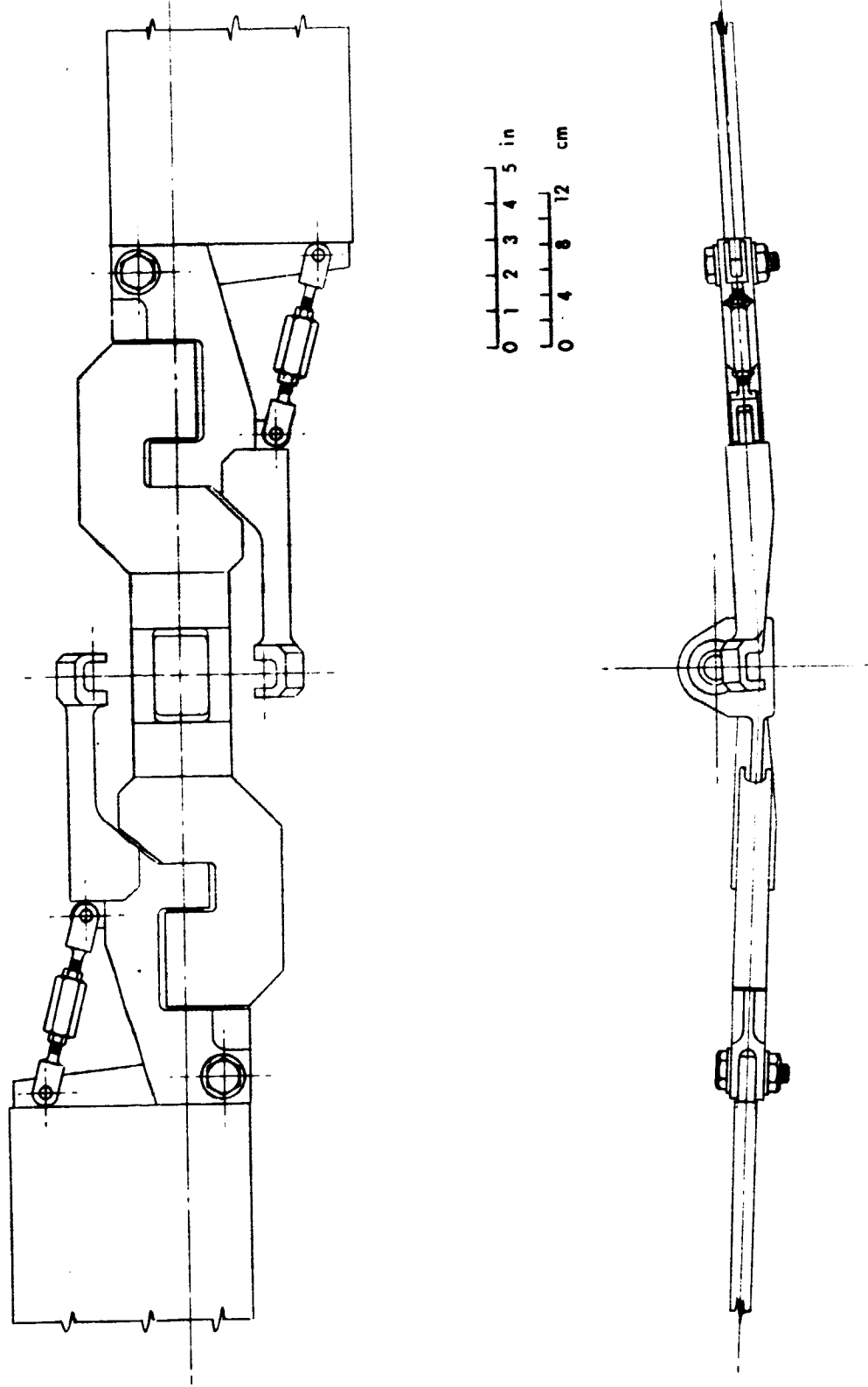


Figure 5.- Sketch of hub assembly.

ORIGINAL PAGE IS  
OF POOR QUALITY

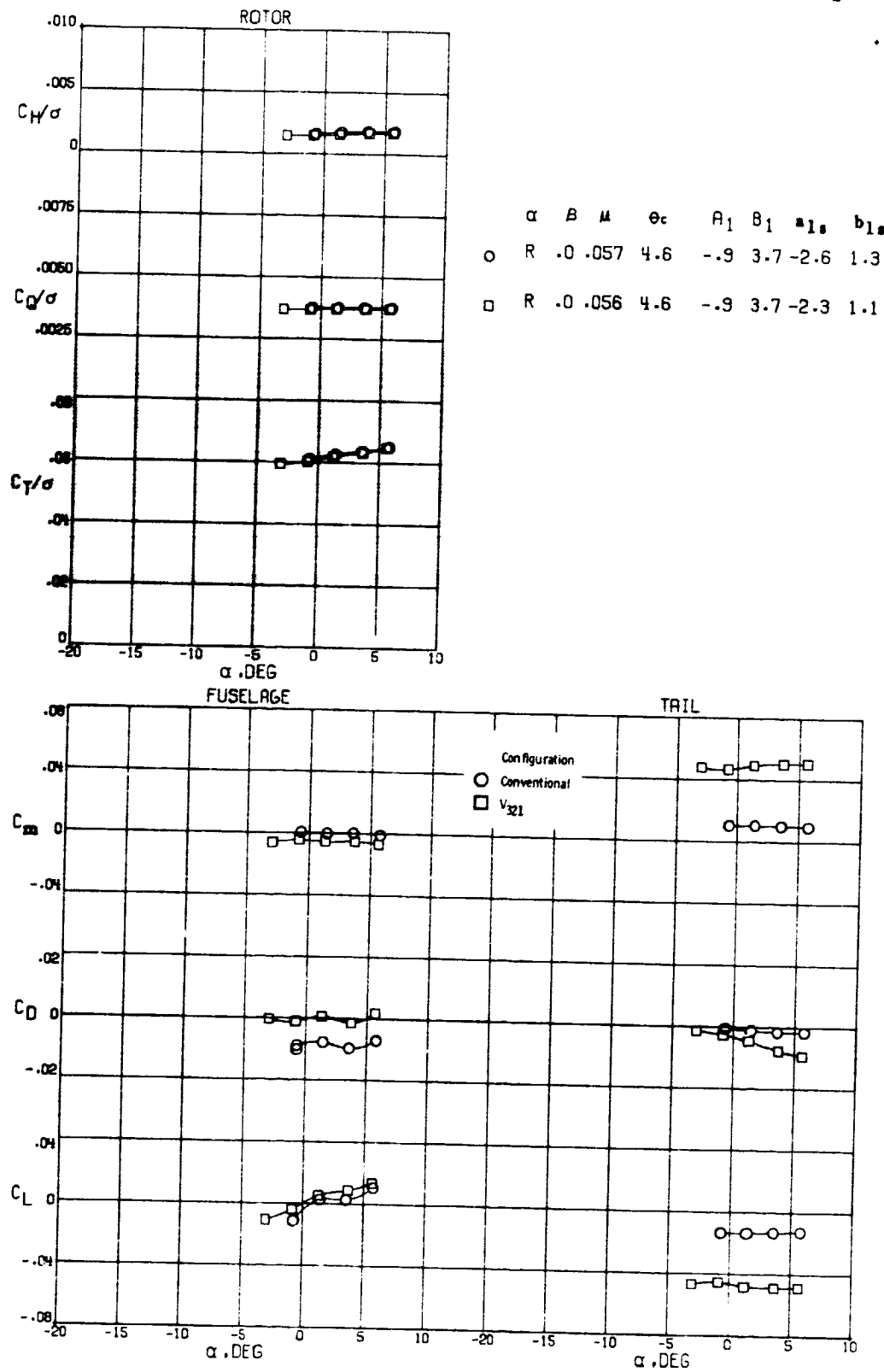


Figure 6.- Longitudinal aerodynamic characteristics of the conventional tail and the baseline V-tail in 1-g flight at three advance ratios.

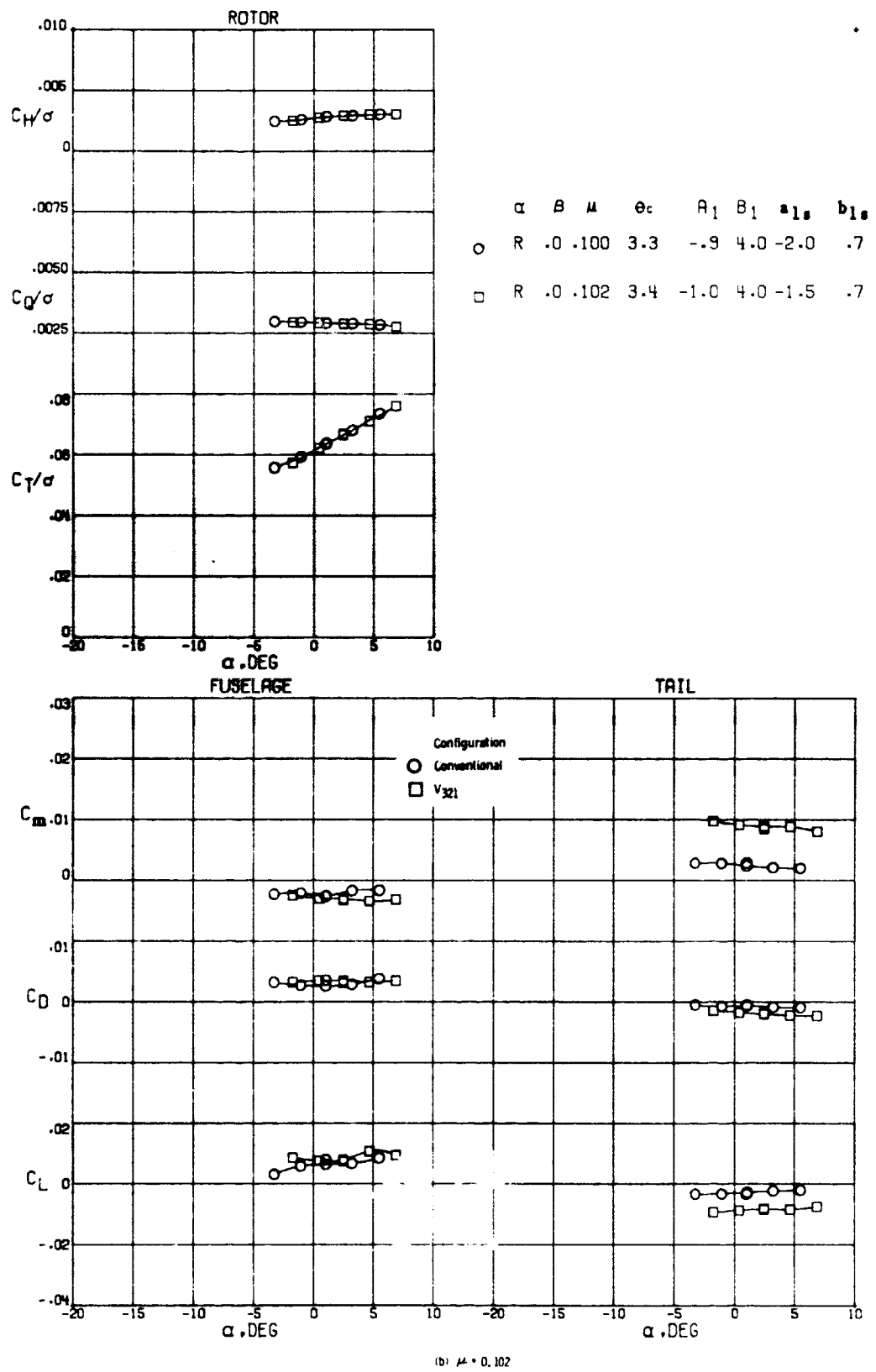
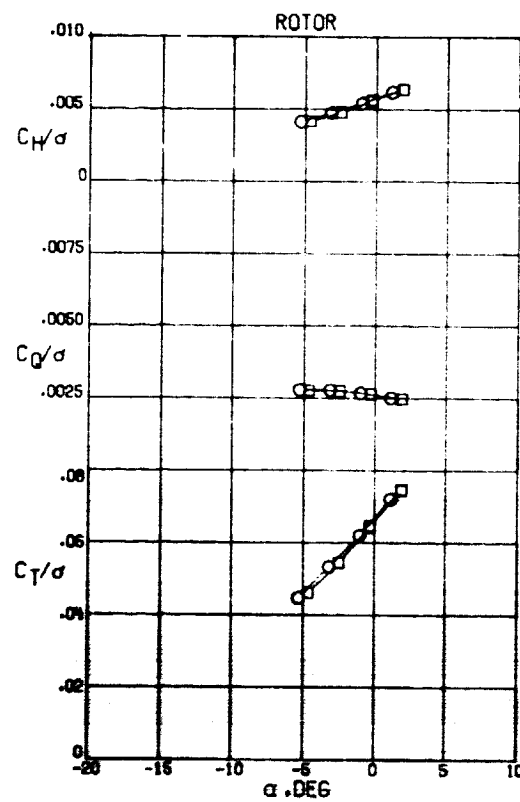


Figure 6 - Continued.

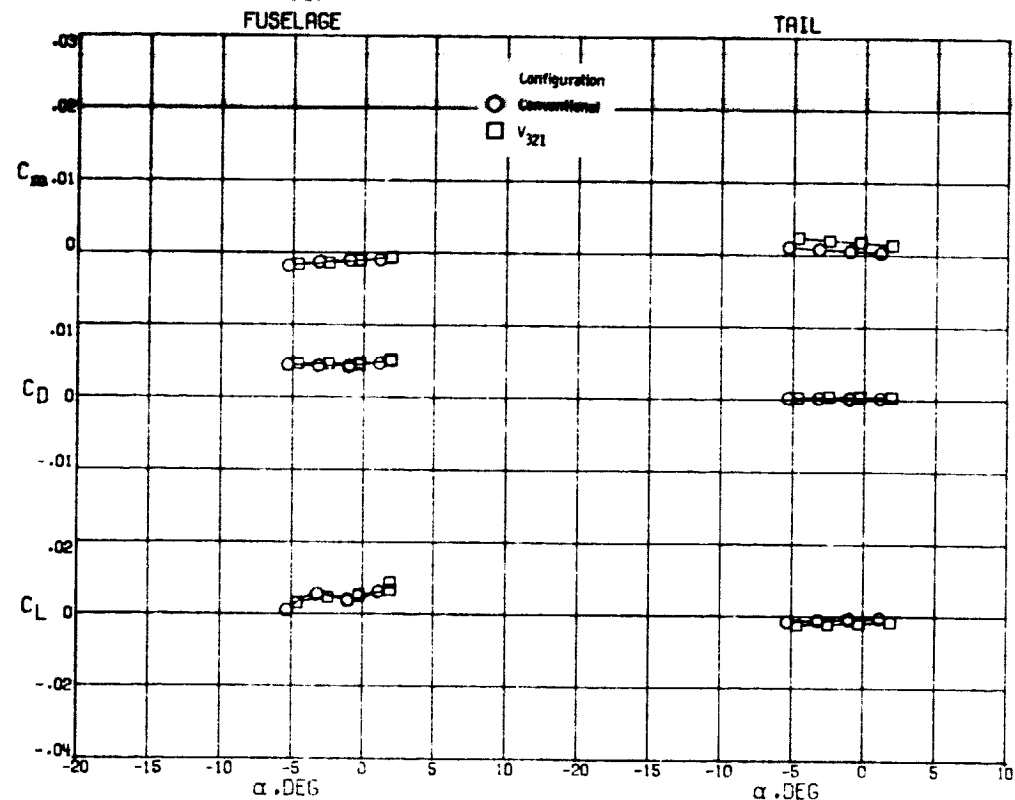
ORIGINAL PAGE IS  
OF POOR QUALITY



$\alpha \quad B \quad \mu \quad \theta_c \quad A_1 \quad B_1 \quad a_{1s} \quad b_{1s}$

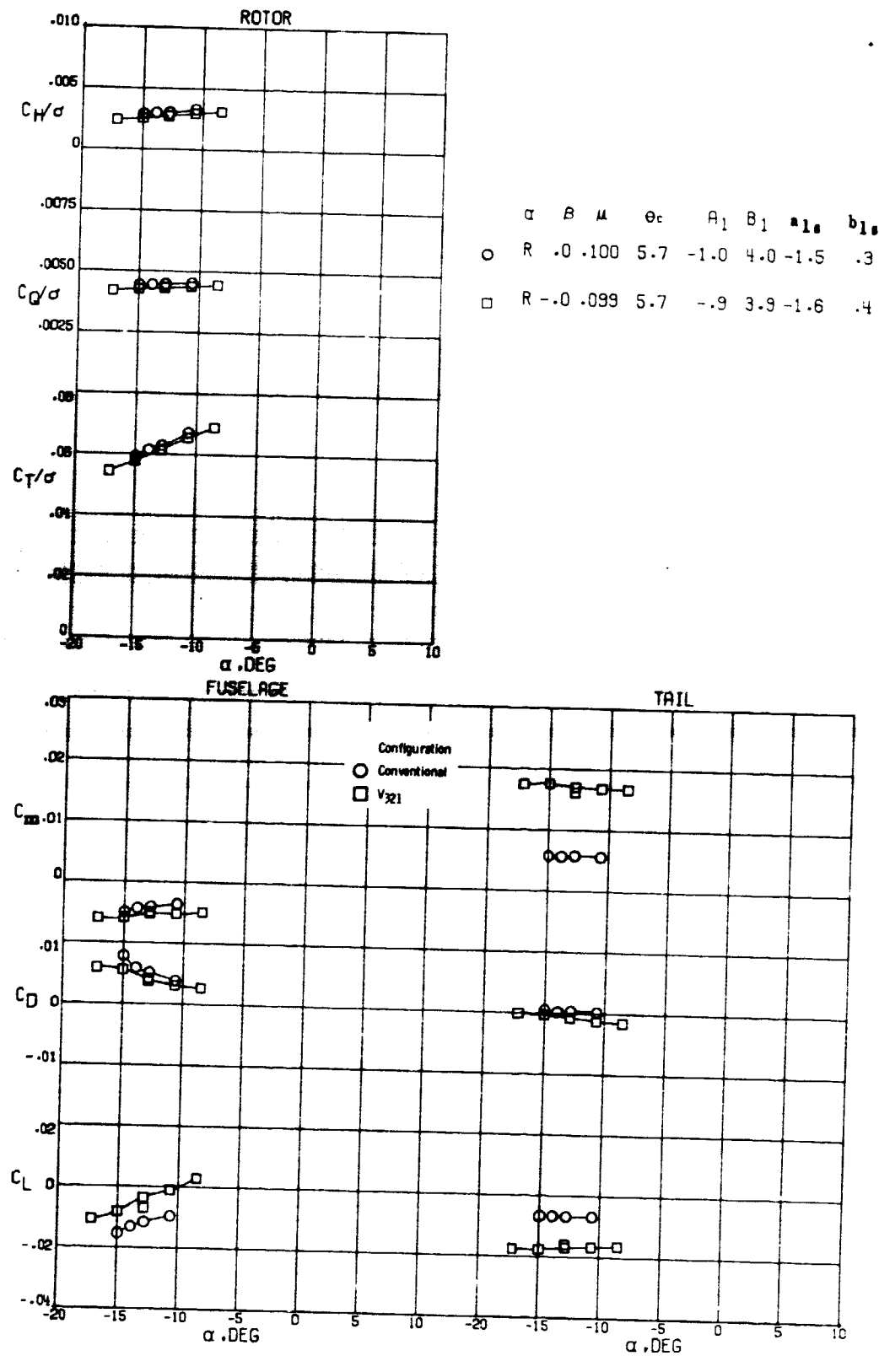
○  $R = 0.190$  3.2 -1.0 4.6 -1.4 .3

□  $R = 0.193$  3.2 -1.0 4.6 -.9 .2



(C)  $\mu = 0.192$

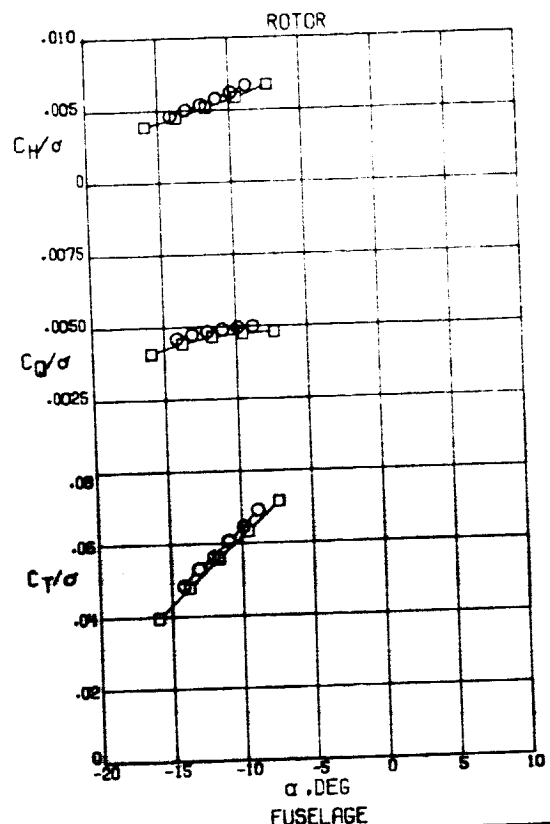
Figure 6 - Concluded.



(a)  $\mu = 0.102$

Figure 7. Longitudinal aerodynamic characteristics of the conventional tail and the baseline V-tail in climb at two advance ratios.

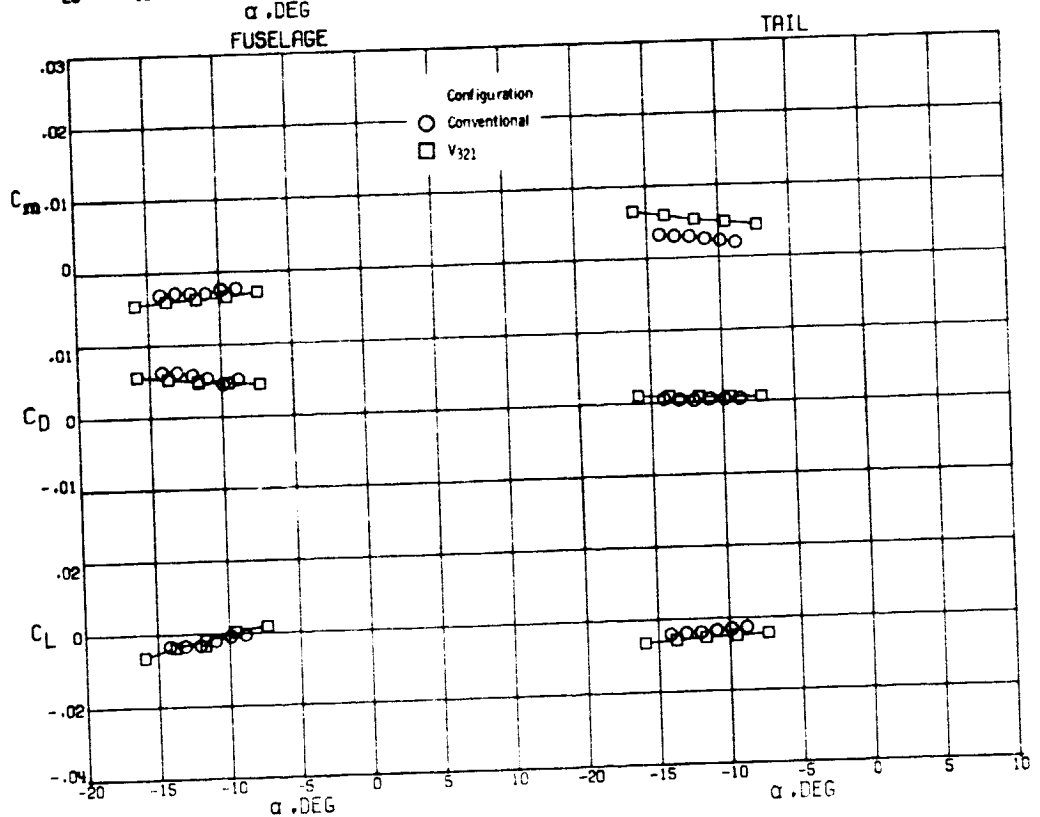
ORIGINAL PAGE IS  
OF POOR QUALITY



$\alpha \quad \beta \quad \mu \quad \theta_c \quad A_1 \quad B_1 \quad a_{1s} \quad b_{1s}$

○  $R = .1$  .189 6.7 -.9 5.4 -1.2 .2

□  $R = .0$  .186 6.7 -1.0 5.4 -1.3 .3



(b)  $\mu = 0.192$

Figure 7. - Concluded.

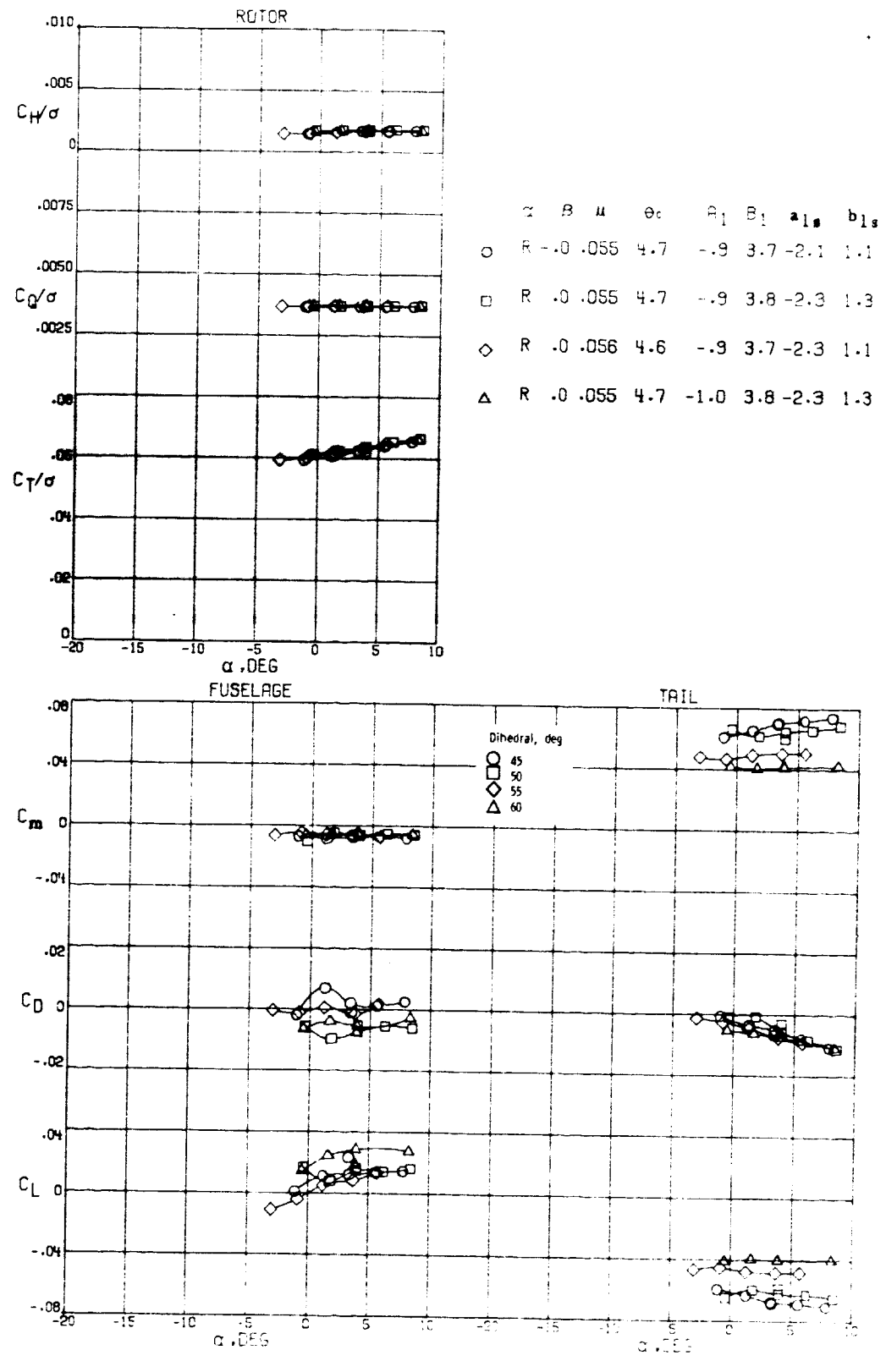
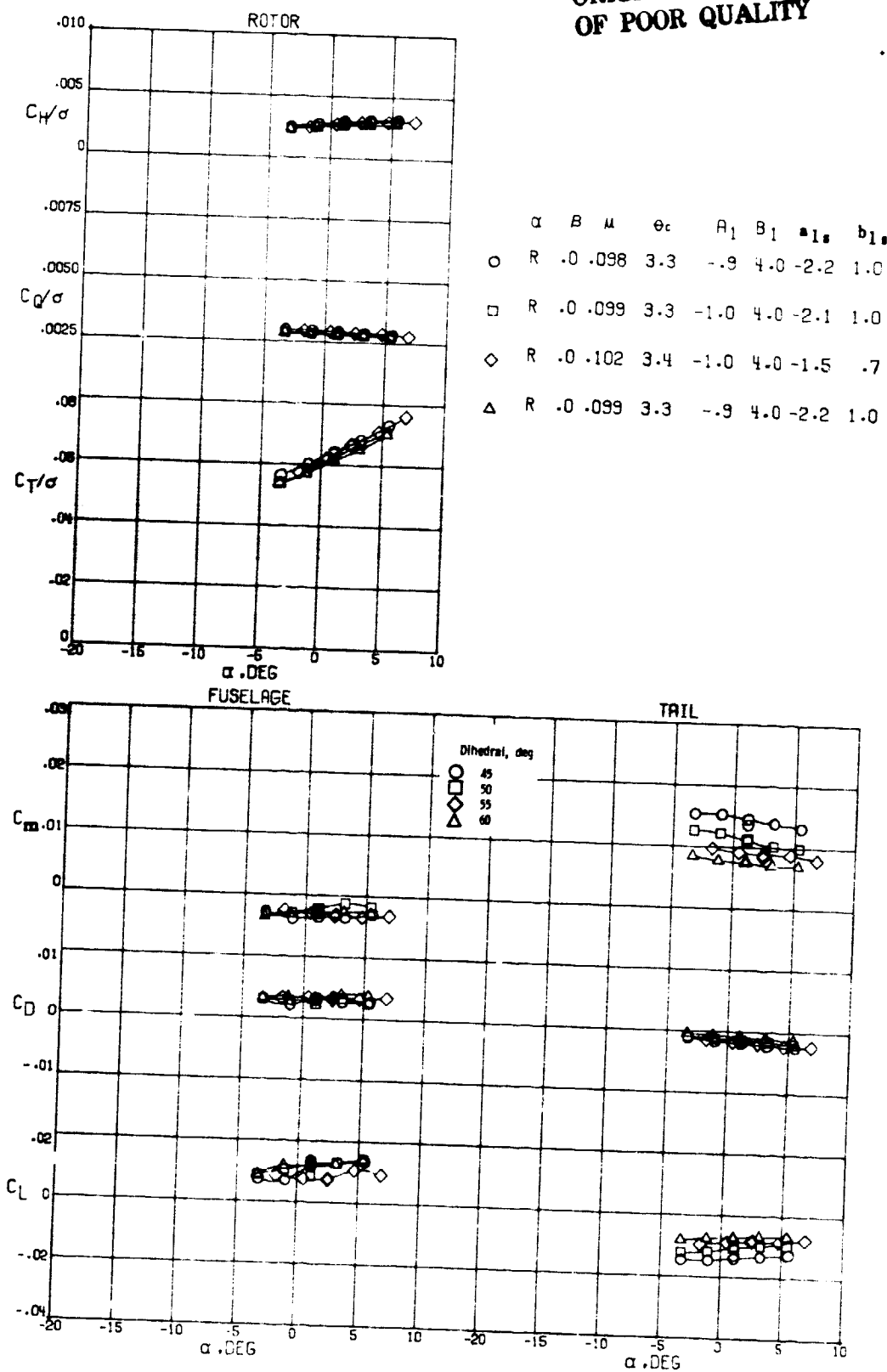


Figure 8.- Effect of V-tail dihedral on the longitudinal aerodynamic characteristics of the model at three advance ratios.

ORIGINAL PAGE IS  
OF POOR QUALITY



(b)  $\mu = 0.102$

Figure 3. - Continued.

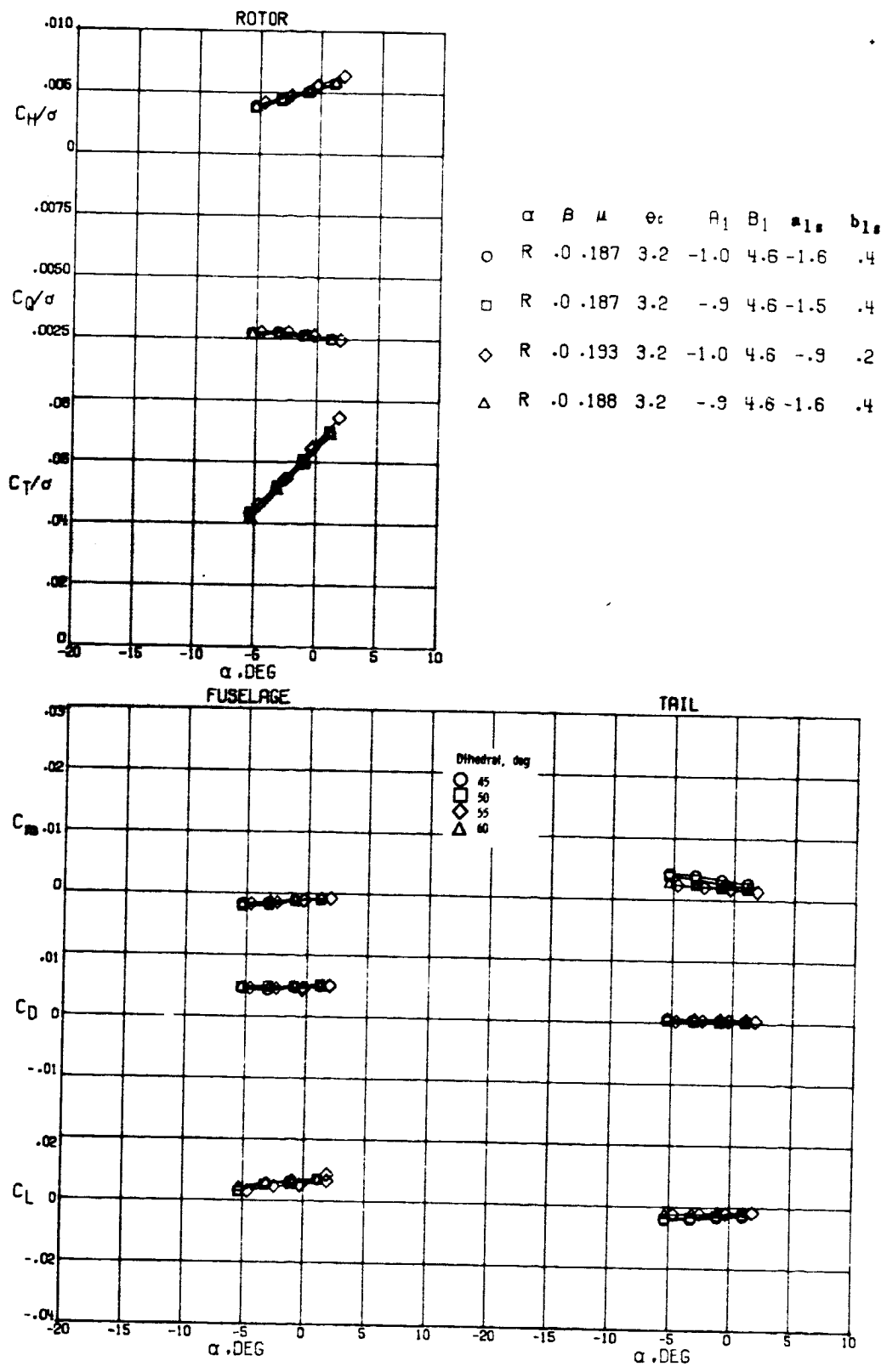


Figure 8.- Concluded.

ORIGINAL PAGE IS  
OF POOR QUALITY

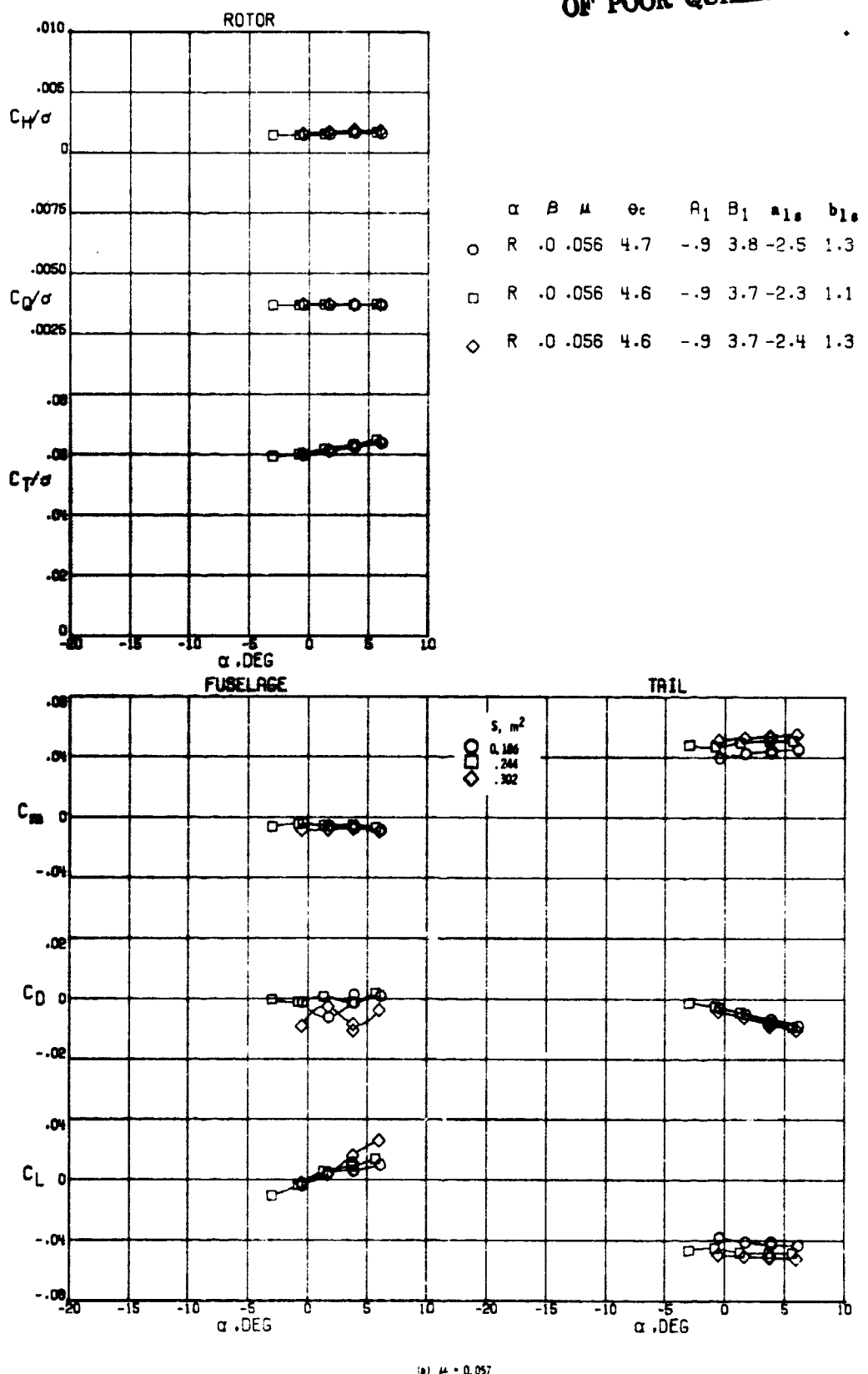


Figure 9.- Effect of V-tail planform area on the longitudinal aerodynamic characteristics of the model at three advance ratios.

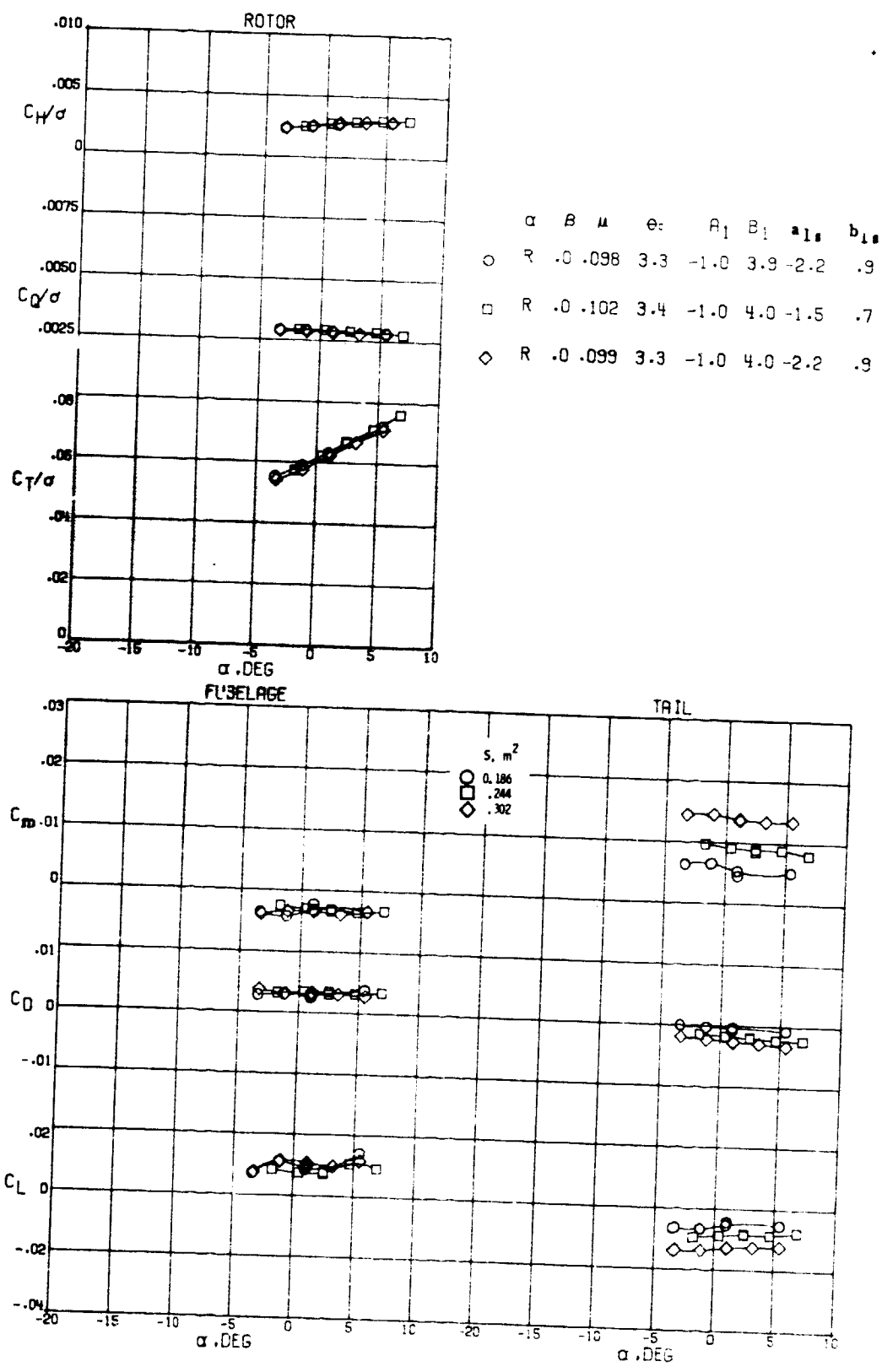


Figure 9. - Continued.

ORIGINAL PAGE IS  
OF POOR QUALITY

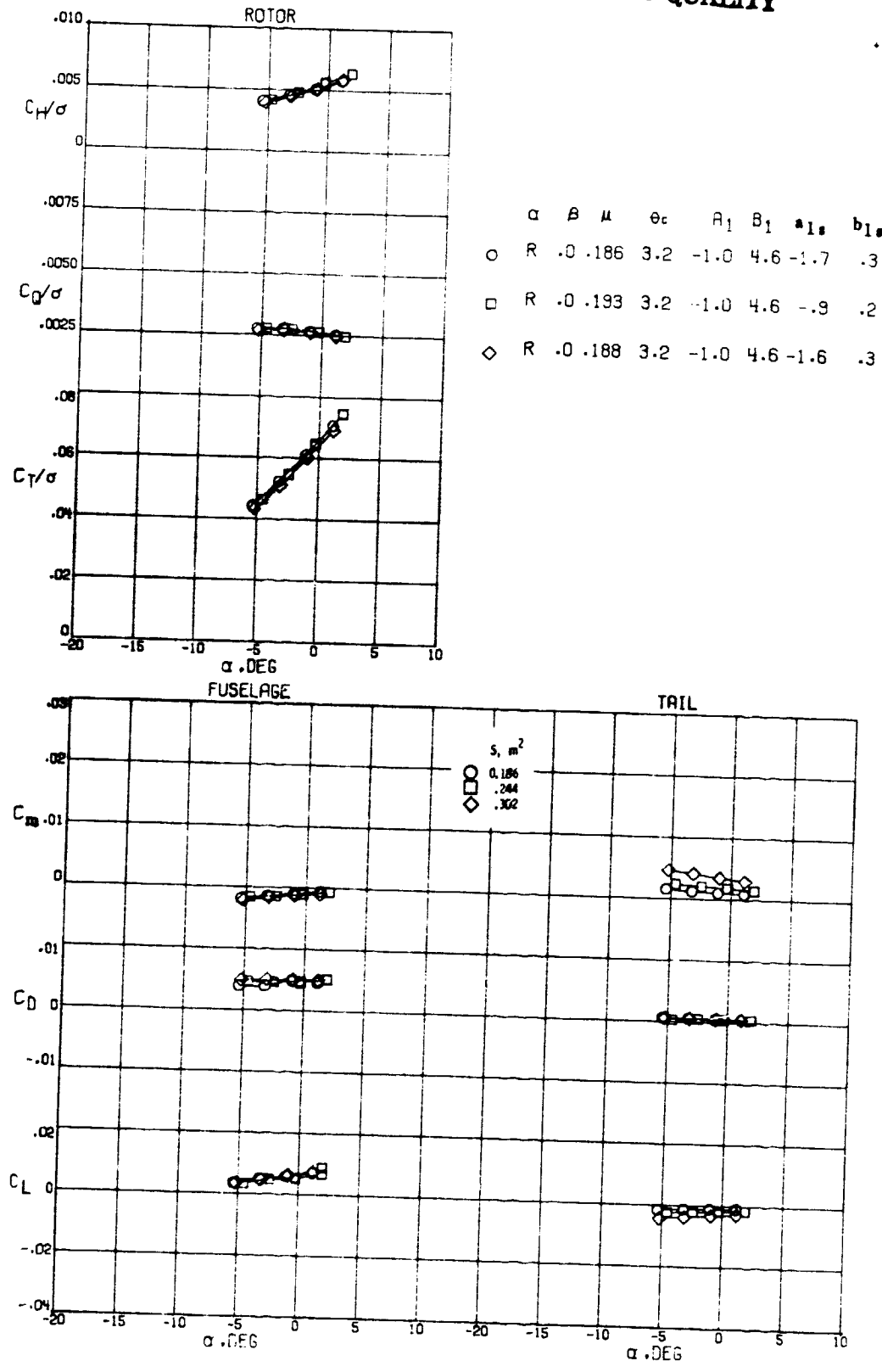


Figure 9. - Concluded.

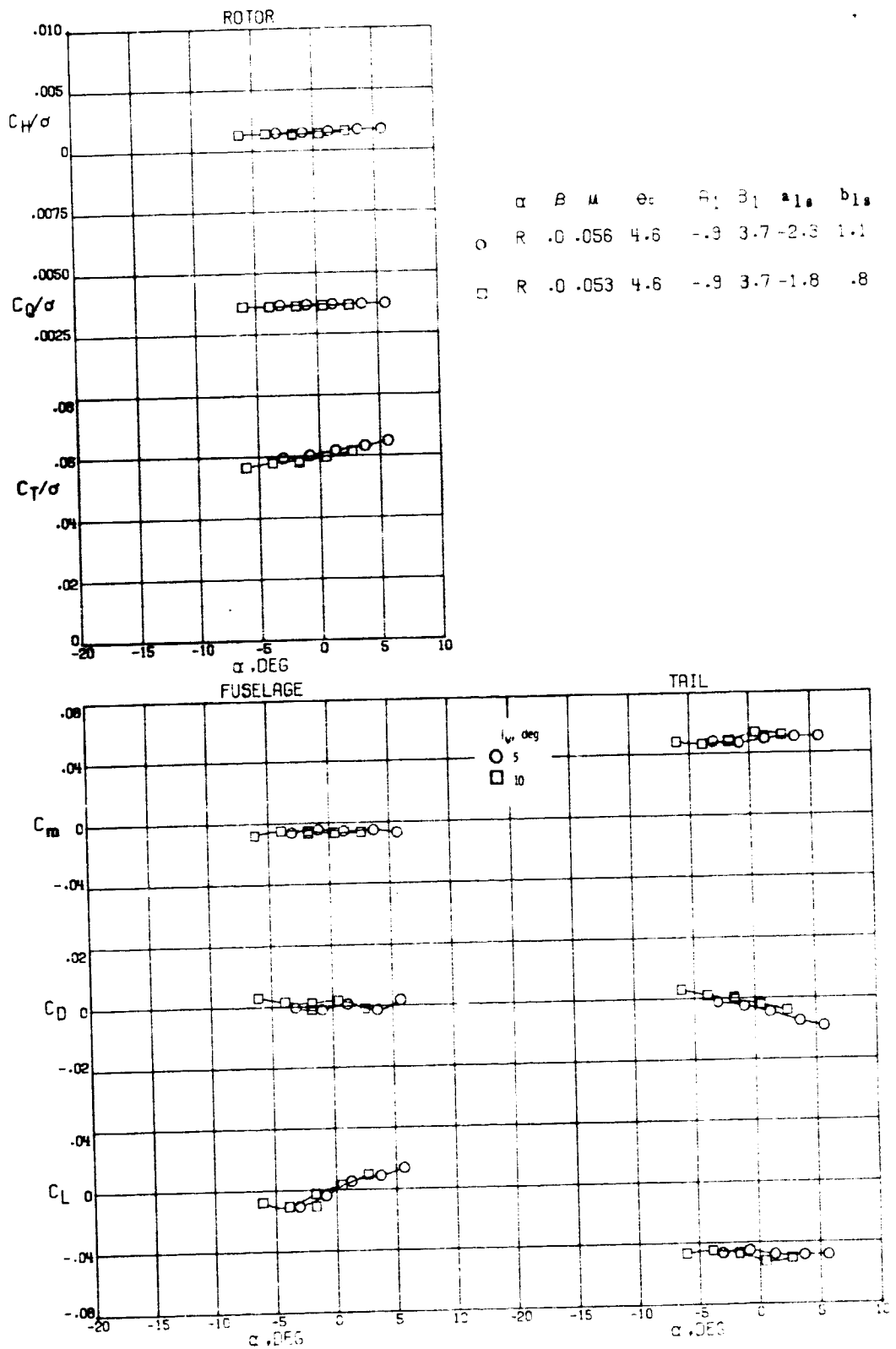
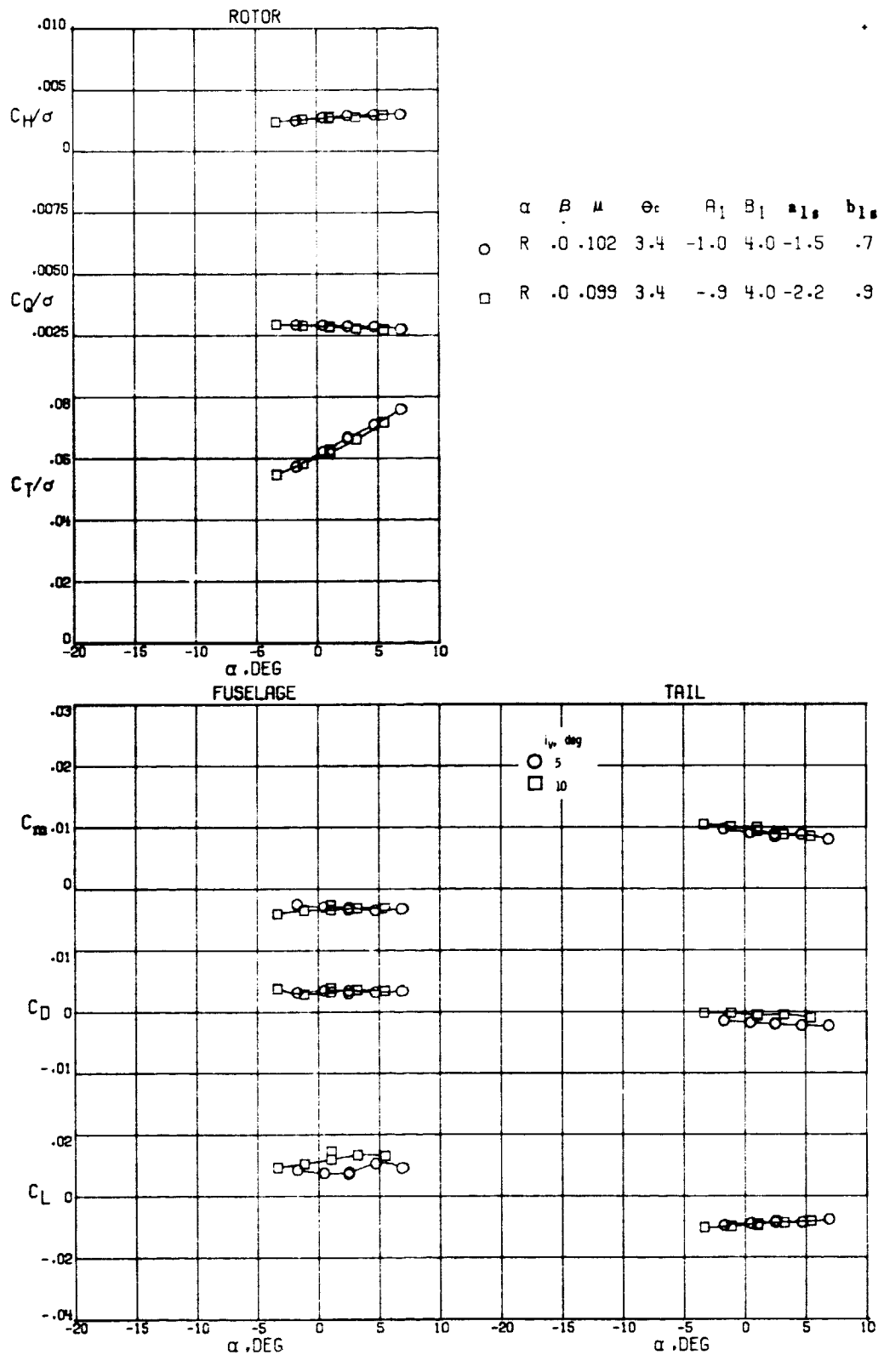


Figure 10c- Effect of V-tail incidence on the longitudinal aerodynamic characteristics of the model at three advance ratios.

ORIGINAL PAGE IS  
OF POOR QUALITY



(b)  $\mu = 0.102$

Figure 10.- Continued.

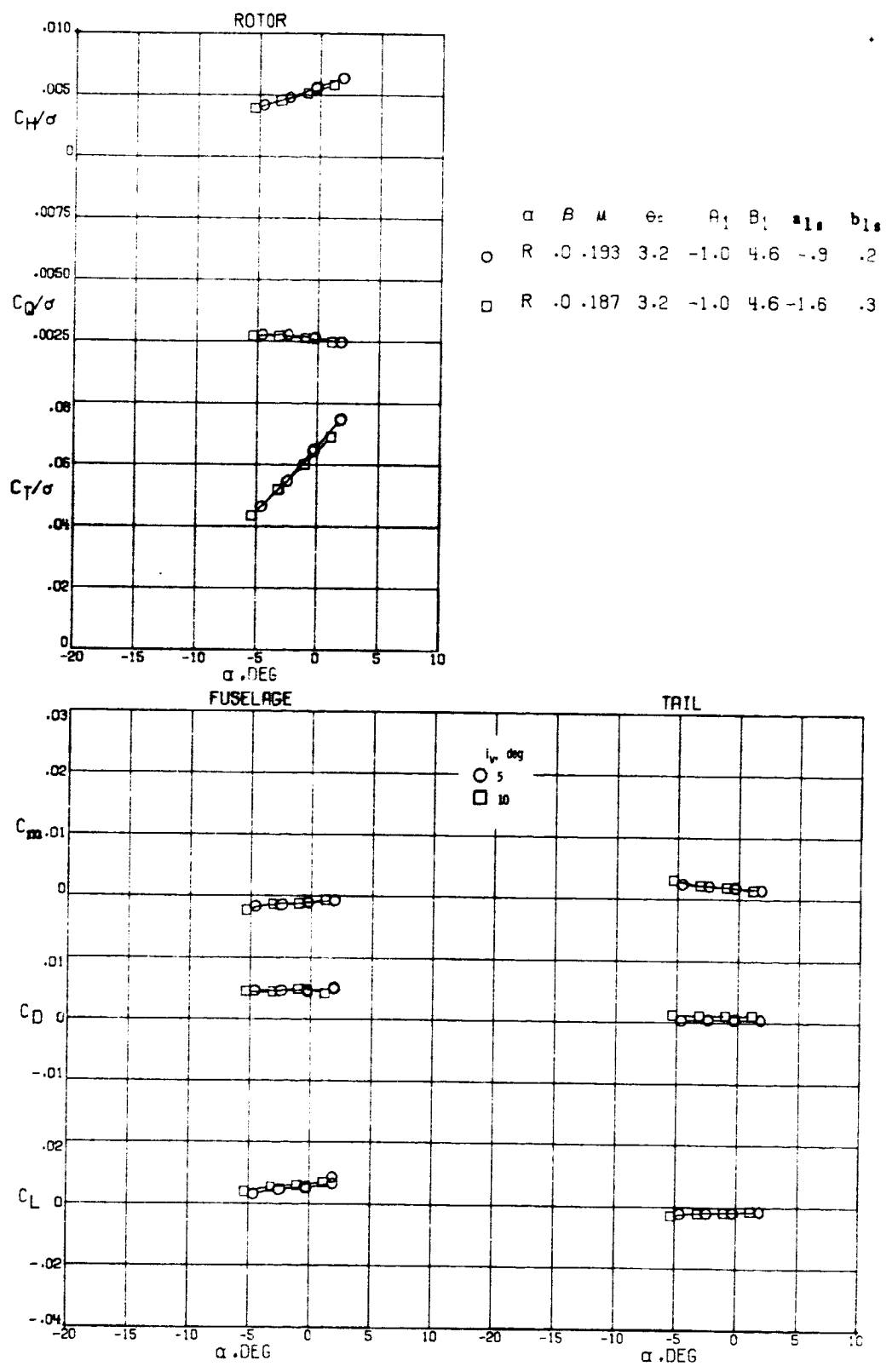


Figure 10.- Concluded.

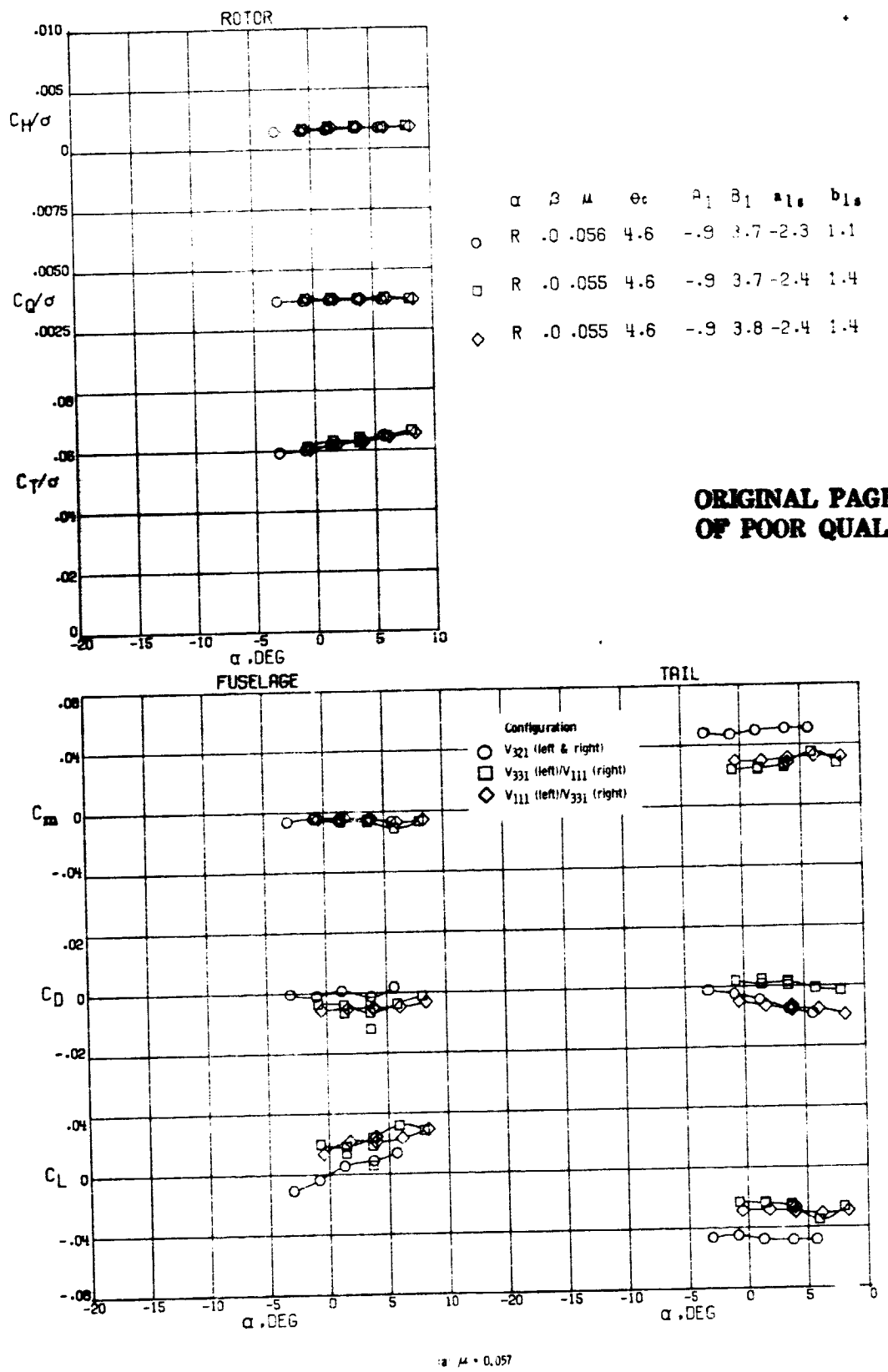


Figure 11. - Comparison of the longitudinal aerodynamic characteristics of the baseline V-tail with the right or left tail surfaces removed.

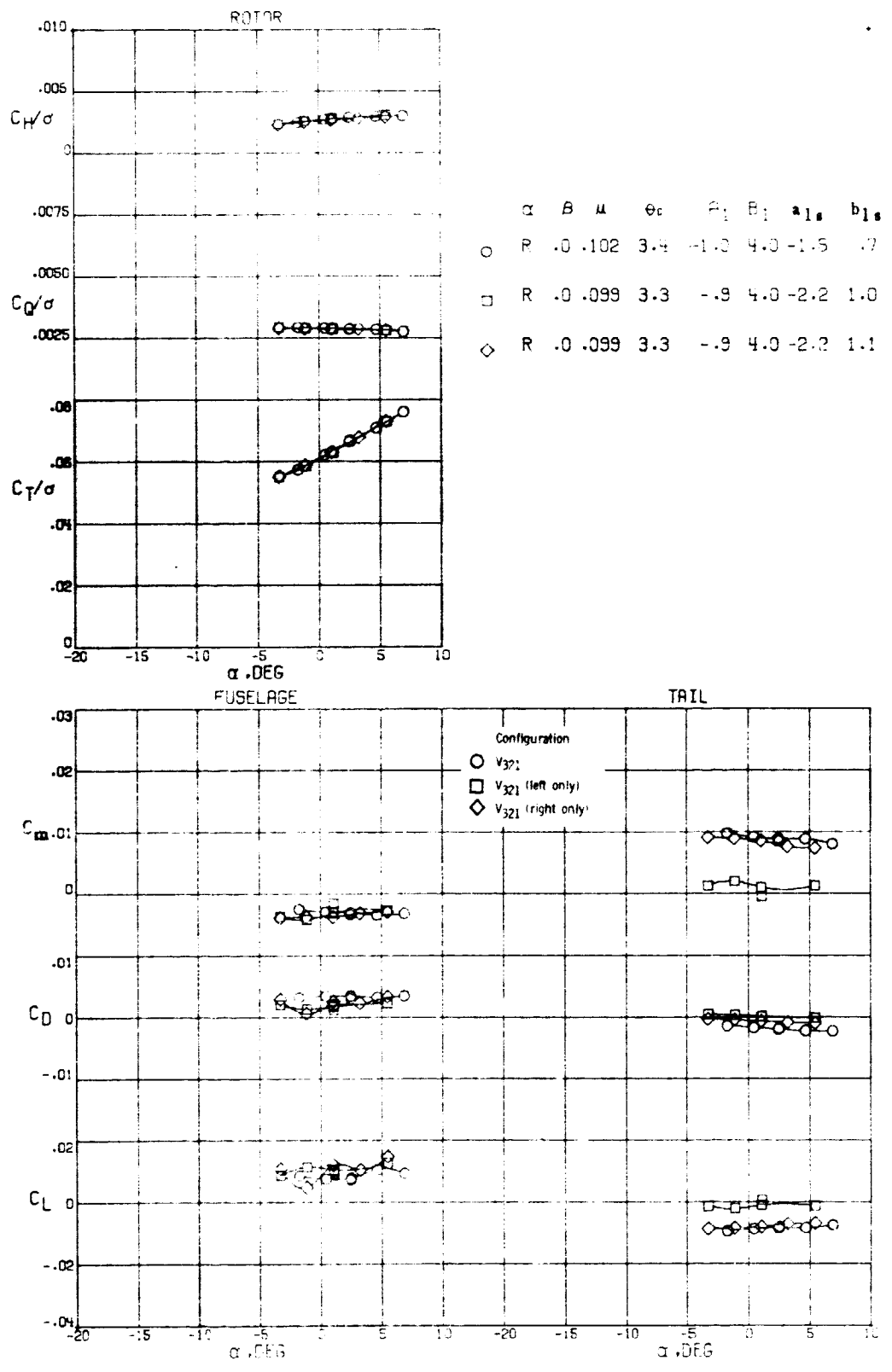
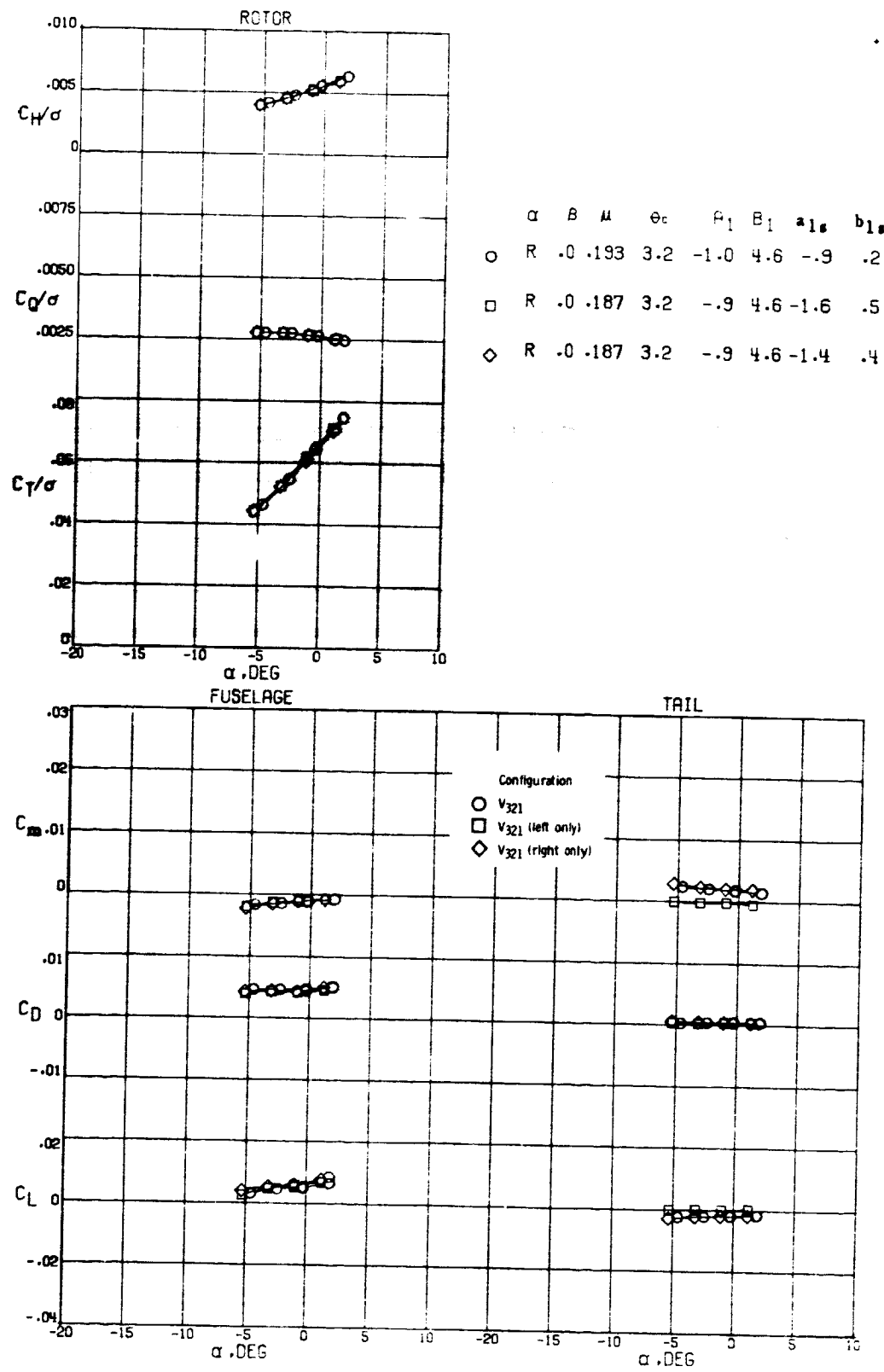


Figure 11. - Continued.



(c)  $\mu = 0.192$

Figure 11. - Concluded.

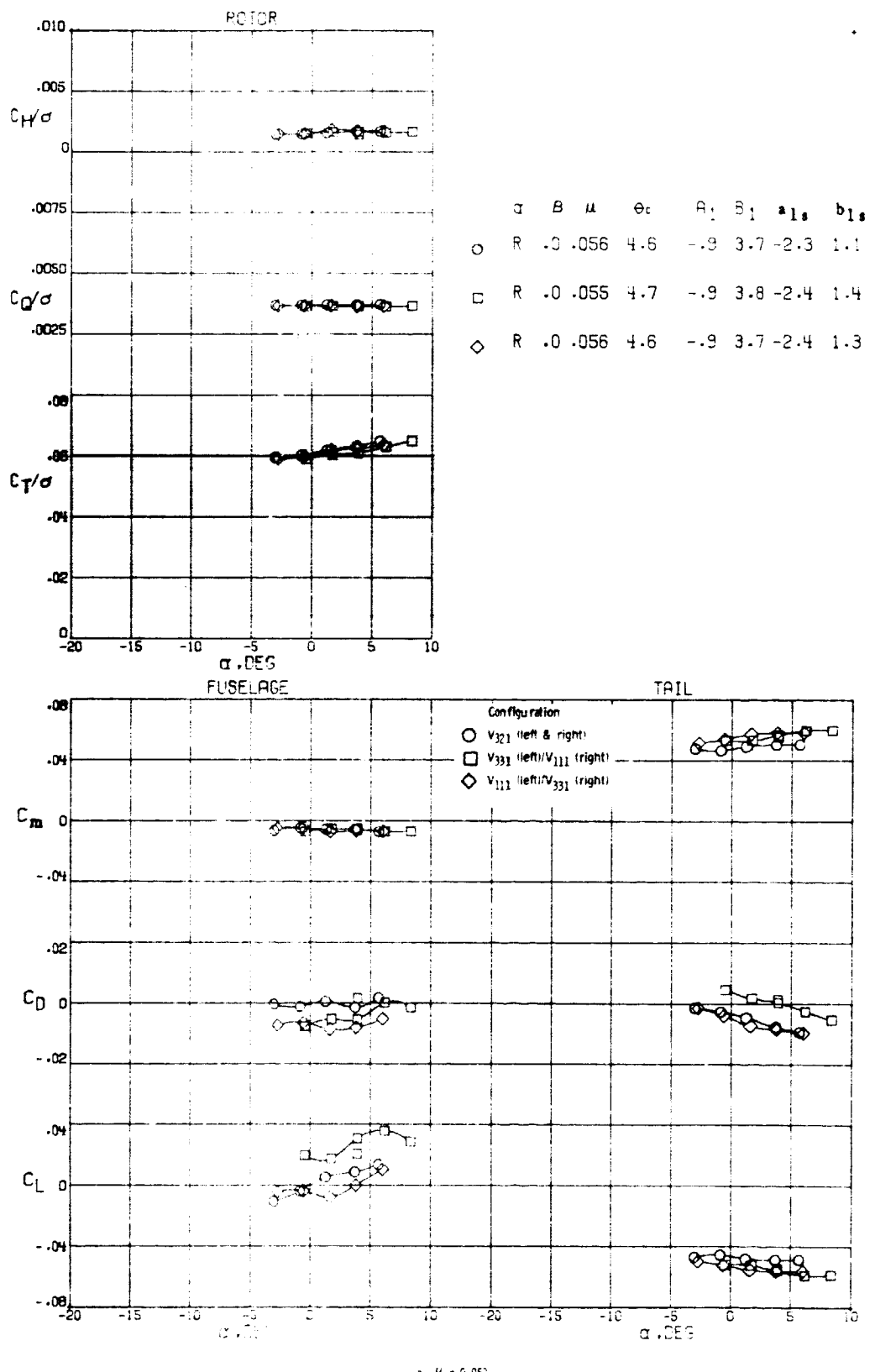


Figure 12 - Comparison of the aerodynamic characteristics of the baseline V-tail with two new synthetic control configurations.

ORIGINAL PAGE IS  
OF POOR QUALITY

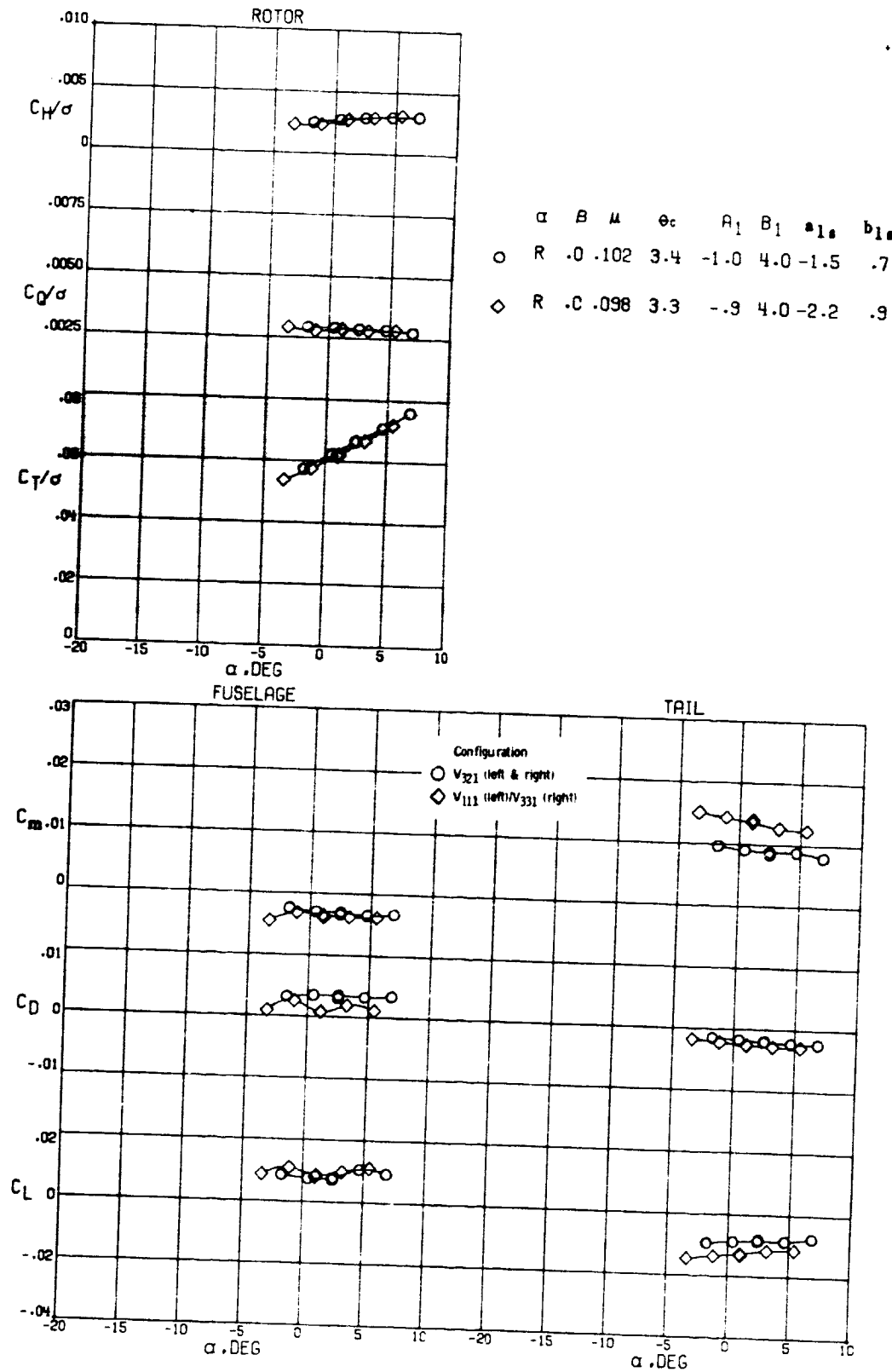


Figure 12.- Continued.

(b)  $\mu = 0, 102$

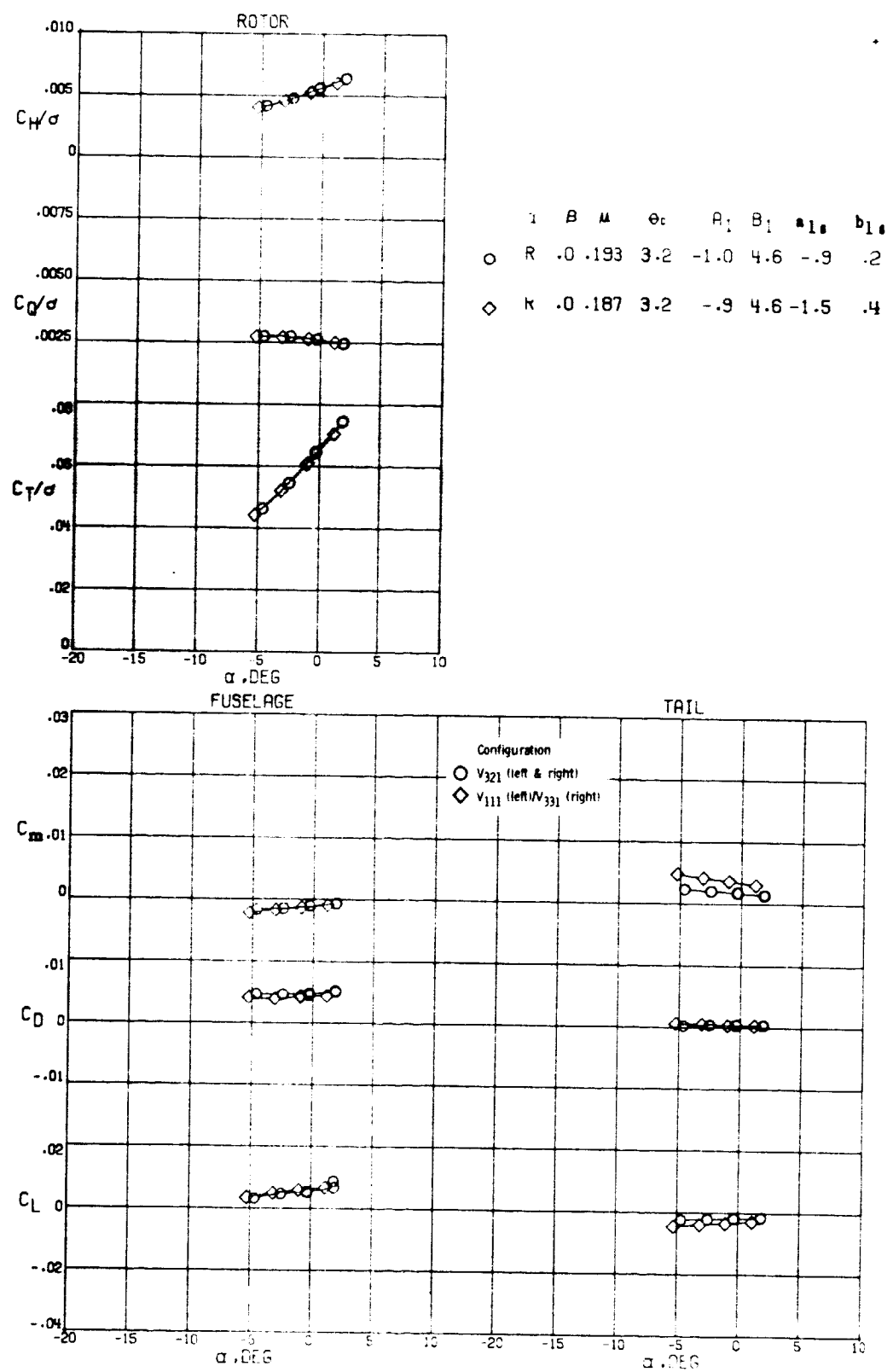


Figure 12 - Concluded.

(c)  $\mu = 0.192$

ORIGINAL PAGE IS  
OF POOR QUALITY

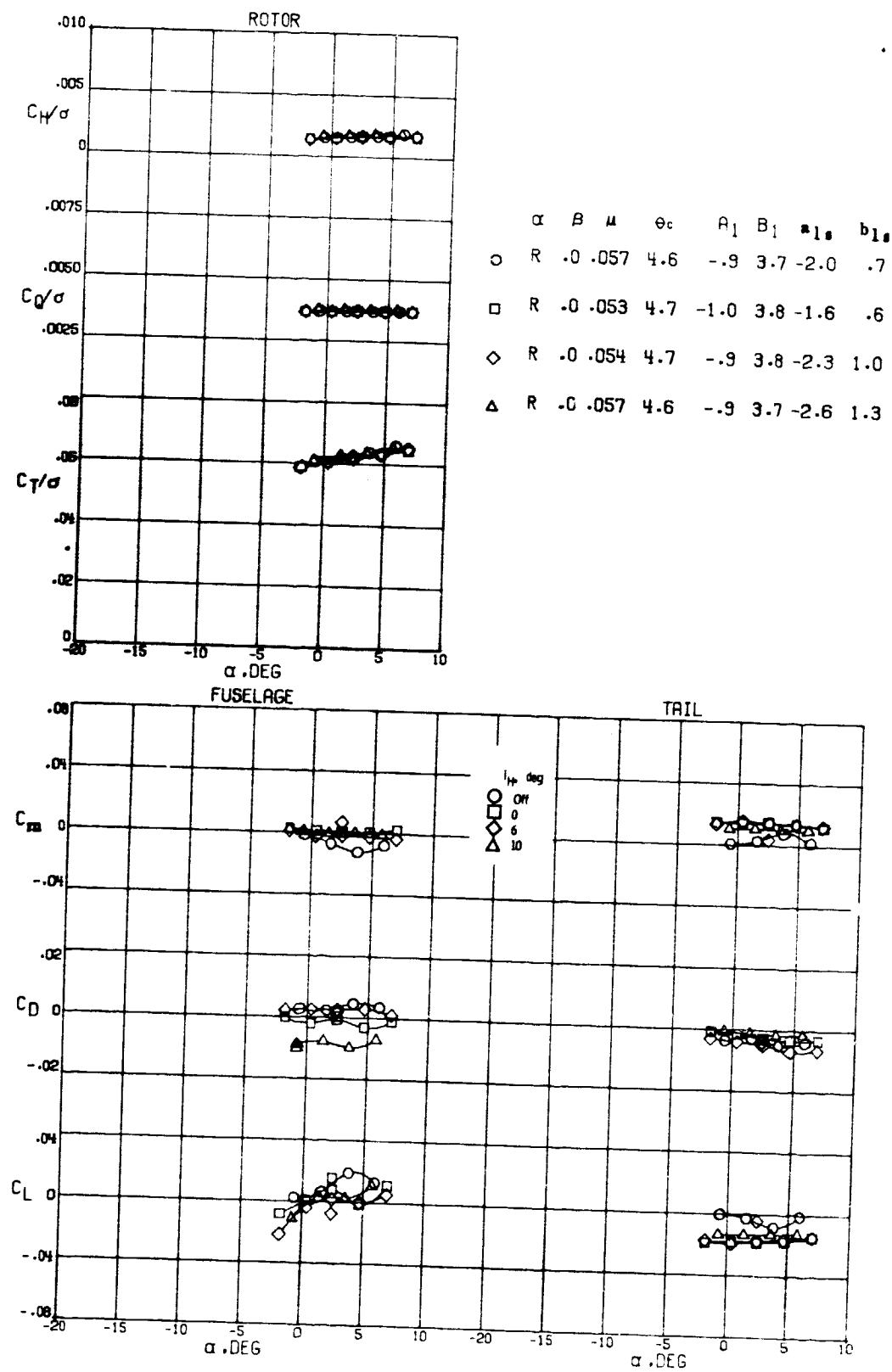


Figure 13.—Effect of horizontal tail (conventional) incidence on the longitudinal aerodynamic characteristics of the model.

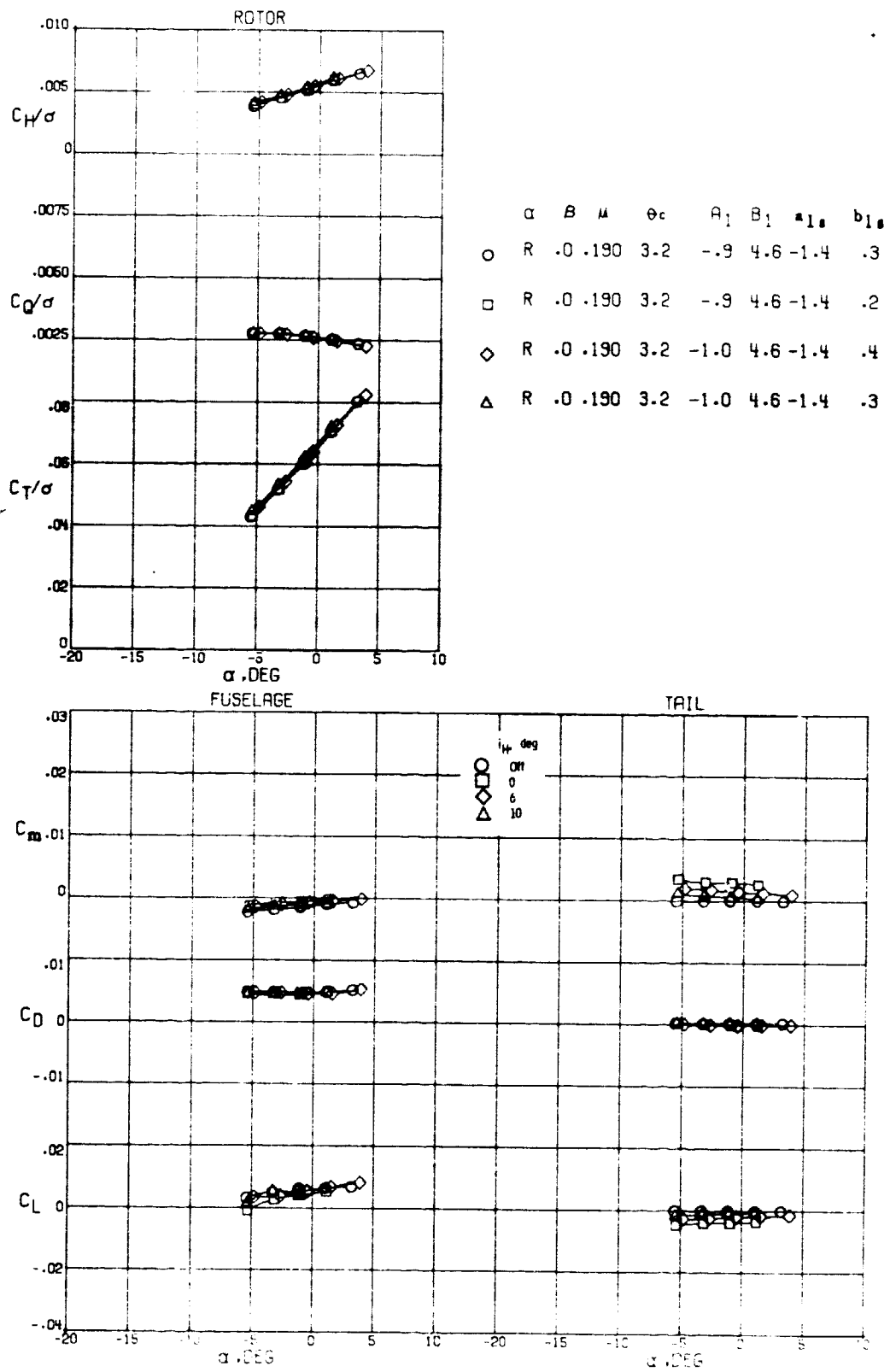
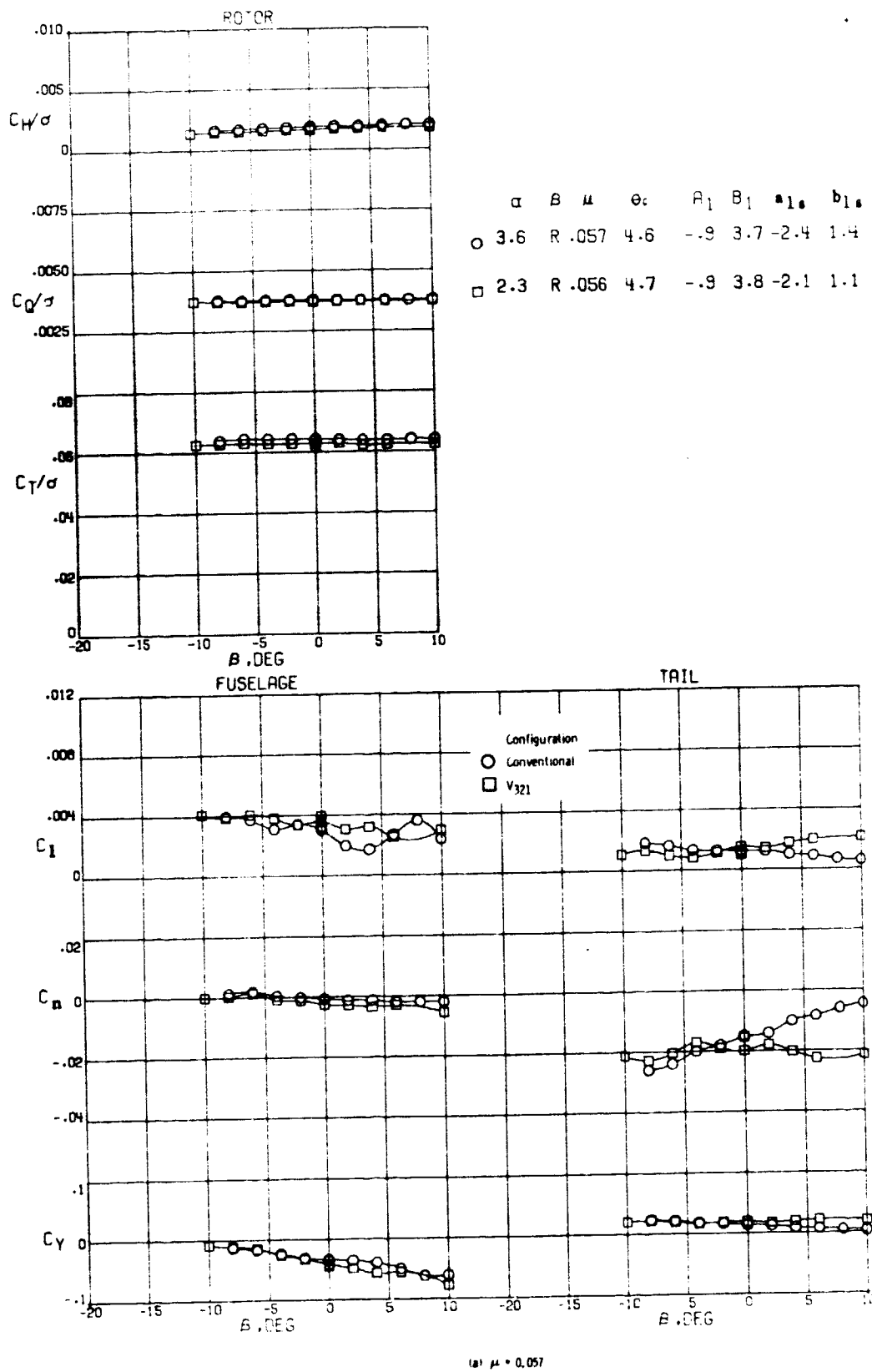


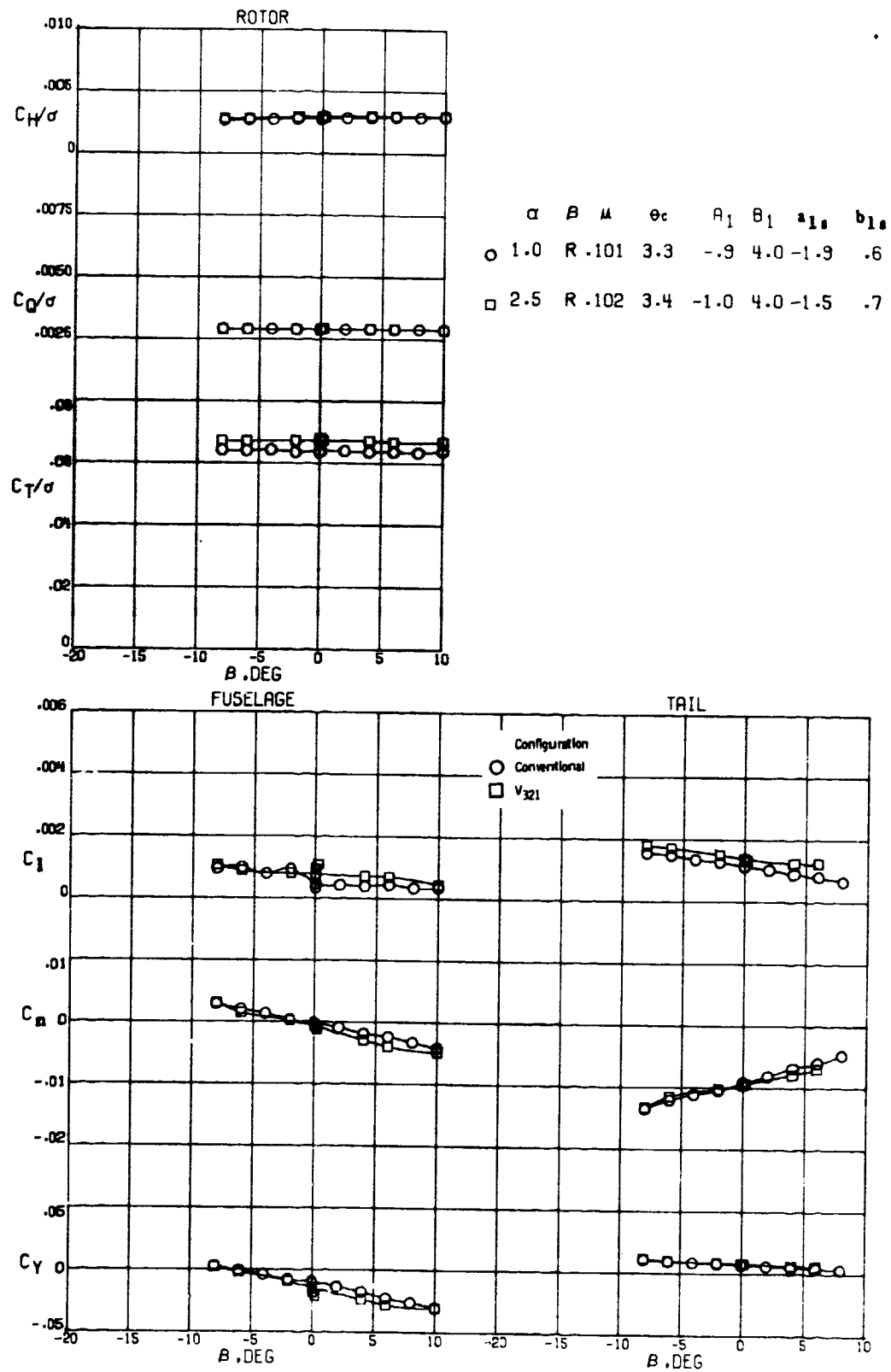
Figure 13.- Concluded.

ORIGINAL PAGE IS  
OF POOR QUALITY



(a)  $\mu = 0.057$

Figure 14.- Lateral-directional characteristics of the conventional tail and the baseline V-tail in 1-g flight at three advance ratios.



(b)  $\mu = 0.102$

Figure 14.- Continued.

ORIGINAL PAGE IS  
OF POOR QUALITY

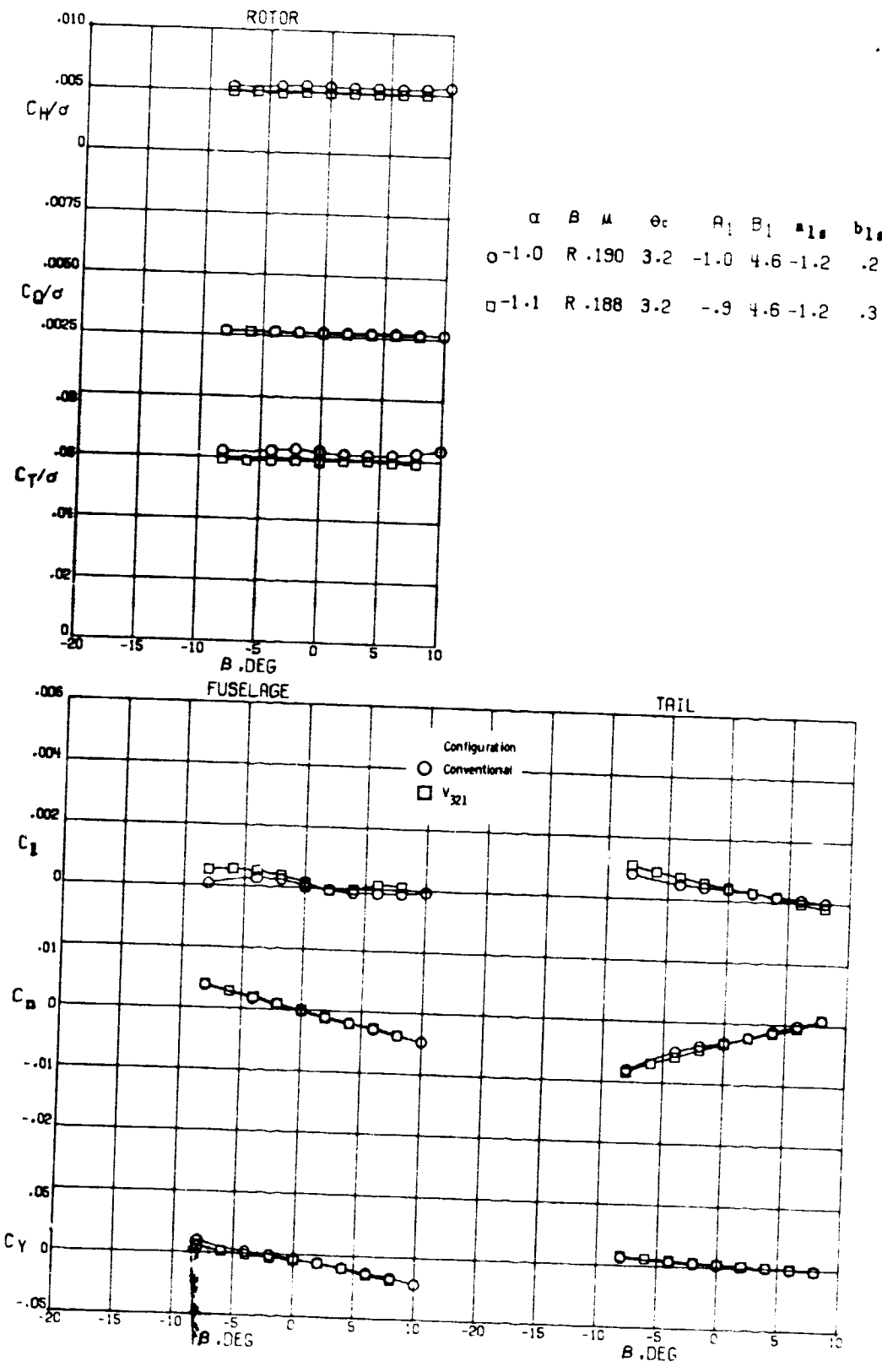


Figure 14.- Concluded.

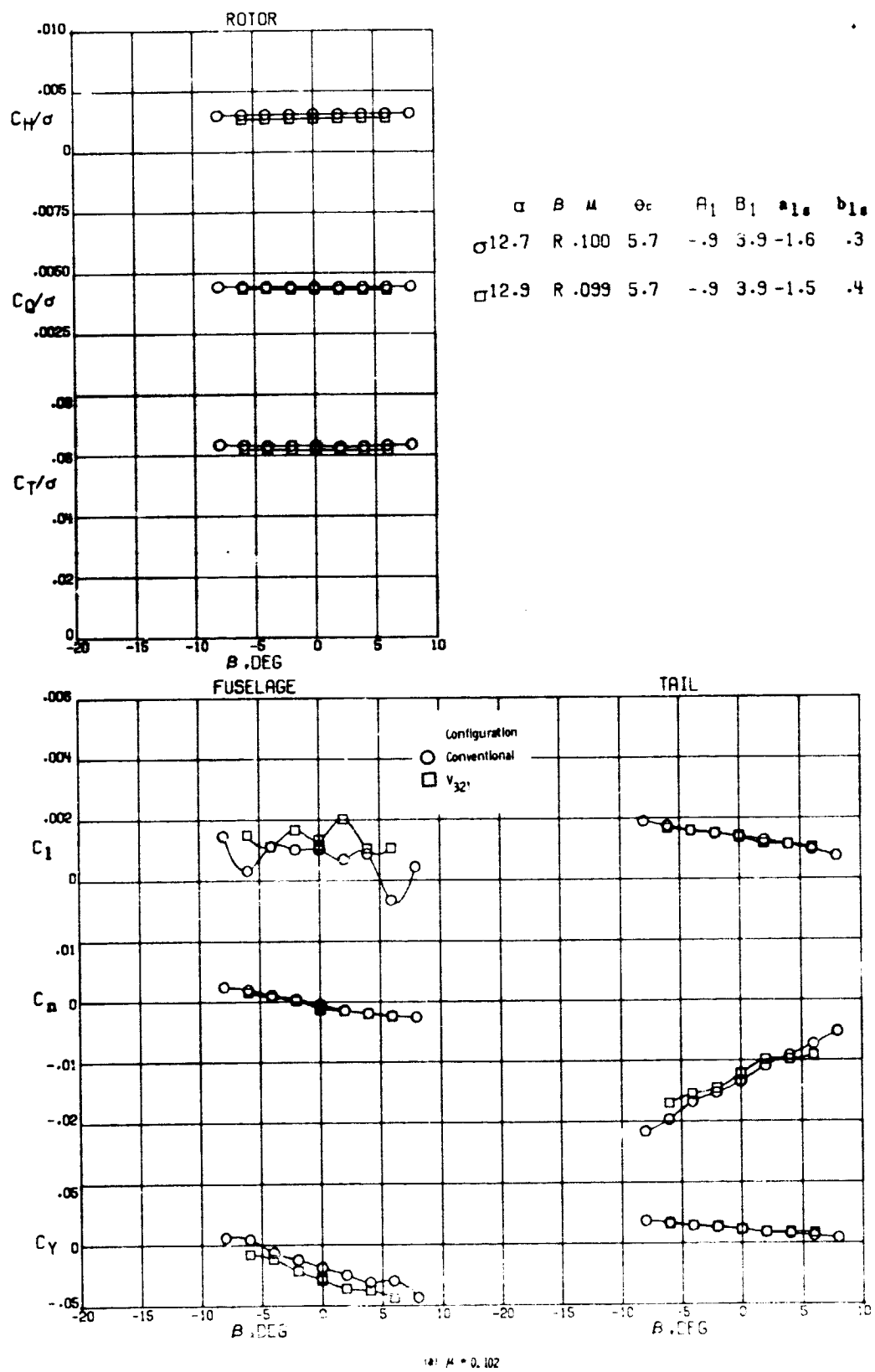


Figure 15.- Lateral-directional characteristics of the conventional tail and the baseline V-tail in climb at two advance ratios.

ORIGINAL PAGE IS  
OF POOR QUALITY

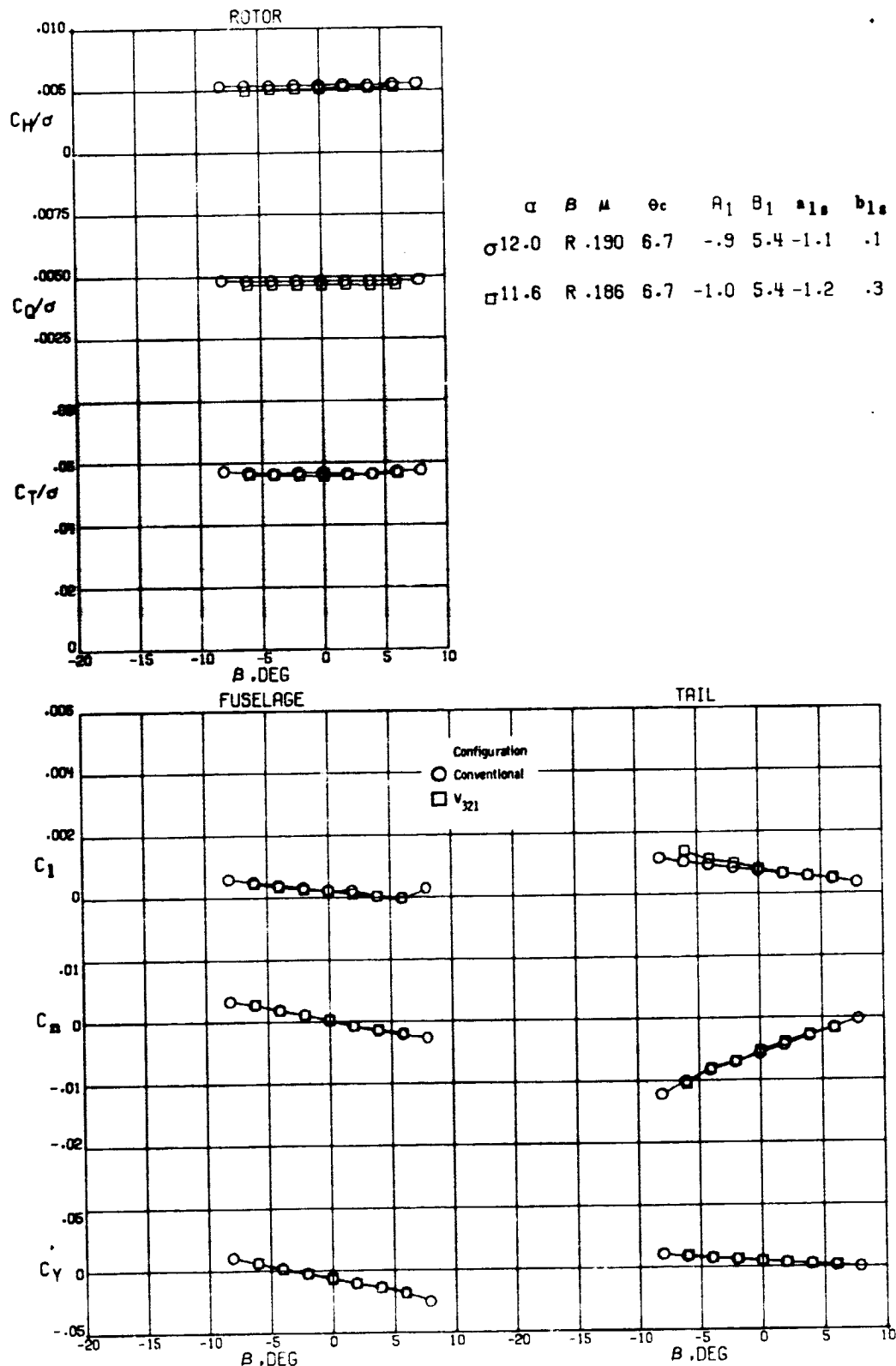


Figure 15.- Concluded.

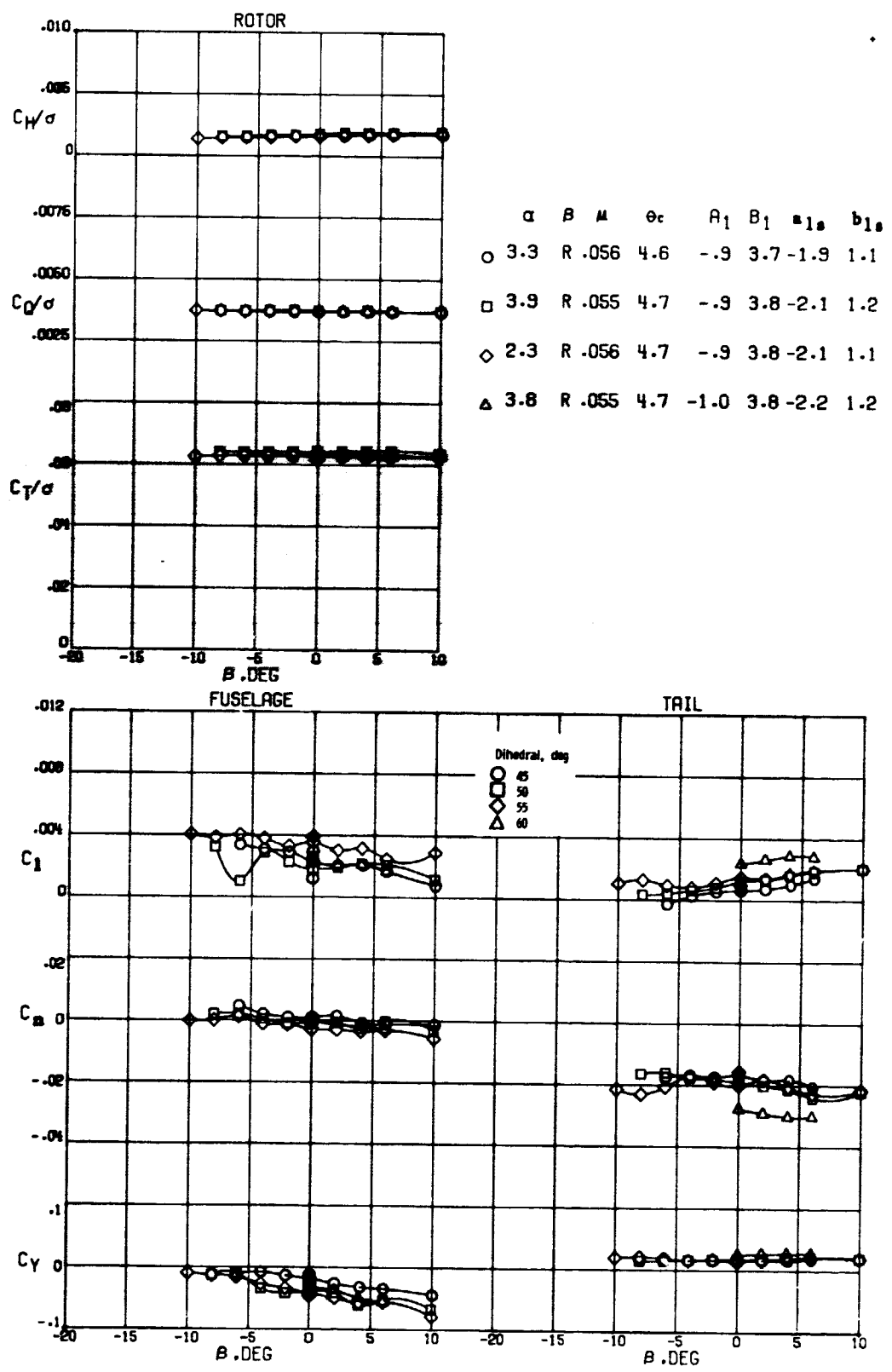
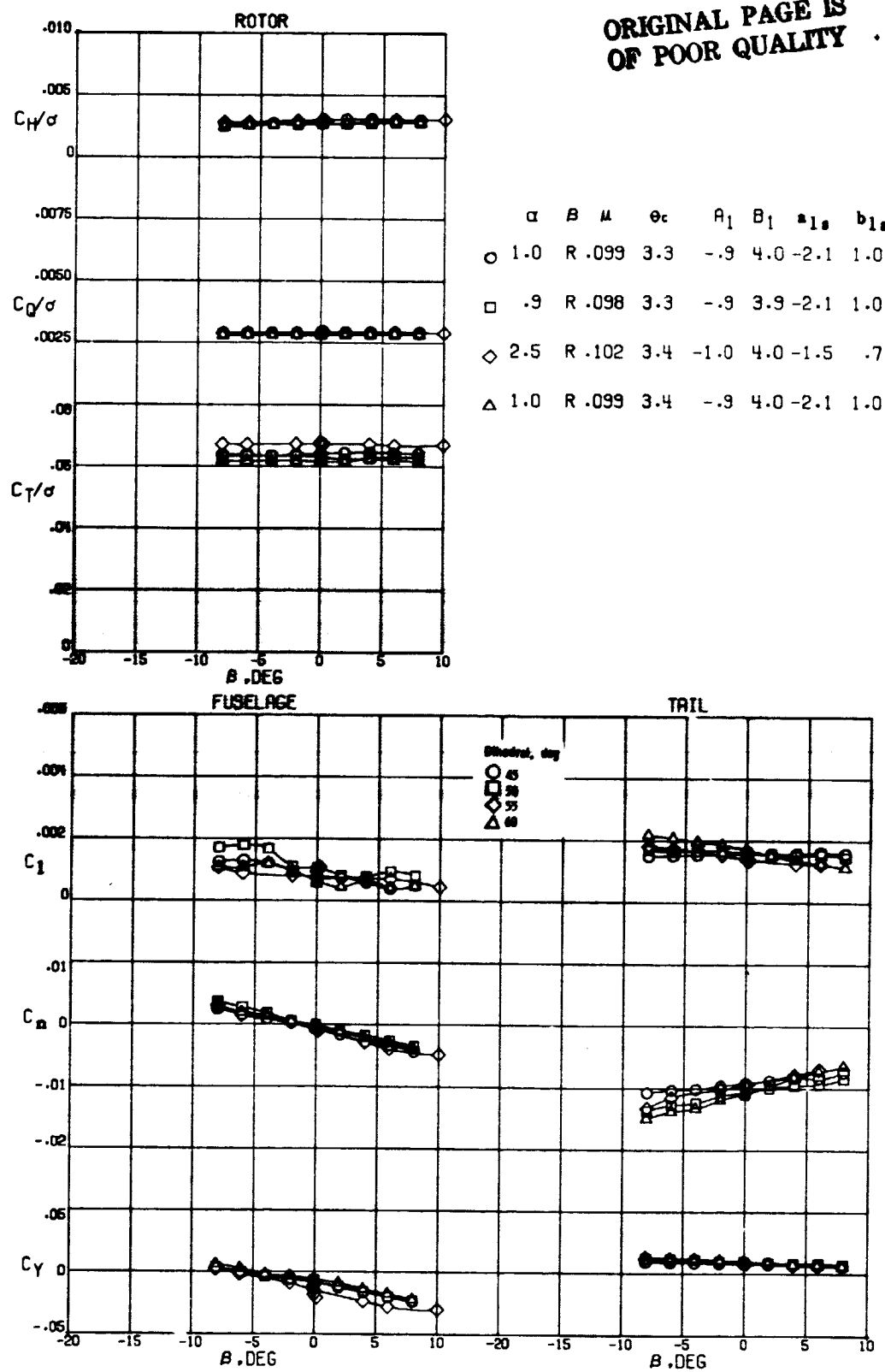
(a)  $\mu = 0.057$ 

Figure 16. - Effect of V-tail dihedral on the lateral-directional characteristics of the model at three advance ratios.

ORIGINAL PAGE IS  
OF POOR QUALITY



(b)  $\mu = 0.102$

Figure 16.- Continued.

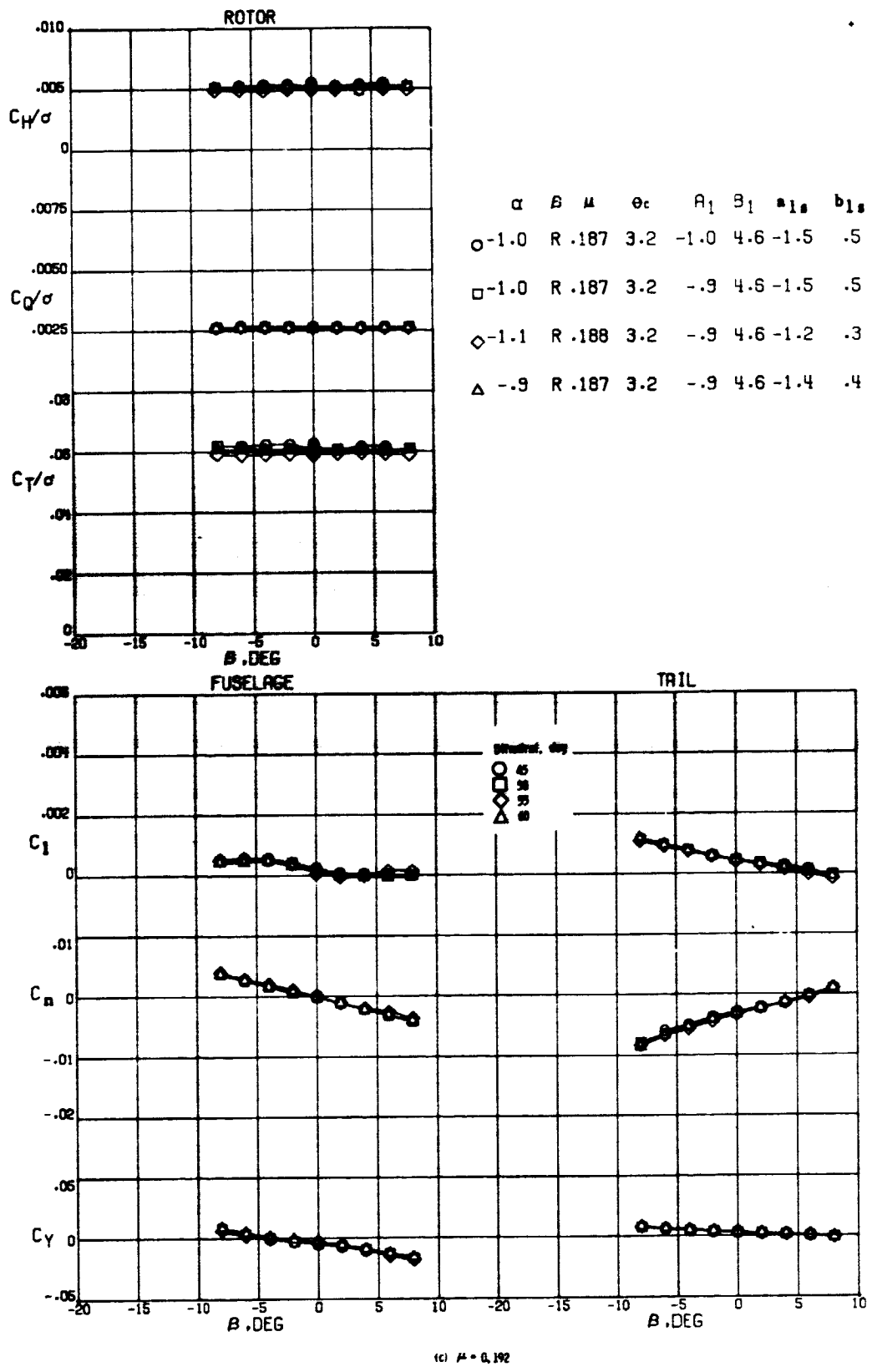


Figure 16 - Concluded.

ORIGINAL PAGE IS  
OF POOR QUALITY

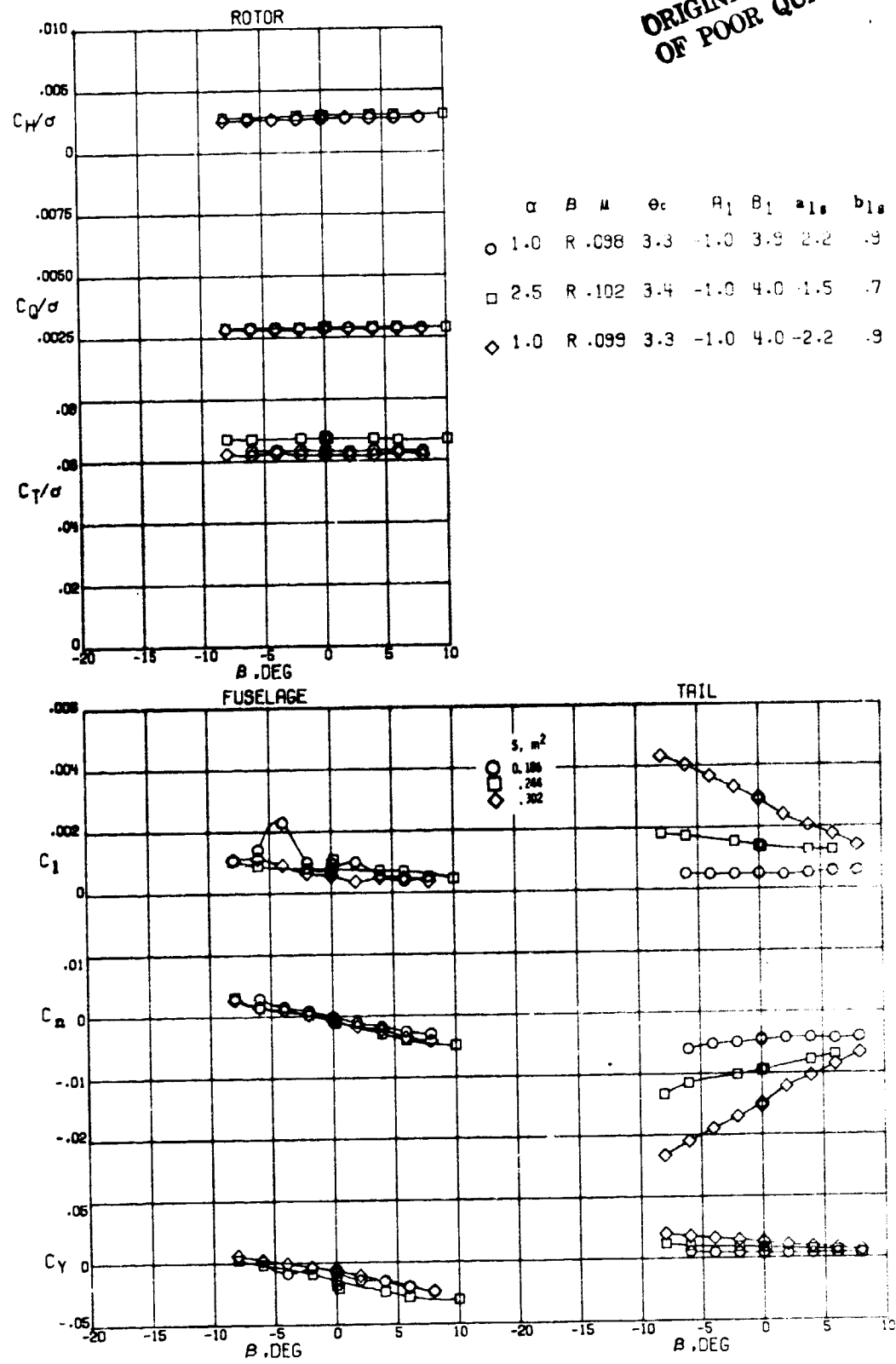
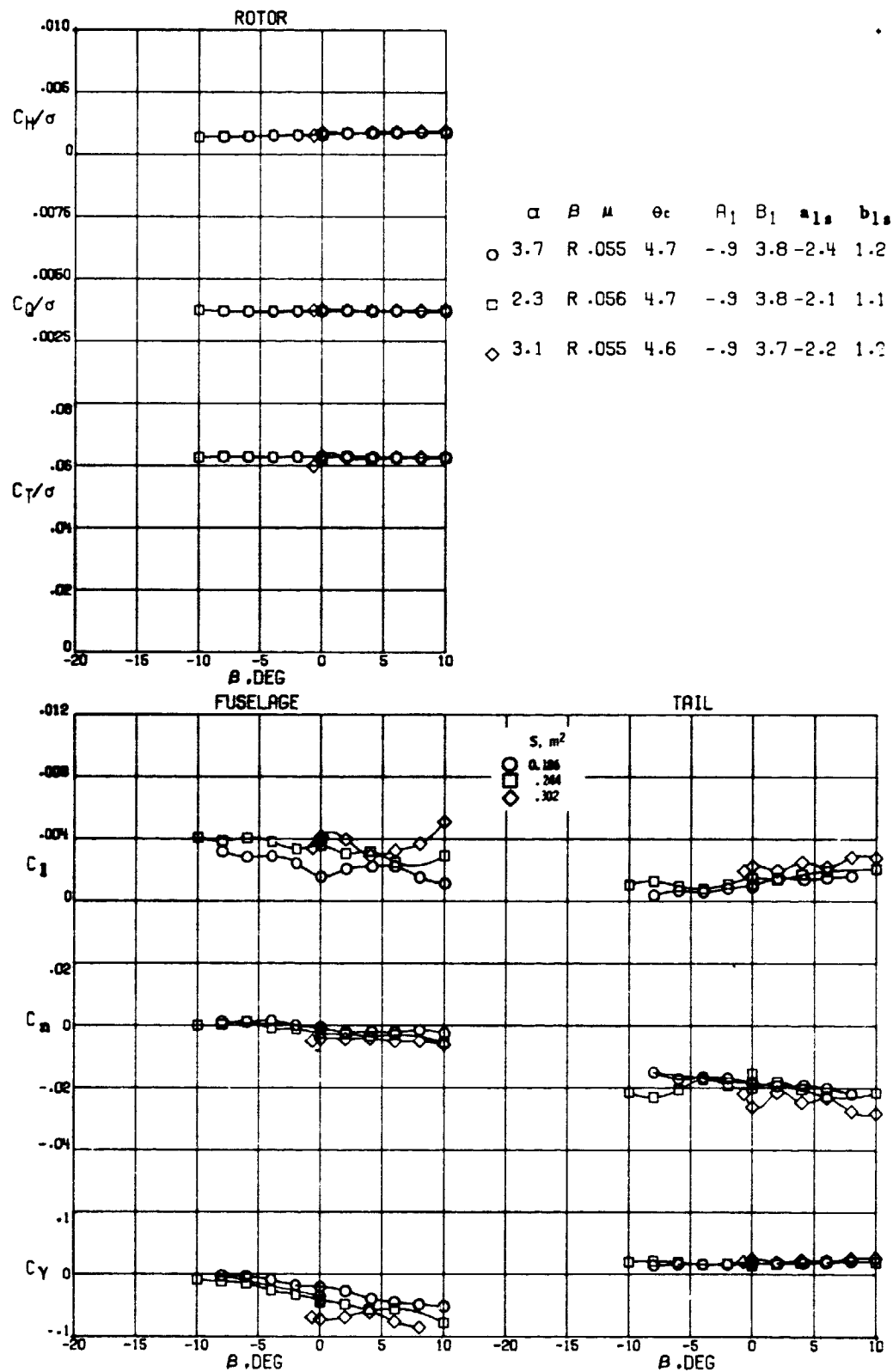


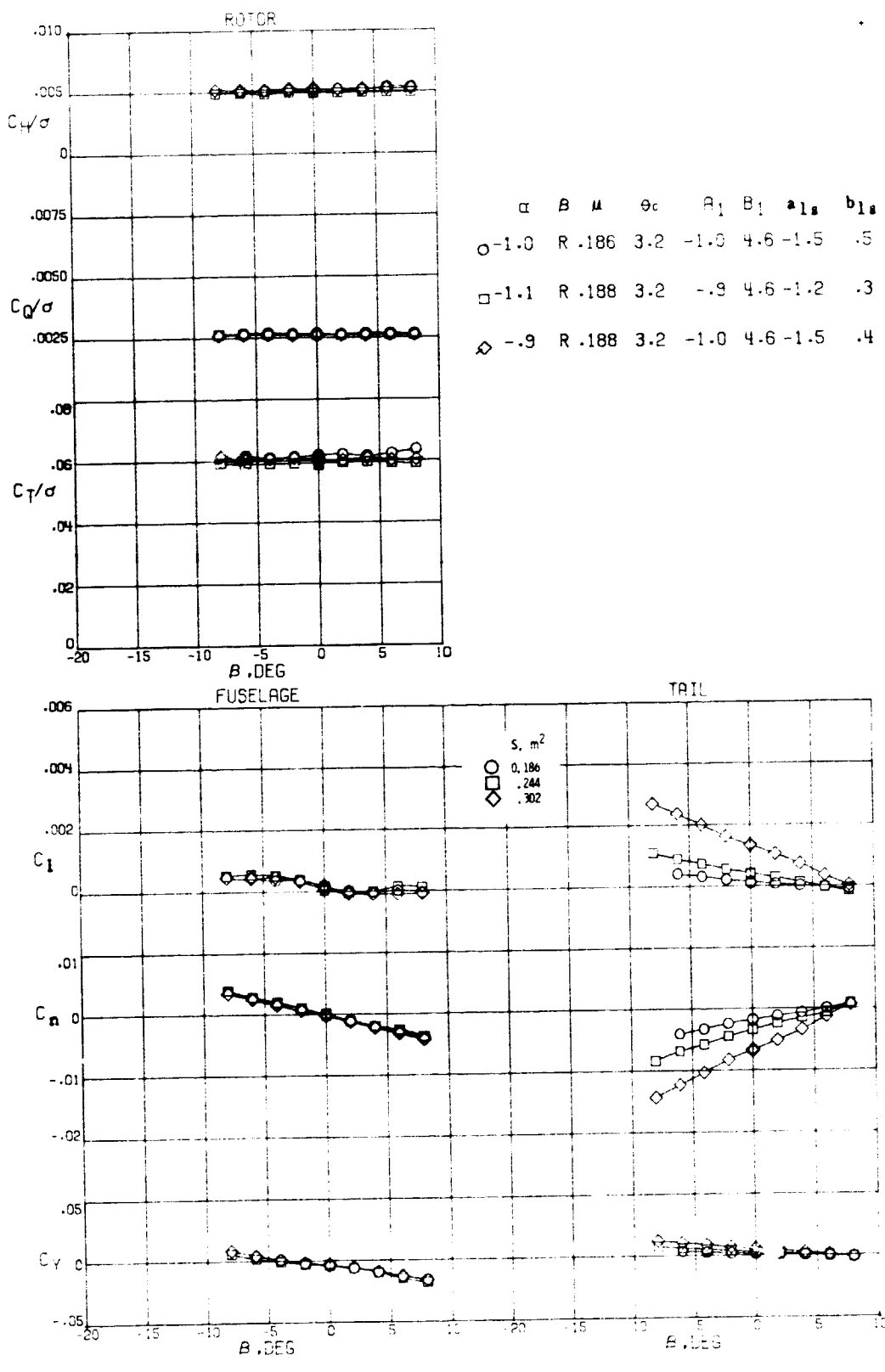
Figure 17.- Continued.



(a)  $\mu = 0.057$

Figure 17.- Effect of V-tail planform area on the lateral-directional characteristics of the model at three advance ratios.

ORIGINAL PAGE IS  
OF POOR QUALITY



(c)  $\mu = 0.192$

Figure 17.- Concluded.

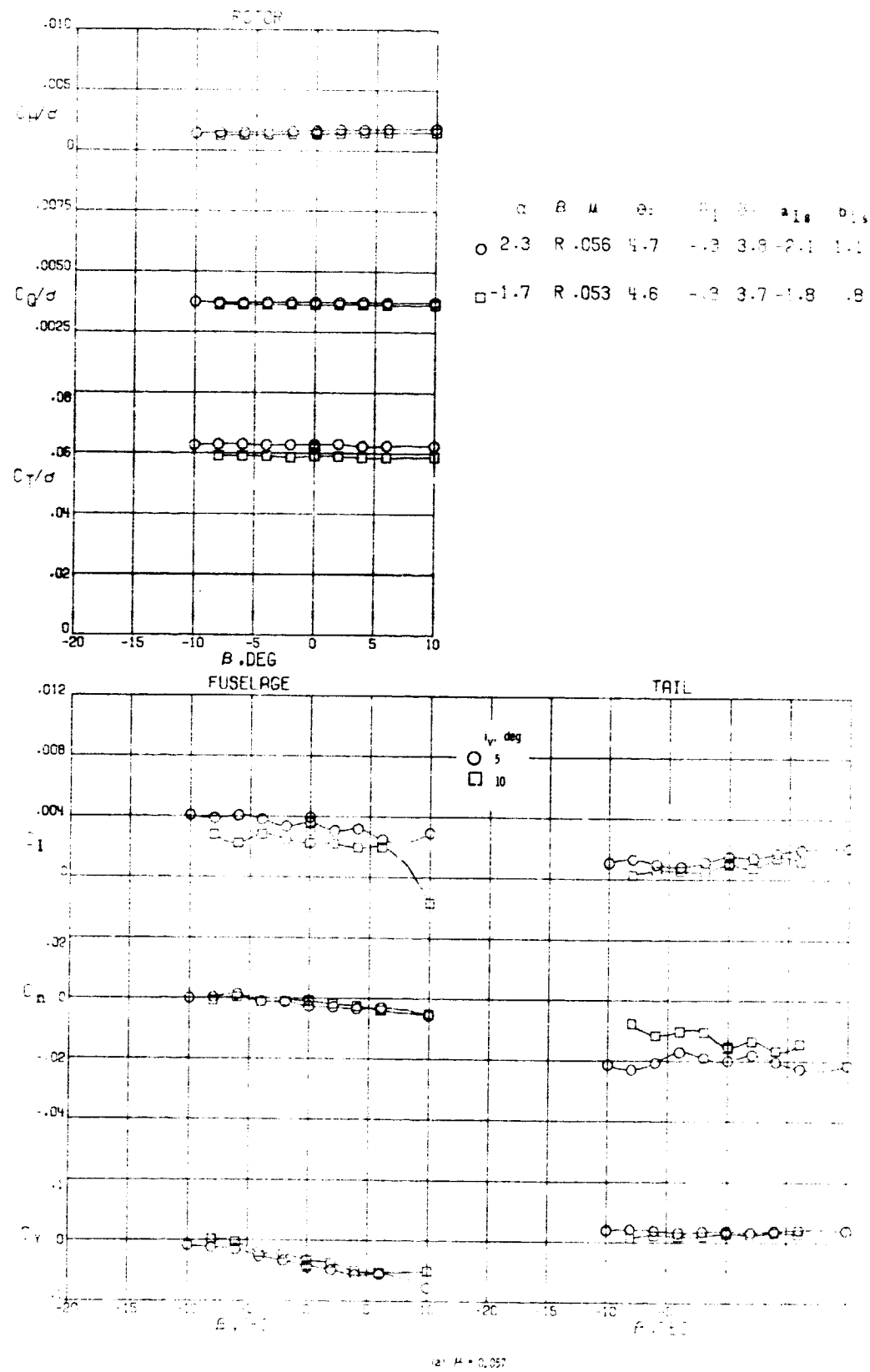


Figure 18 - Effect of vertical tail position on the aerodynamic characteristics of the model at three advance ratios.

ORIGINAL PAGE IS  
OF POOR QUALITY

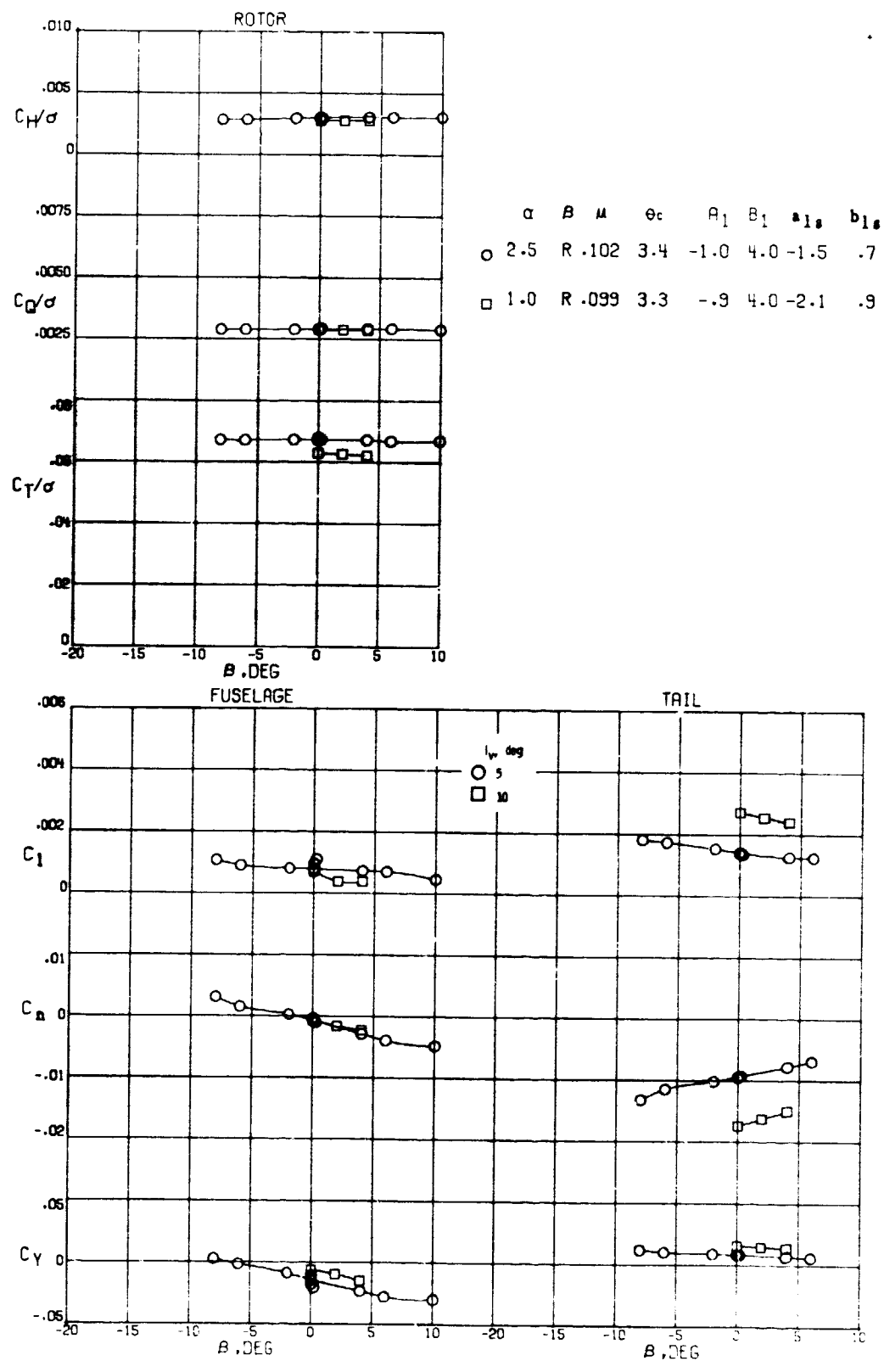
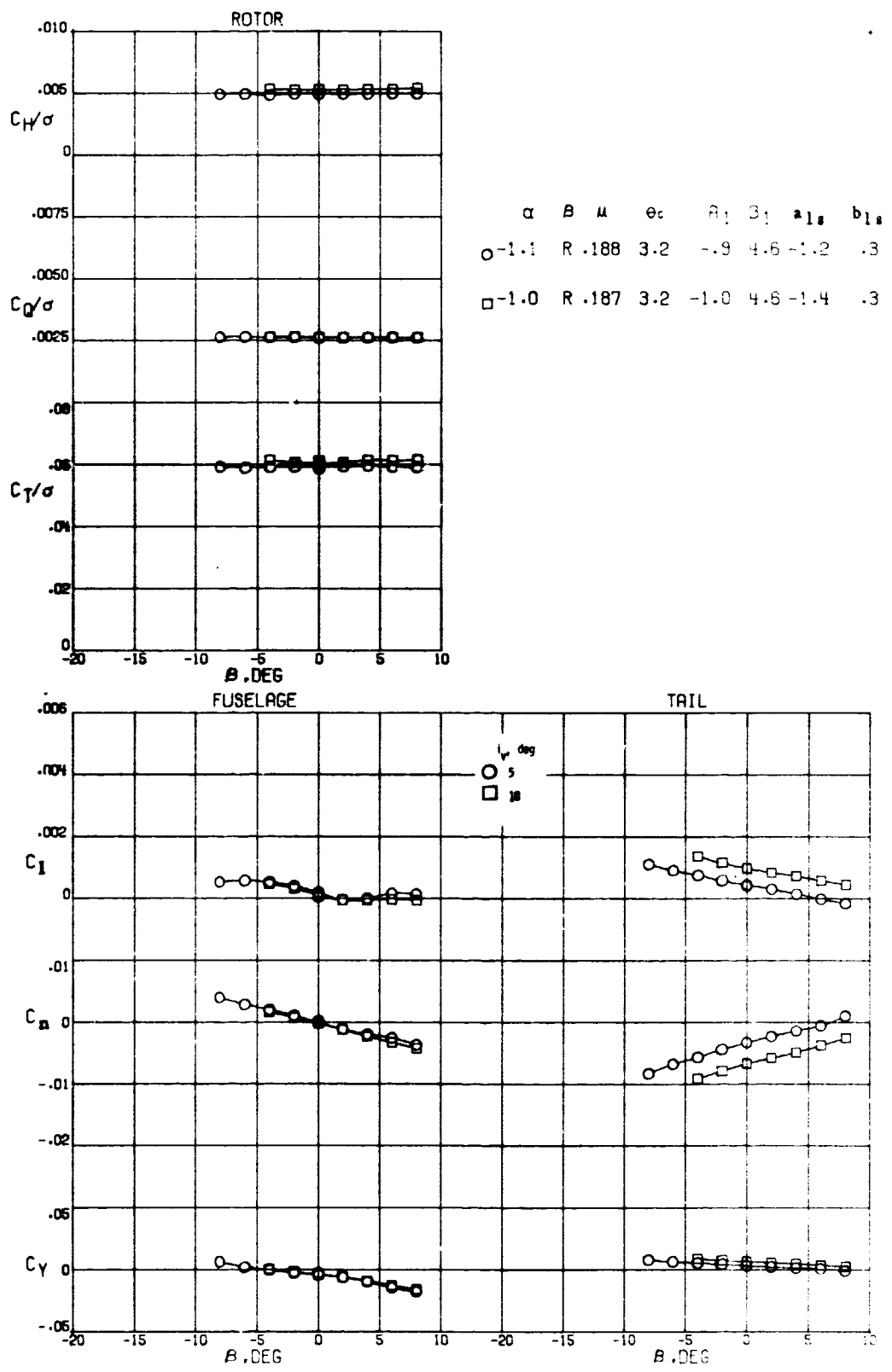


Figure 18.- Continued.



(C)  $\mu = 0.192$

Figure 18.- Concluded.

ORIGINAL PAGE IS  
OF POOR QUALITY

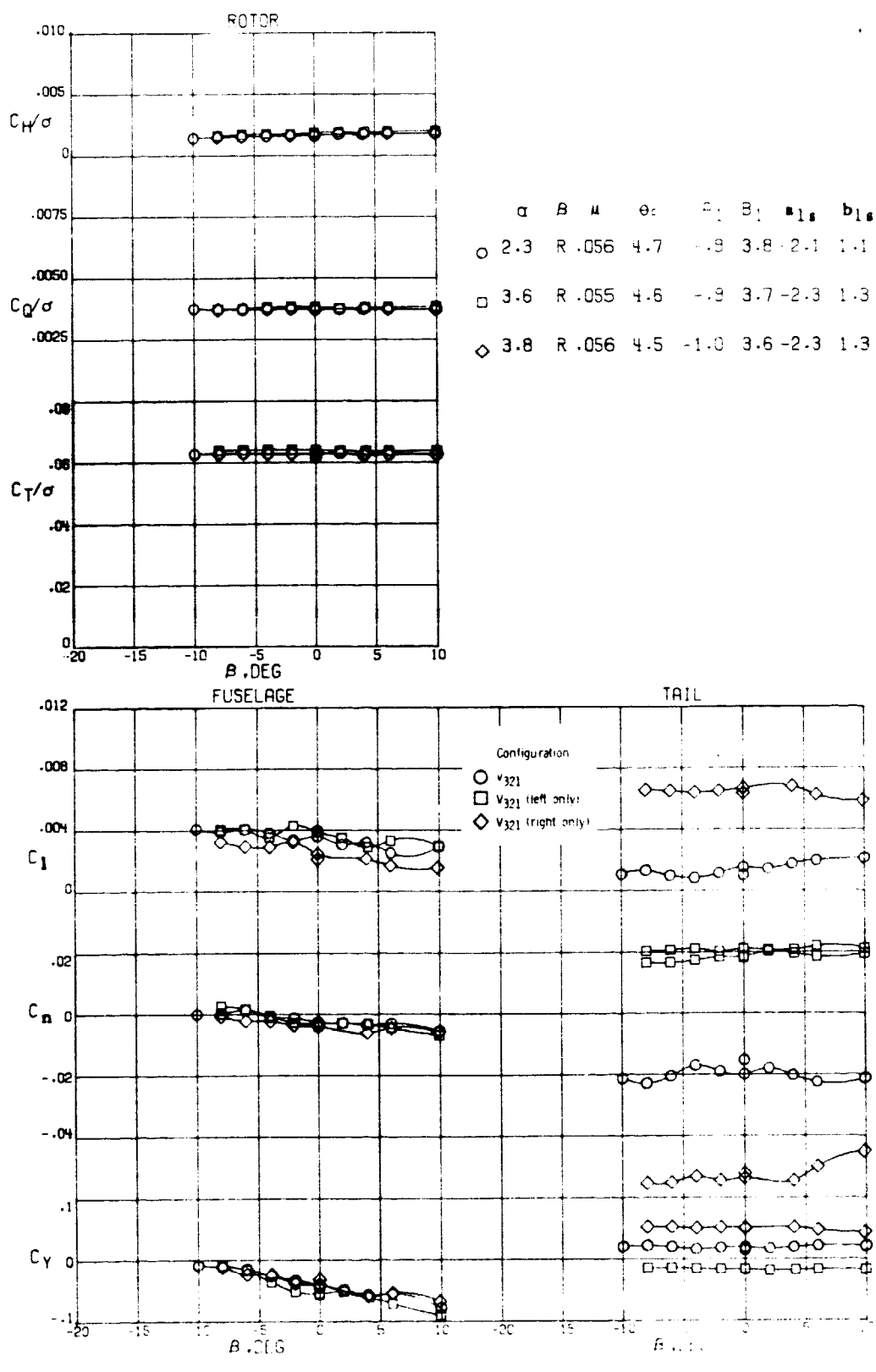
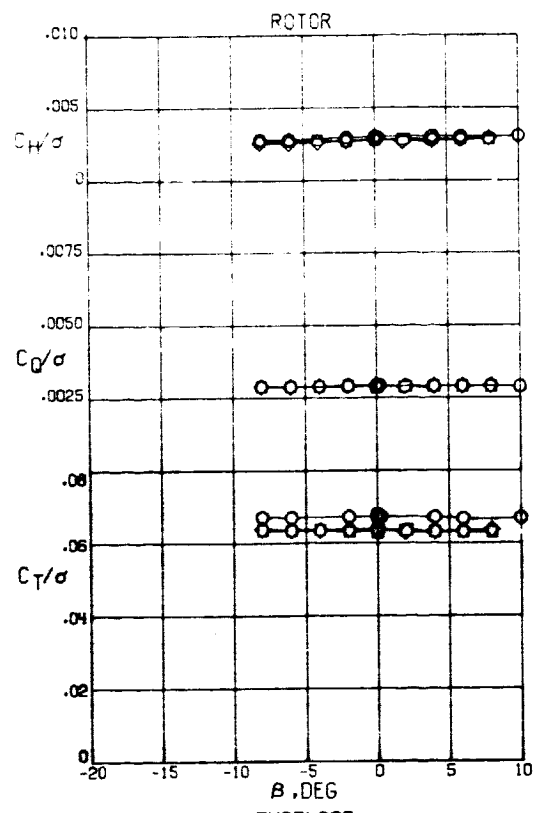
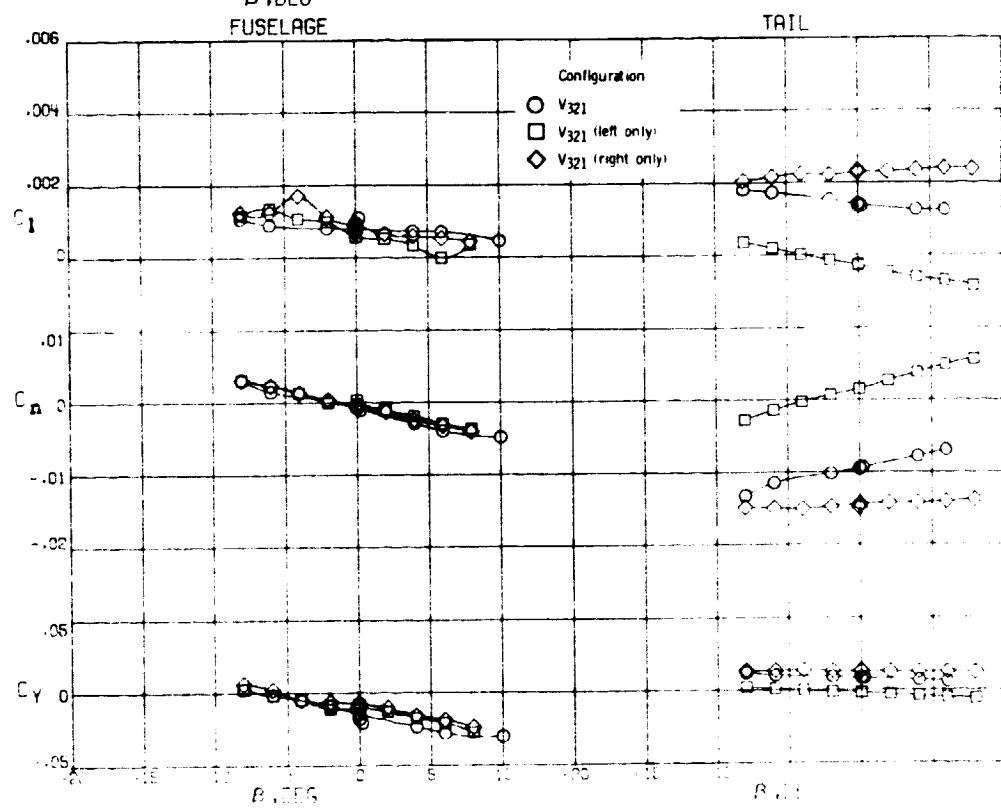


Figure 19. - Comparison of the lateral-directional characteristics of the baseline V-tail with the right or left tail surfaces removed.

at  $M = 0.357$



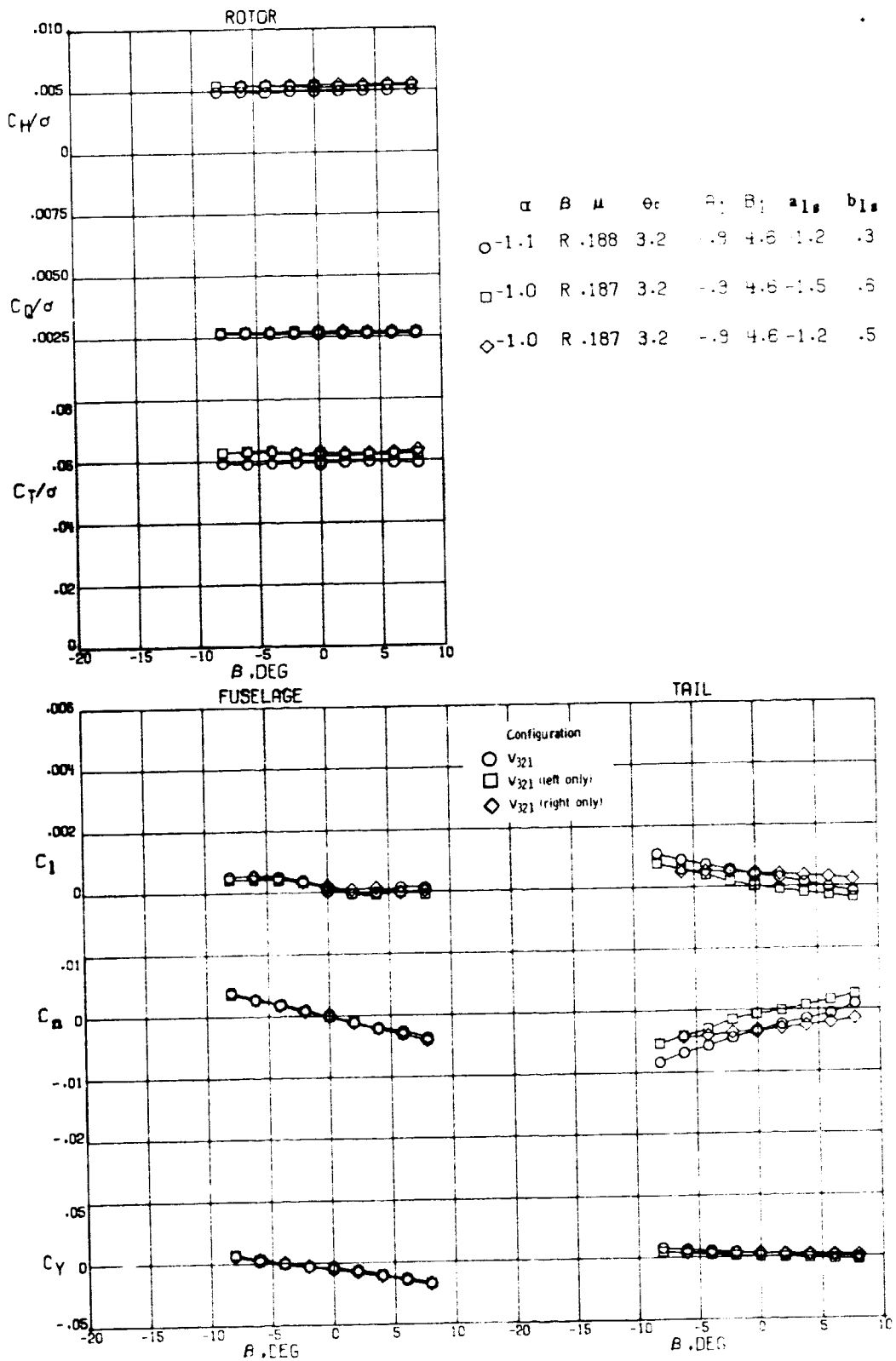
$\alpha$	$B$	$u$	$\theta_c$	$w_1$	$B_1$	$a_{ls}$	$b_{ls}$
2.5	R .102	3.4	-1.0	4.0	1.5	.7	
1.0	R .099	3.3	-1.0	4.0	-2.2	1.0	
1.0	R .099	3.3	-1.0	4.0	-2.1	1.0	



(b)  $A = 0.102$

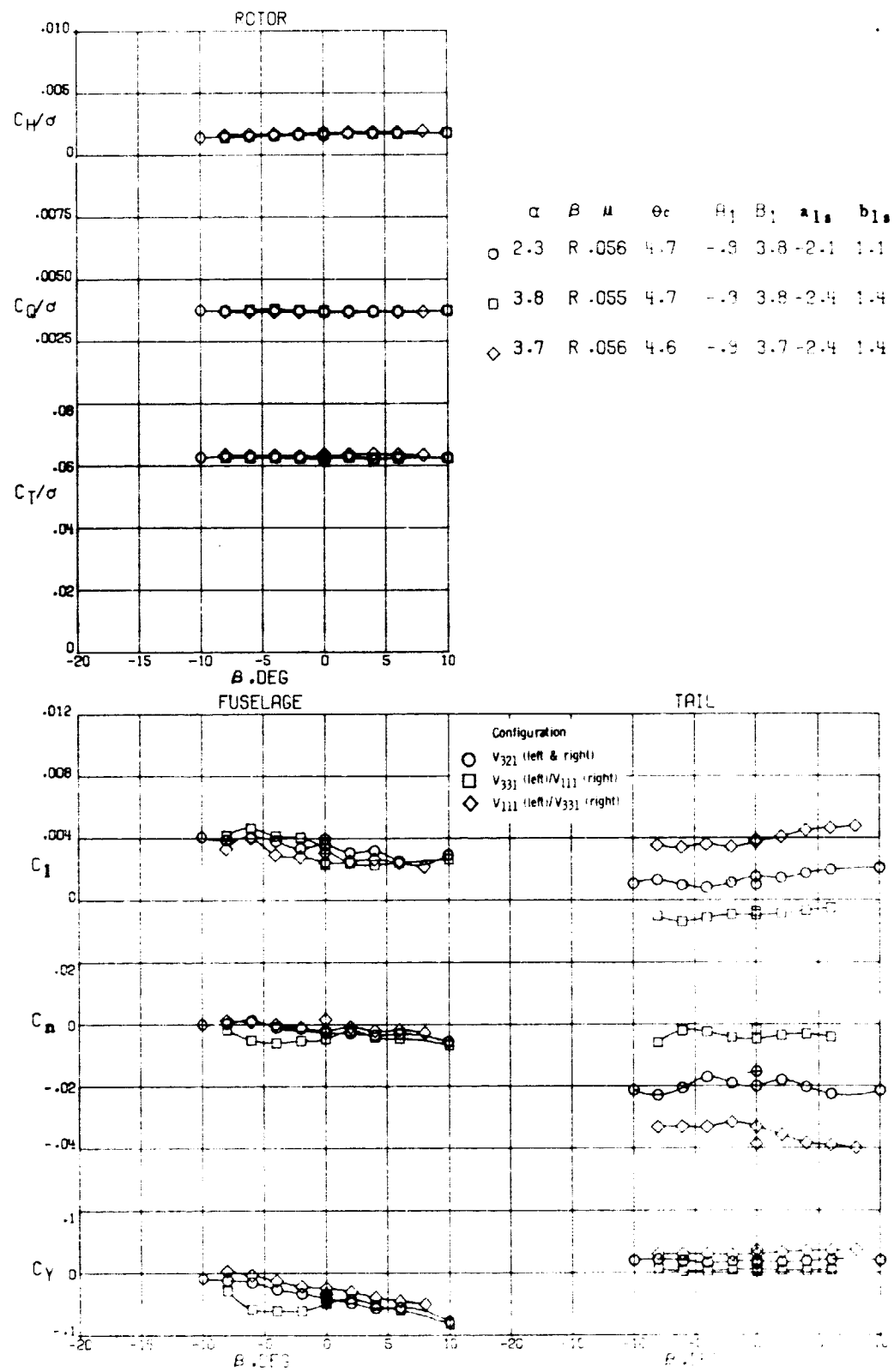
Figure 19.- Continued.

ORIGINAL PAGE IS  
OF POOR QUALITY



(c)  $\mu = 0.192$

Figure 19.- Concluded.



$\alpha = 2.3 \quad R = .057$

Figure 20. Comparison of the lateral-directional characteristics of the baseline V-tail with two nonsymmetric dihedral configurations.

ORIGINAL PAGE IS  
OF POOR QUALITY

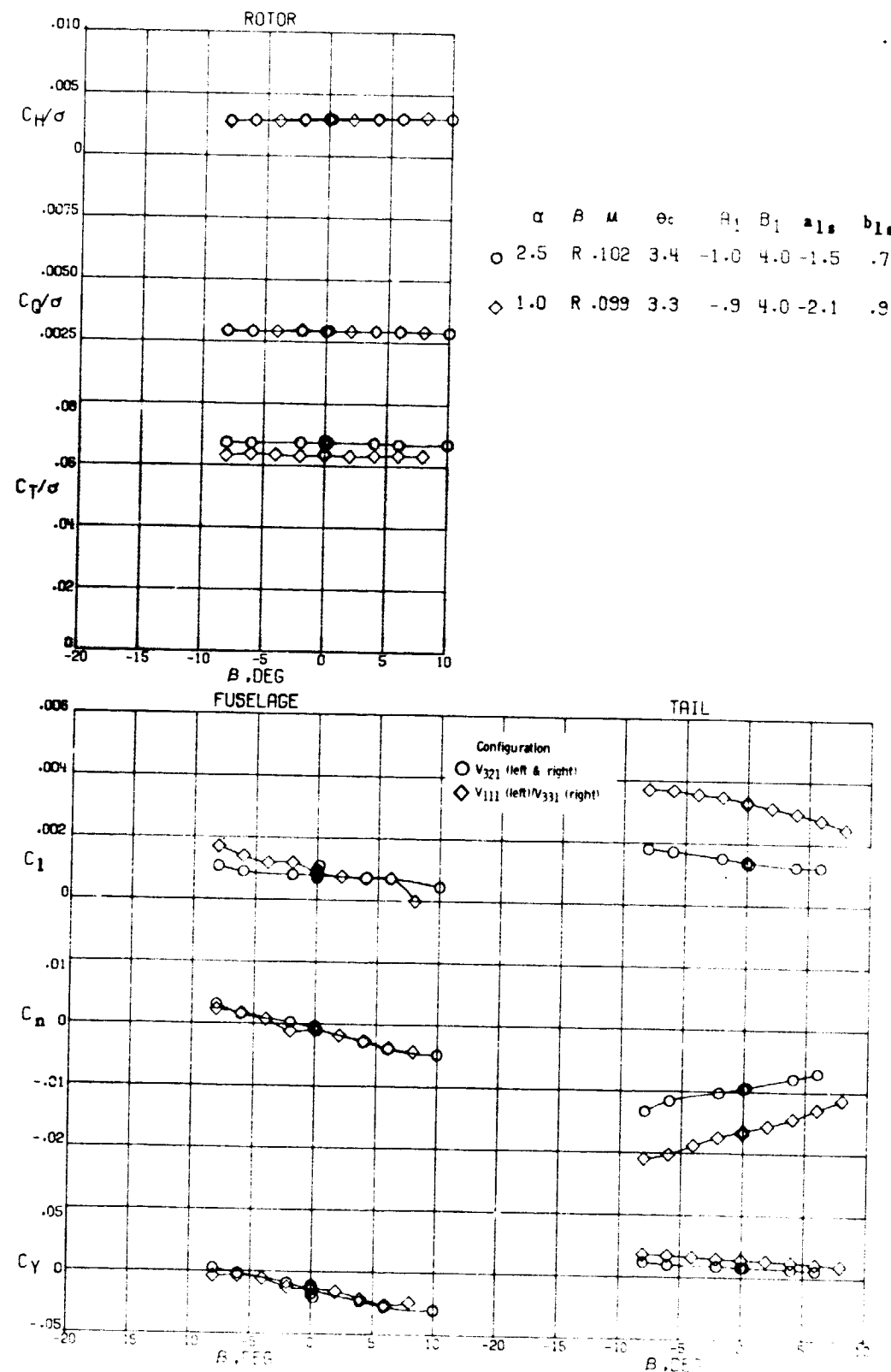


Figure 20. - Continued.

(b)  $\mu = 0.102$

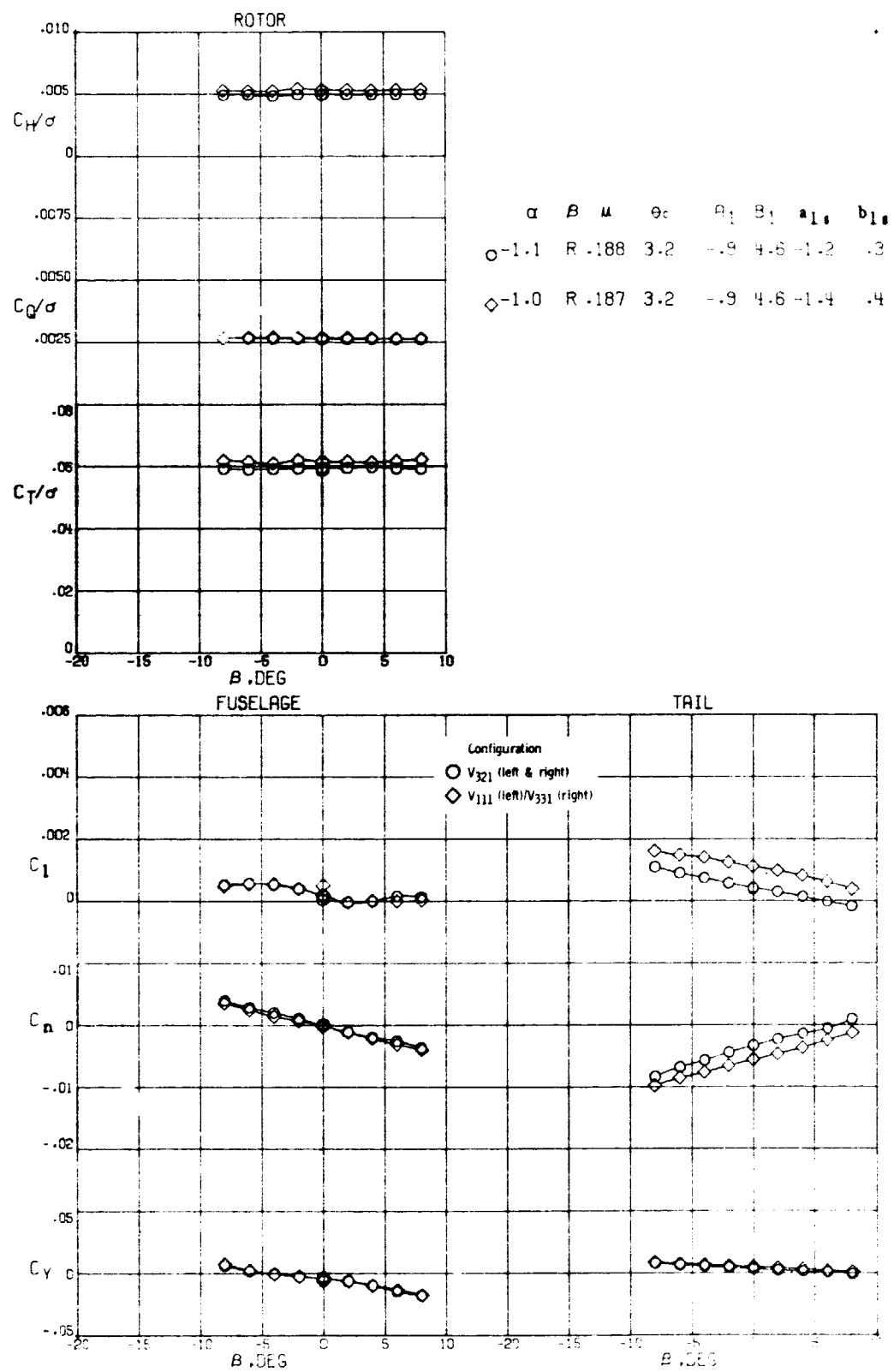
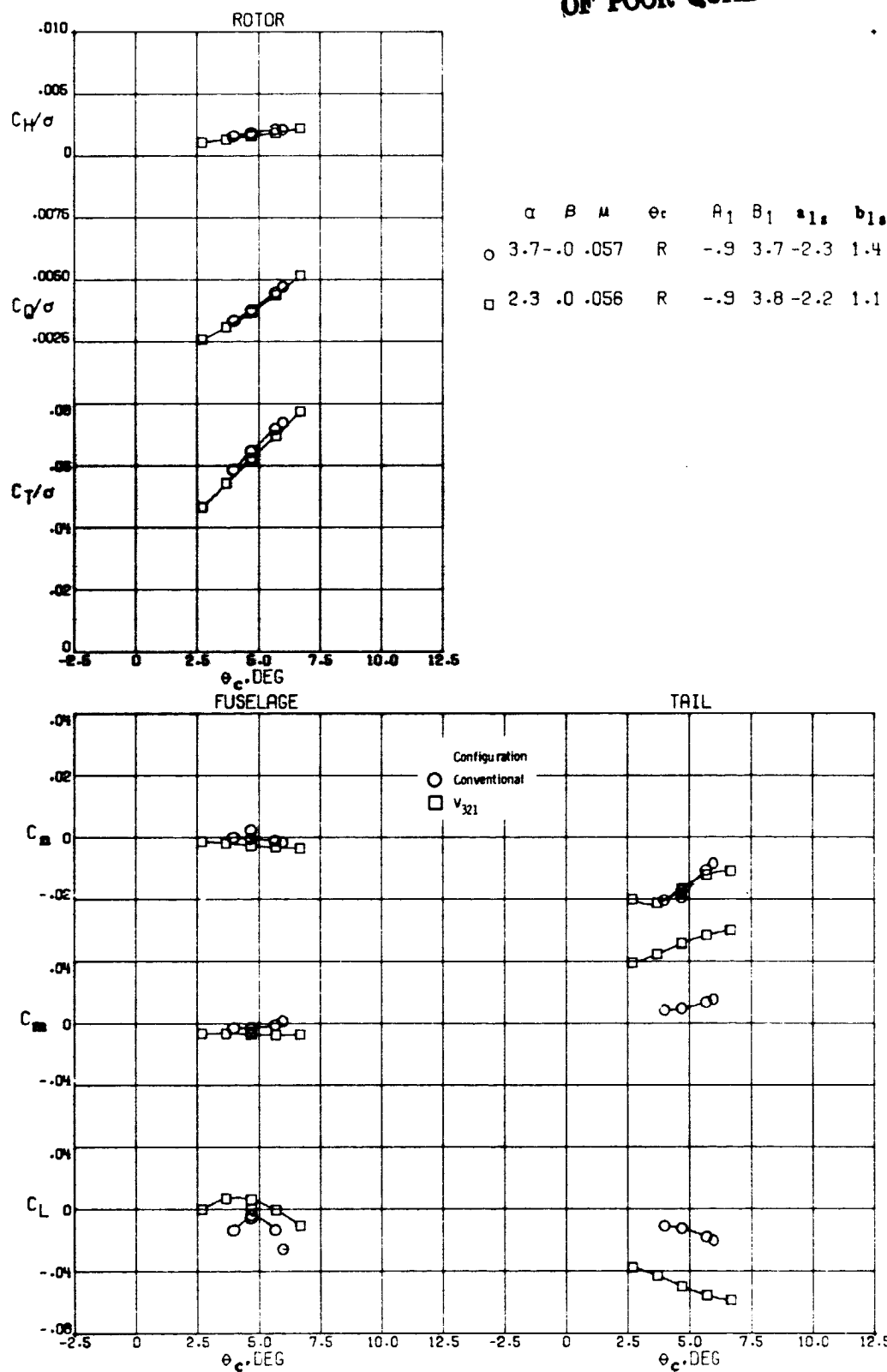


Figure 20. - Concluded.

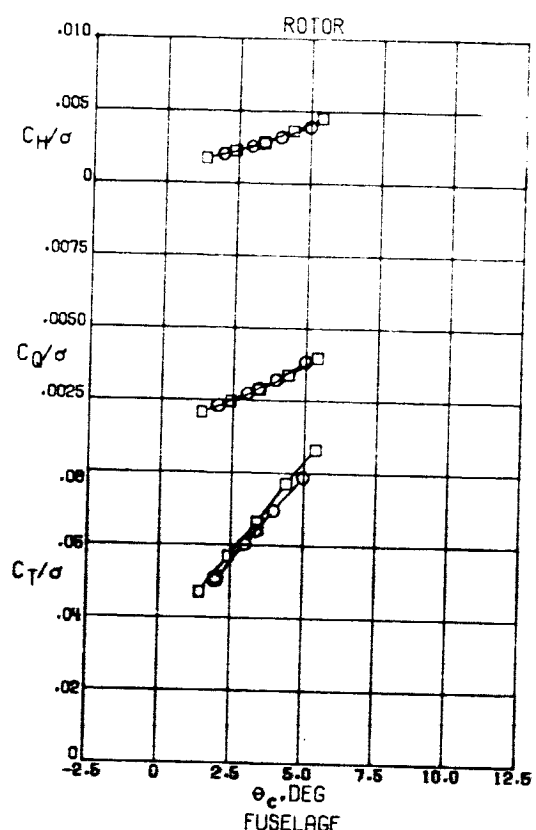
(C)  $\mu = 0.192$

ORIGINAL PAGE IS  
OF POOR QUALITY

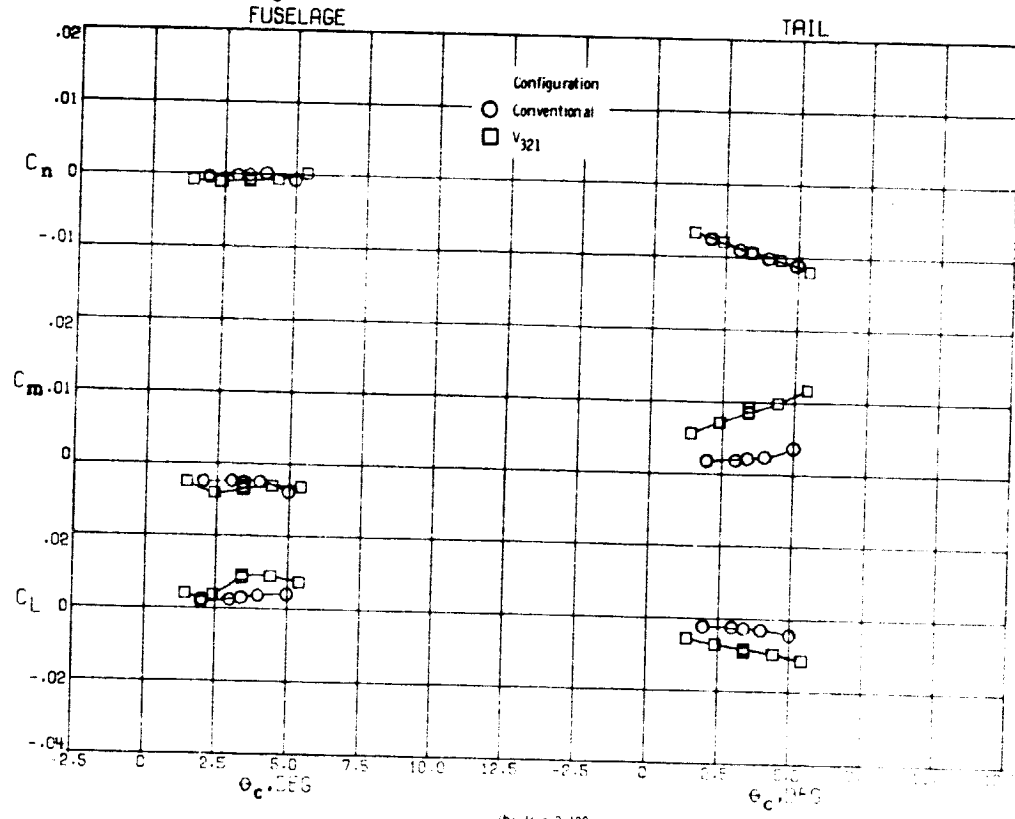


(a)  $H = 0.057$

Figure 21 - Comparison of rotor collective effects on the conventional tail and the baseline V-tail.



$\alpha \quad \beta \quad \mu \quad \theta_c \quad \beta_1 \quad b_1 \quad a_{1s} \quad b_{1s}$   
 ○ 1.0 .0 .100 R -.9 4.0 -2.0 .7  
 □ 2.5 .0 .102 R -1.0 4.0 -1.4 .6



b:  $\mu = 0.102$

Figure 21. - Continued.

ORIGINAL PAGE IS  
OF POOR QUALITY

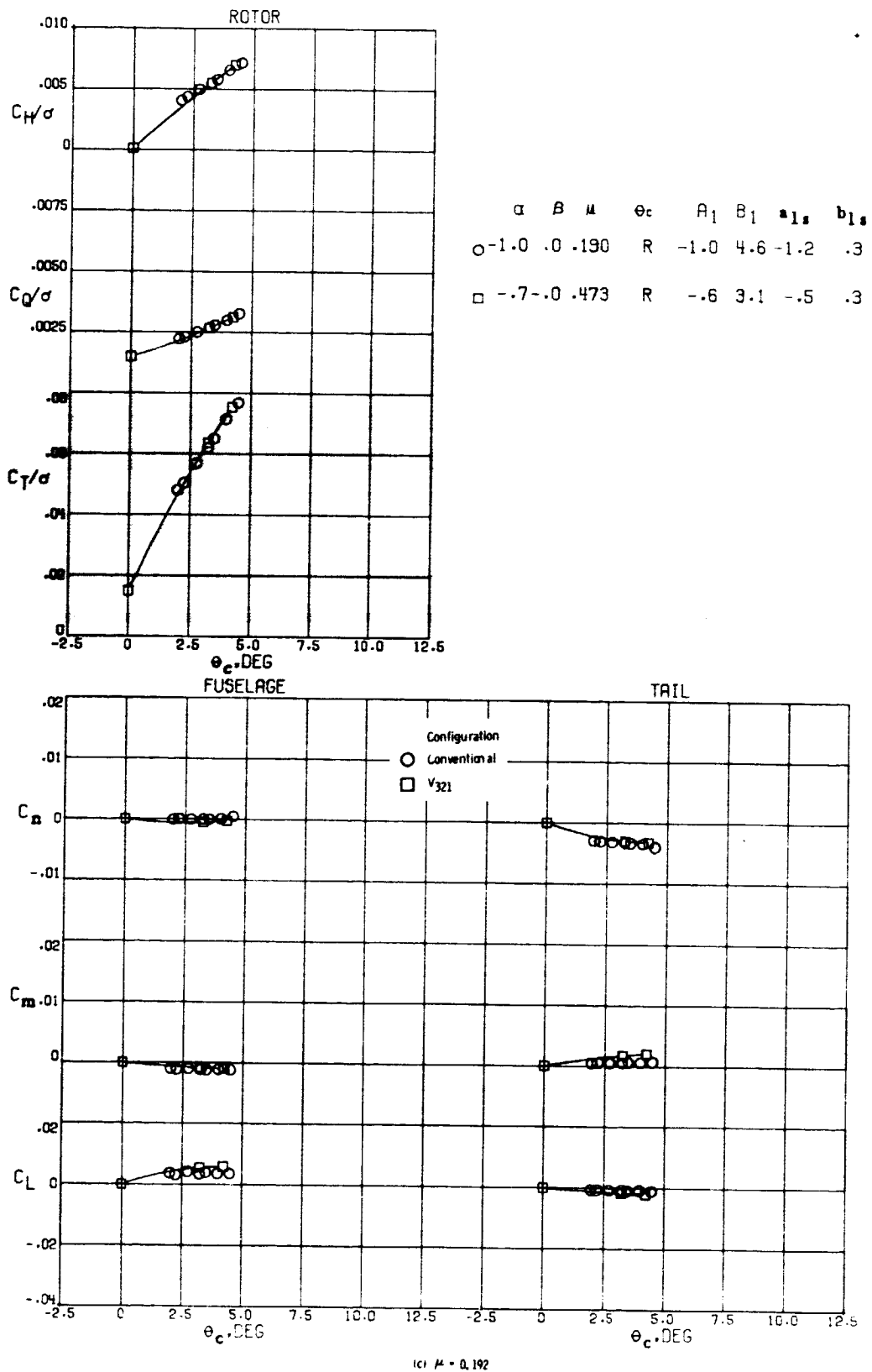
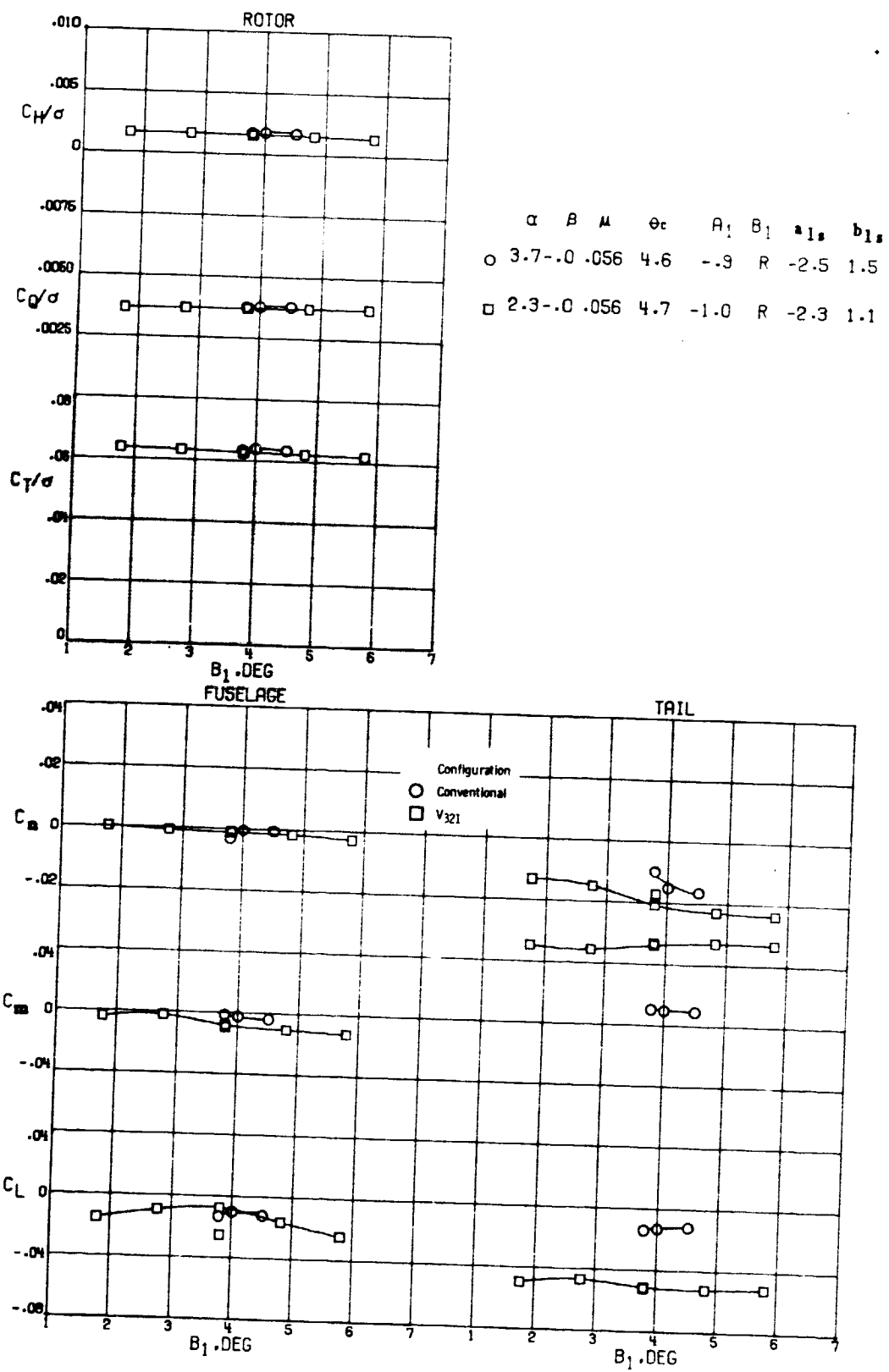


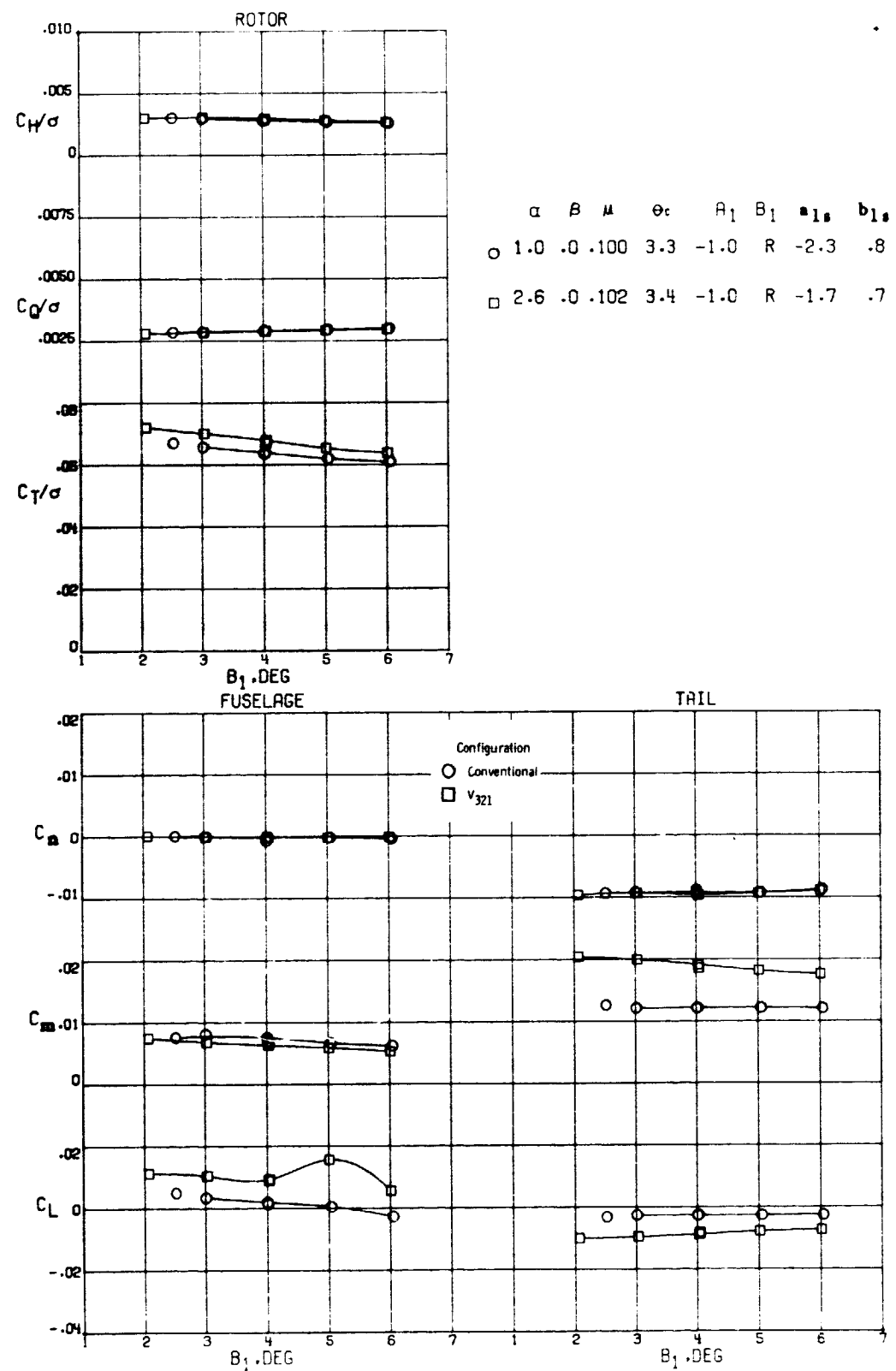
Figure 21.- Concluded.



(a)  $\mu = 0.057$

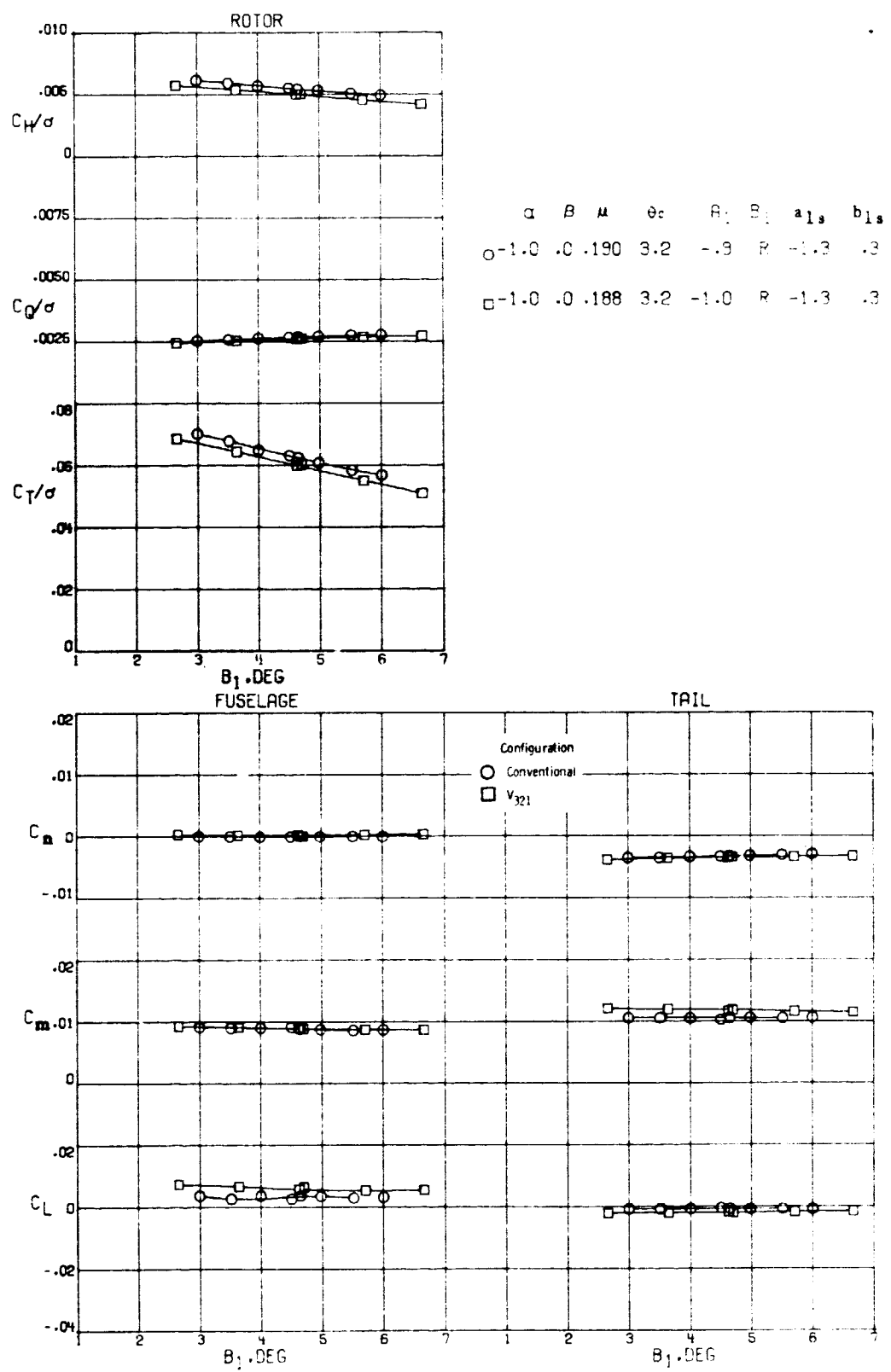
Figure 22.- Comparison of rotor longitudinal cyclic effects on the conventional tail and the baseline V-tail.

ORIGINAL PAGE IS  
OF POOR QUALITY



(b)  $\mu = 0, 102$

Figure 22. - Continued.



$\alpha = 0.192$

Figure 22.- Concluded.

ORIGINAL PAGE IS  
OF POOR QUALITY

**END**

**DATE**

**FILMED**

**NOV 17 1978**